

# Characterization of Synaptopodin 2 Subcellular Trafficking during Phenotype Modulation of Vascular Smooth Muscle Cells and Beyond

Inaugural-Dissertation

zur

Erlangung des Doktorgrades (Dr. rer. nat.)

der Mathematisch-Naturwissenschaftlichen Fakultät

der Universität zu Köln



Vorgelegt von

***Mostafa Abootorabi Ardestani***

Cologne, Germany, 2015

[Die vorliegende Arbeit wurde in der Zeit vom November 2011 bis Januar 2015, unter der Anleitung von Frau Prof. Dr. Gabriele Pfitzer und Frau Dr. Mechthild M. Schroeter am Institute für vegetative Physiologie der medizinischen Fakultät der Universität Köln, angefertigt.]

[This study was undertaken under the guidance of Prof. Dr. Gabriele Pfitzer and Dr. Mechthild M. Schroeter in the period between November 2011 and January 2015 at the Institute of Vegetative Physiology of the Medical faculty of the University of Cologne.]

Thesis Supervisor: Prof. Dr. Gabriele Pfitzer

Thesis Committee Chair: Prof. Dr. Thorsten Hoppe

Thesis Reader: Prof. Dr. Günter Schwarz

Thesis Reader: Prof. Dr. Angelika A. Noegel

Date of Oral Exam: 2015-04-14

*To My Beloved  
Family*

“Imagination is more important than knowledge. For knowledge is limited to all we now know and understand, while imagination embraces the entire world, and all there ever will be to know and understand.”

**Albert Einstein**

**Table of Contents\_Toc410319457**

<b>1</b>	<b>Introduction</b>	<b>18</b>
1.1	<b>Muscle</b>	<b>18</b>
1.1.1	Vascular smooth muscle	18
1.1.2	Molecular basis of contraction and relaxation	20
1.1.3	Smooth muscle cells phenotype plasticity and disease	22
1.1.4	Actin cytoskeleton	23
1.1.4.1	Actin and actin filaments	23
1.2	<b>Synaptopodin family</b>	<b>25</b>
1.2.1	Synaptopodin	26
1.2.2	Synaptopodin 2	26
1.2.3	Synaptopodin 2-like	28
1.3	<b>Protein-Protein interaction</b>	<b>29</b>
1.3.1	Förster resonance energy transfer	30
1.3.2	Bimolecular fluorescence complementation (BIFC)	31
1.4	<b>Aim of the project</b>	<b>33</b>
<b>2</b>	<b>Materials and Methods</b>	<b>34</b>
2.1	<b>General materials</b>	<b>34</b>
2.2	<b>Methods</b>	<b>49</b>
2.2.1	Molecular biology methods	49
2.2.1.1	Total RNA isolation and cDNA synthesis	49
2.2.1.1.1	<b>Total RNA isolation by MAXWELL machine</b>	49
2.2.1.1.2	<b>cDNA synthesis</b>	50
2.2.1.2	Preparative PCR	50
2.2.1.2.1	<b>Purification of PCR products</b>	51
2.2.1.2.2	<b>Sub-Cloning</b>	52
2.2.1.2.3	<b>Transformation</b>	53
2.2.1.2.4	<b>Colony PCR</b>	53
2.2.1.2.5	<b>Preparation of plasmid DNA</b>	54
2.2.1.2.6	<b>Test digest screening</b>	55
2.2.1.2.7	<b>DNA sequencing</b>	55
2.2.1.3	Quantitative polymerase chain reaction (qRT-PCR)	55
2.2.1.3.1	<b>Analysis of qRT-PCR data</b>	56
2.2.2	Cell biology methods	57
2.2.2.1	Isolation of vascular smooth muscle cells from rat aorta	57
2.2.2.2	Cell culture and treatments	59
2.2.2.3	Immunofluorescence staining	61
2.2.2.4	Confocal microscopy	62
2.2.3	Biochemical and analytical methods	63
2.2.3.1	Characterization of isolated VSMCs	63
2.2.3.2	Fluorescence activated cell sorting assay (FACS)	63
2.2.3.3	Subcellular fractionation	63
2.2.3.4	SDS-PAGE and Western blot analysis	65
2.2.3.5	Estimation of F/G-Actin ratio	66
2.2.4	Preparation of collagen I and laminin coated polyacrylamide matrices	67
2.2.5	Stiffness measurement of polyacrylamide by atomic force microscopy	67

2.2.6	Bimolecular fluorescence complementation assay (BIFC)	68
2.2.7	FACS-BIFC based assay	69
2.2.8	Statistics	70
<b>3</b>	<b>Results</b>	<b>71</b>
3.1	Over 95% of the isolated cells were vascular smooth muscle cells	71
3.2	Isolated primary VSMCs expressed the smooth muscle marker proteins	72
3.3	Immunofluorescence studies demonstrated co-localization of SYNPO2, smMHC, and $\alpha$ -SMA	73
3.4	Alteration of marker proteins during phenotype switch	73
3.5	Phenotype switch of VSMCs alters subcellular distribution of SYNPO2	75
3.6	Controlling of phenotype switch using ECM proteins	77
3.7	Cultivation the cells on ECM proteins pre-coated matrices alter subcellular localization of SYNPO2	80
3.8	Actin cytoskeleton turnover affects subcellular distribution of SYNPO2	81
3.9	Heat Shock Stress did not affect the Subcellular Localization of SYNPO2 in VSMCs	83
3.10	Subcellular distribution of SYNPO2 is controlled by cAMP	84
3.11	Inhibition of PKA and CaMK-II reduced the accumulation of SYNPO2 in the nucleus of VSMCs	86
3.12	ROCK signaling does not affect subcellular localization of SYNPO2	88
3.13	Treatment with okadaic acid resulted in a reduction of nuclear SYNPO2- displaying cells	89
3.14	Characterization of expression level of 14-3-3 isoforms in VSMCs	90
3.15	Analysis of subcellular localization of SYNPO2 and its interaction with 14-3-3 $\beta/\gamma$ , and importin $\alpha$ using fluorescent fused proteins and BIFC assay	91
3.16	Subcellular localization of YFP-fused SYNPO2 & CFP-fused 14-3-3 $\gamma/\beta$ , importin $\alpha$	92
3.17	Analysis of SYNPO2, 14-3-3 $\gamma/\beta$ and importin $\alpha$ interaction by using BIFC	95
3.17.1	SYNPO2 interacts with 14-3-3 $\gamma$ in the cytoplasm and not in the nucleus	95
3.17.2	SYNPO 2 and 14-3-3 $\beta$ accumulate and form loop-like complexes in the nucleus	96
3.17.3	Preferred interaction of SYNPO2 and importin $\alpha$ in the nucleus	97
3.18	Visualization of SYNPO2 homo-dimer using BIFC and FACS-BIFC based assay	99
<b>4</b>	<b>Discussion</b>	<b>100</b>
4.1	Current state of knowledge as relevant to this work	100
4.2	Phenotype switch of VSMCs affects the subcellular distribution of SYNPO2	102
4.3	Actin dynamics and subcellular distribution of SYNPO2 in VSMCs	105
4.4	The cAMP mediated signaling is involved in the subcellular shuttling of SYNPO2 between the nucleus and the cytoplasm	108
4.5	Imaging of SYNPO2, 14-3-3 $\gamma/\beta$ , and Importin $\alpha$ interaction in living cells	111

4.6	Visualization of SYNPO2 homo-dimerization using BIFC assay in living cells	116
<b>5</b>	<b><i>Conclusion and Outlook</i></b>	<b>118</b>
<b>6</b>	<b><i>Bibliography</i></b>	<b>121</b>
<b>7</b>	<b><i>Supplementary information</i></b>	<b>141</b>
7.1	Synaptopodin 2	141
7.2	14-3-3 $\gamma$	142
7.3	14-3-3 $\beta$	142
7.4	Importin $\alpha$	143
7.5	Plasmids	144
7.5.1	pEYFP-N1-SYNPO2 and pEYFP-C1-SYNPO2	144
7.5.2	pECFP-N1-14-3-3 $\gamma$ and pECFP-C1-14-3-3 $\gamma$	145
7.5.3	pECFP-N1-14-3-3 $\beta$ and pECFP-C1-14-3-3 $\beta$	146
7.5.4	pECFP-N1-importin $\alpha$ and pECFP-C1-importin $\alpha$	147
7.5.5	$\Delta$ C- and $\Delta$ N-YFP-SYNPO2	148
7.5.6	$\Delta$ C- and $\Delta$ N-YFP-14-3-3 $\gamma$	149
7.5.7	$\Delta$ C- and $\Delta$ N-YFP-14-3-3 $\beta$	150
7.5.8	$\Delta$ C- and $\Delta$ N-YFP- Importin $\alpha$	151
7.6	BIFC control experiments	152
<b>8</b>	<b><i>Acknowledgment</i></b>	<b>154</b>
<b>9</b>	<b><i>Erklärung</i></b>	<b>156</b>
<b>10</b>	<b><i>Curriculum Vitae</i></b>	<b>157</b>

## I. List of Figures

Fig. 1 Schematic illustration of (A) skeletal and (B) smooth muscles (according to Lodish 4th Ed).	18
Fig. 2 Schematic illustration of the signals that regulate and control the smooth muscle cell contraction and relaxation (according to Puetz et al 2009) <sup>16</sup> .	21
Fig. 3 Schematic illustration of actin polymerization/depolymerization.	25
Fig. 4 Schematic illustration of synaptopodin 2 isoforms in human.	27
Fig. 5 Principle of FRET assay used in vivo.	31
Fig. 6 Schematic illustration of the BIFC assay used in this work according to Hu, CD. et al. 2003 <sup>130</sup> .	32
Fig. 7 Schematic illustration: Isolation of vascular smooth muscle cell from rat aorta using enzymatic method.	58
Fig. 8 Fluorescence-activated cell sorting (FACS) analysis of isolated rat aorta vascular smooth muscle cells versus fibroblasts.	71
Fig. 9 Indirect immunofluorescence analysis of marker proteins of isolated VSMCs.	72
Fig. 10 Visualization of SYNPO2 and the contractile marker proteins, smMHC and $\alpha$ -SMA.	73
Fig. 11 Expression analysis of marker proteins in primary rat VSMCs.	75
Fig. 12 Subcellular localization of synaptopodin 2 during isolation and cultivation of primary VSMCs.	77
Fig. 13 Characterization of VSMCs cultivated on polyacrylamide matrices coated with extracellular matrix proteins.	79
Fig. 14 On laminin coated polyacrylamide matrices cultivated VSMCs develop a contractile phenotype.	80
Fig. 15 Subcellular distribution of SYNPO2 during actin cytoskeleton turnover.	82
Fig. 16 Distribution of smooth muscle cells SYNPO2 is independent of heat stress.	83
Fig. 17 cAMP-induced shuttling of SYNPO2 in VSMCs.	85
Fig. 18 Inhibition of both PKA and CaMKII reduced nuclear accumulation of SYNPO2 in the isolated VSMCs.	87
Fig. 19 Inhibition of ROCK had no consequences on the subcellular localization of SYNPO2.	88

Fig. 20 Okadaic acid induced accumulation of SYNPO2 in the cytoplasm. _____	89
Fig. 21 Expression analysis of 14-3-3 isoforms in primary rat VSMCs. _____	90
Fig. 22 Schematic illustration of constructs used for SYNPO2, 14-3-3 $\gamma/\beta$ & importin $\alpha$ interaction and localization analysis by BIFC and a FACS-BIFC based assays. _____	91
Fig. 23 Expression analysis of fluorescent fused proteins. _____	92
Fig. 24 Subcellular distribution of fluorescent fusion proteins in living cells detected by confocal laser scanning microscopy. _____	94
Fig. 25 Interaction between SYNPO2 and 14-3-3 $\gamma$ takes place in the cytoplasm of HEK293 cells. _____	96
Fig. 26 SYNPO2 and 14-3-3 $\beta$ localized and formed a loop structure in the nucleus. _____	97
Fig. 27 Imaging of SYNPO2, importin $\alpha$ interaction using BIFC assay. _____	98
Fig. 28 Imaging of self-association of SYNPO2 to form homo-dimers in living cells. _____	99
Fig. 29 Schematic illustration of actin cytoskeleton dynamics depending on Rho-Rock signaling pathway (modified from Alan Hall, science, 1998). _____	104
Fig. 30 Schematic illustration of PKA (R= regulatory domain, C= catalytic domain) and CaMKII-depending phosphorylation of SYNPO2 used in this work (modified from Faul et al. 2007). _____	109
Fig. 31 Schematic illustration of nuclear-cytoplasmic trafficking of SYNPO2 (According to Faul et al. 2005). _____	114

## II. List of Tables

Table 1 All chemicals used in this work.....	34
Table 2 List of Kits and Materials .....	37
Table 3 All buffers and solutions used in this PhD work.....	38
Table 4 Bacterial and mammalian media.....	40
Table 5 List of used instruments during this work.....	40
Table 6 List of used bacterial for cloning and sub-cloning process. ....	42
Table 7 List of vectors and plasmids used in this work.....	42
Table 8 List of primers used in this work.....	43
Table 9 List of used antibodies in this work.....	47
Table 10 General PCR Mixture used in this work.....	50
Table 11 PCR Programs used in this work.....	51
Table 12 Concentration of TAE agarose for DNA purification .....	51
Table 13 Digestion mixture and using times.....	52
Table 14 Used ligation reaction mixture in this work.....	53
Table 15 Colony PCR reaction mixture.....	54
Table 16 General Real-Time PCR Mixture used in This Work .....	56
Table 17 Real-Time PCR Program used in This Work.....	56
Table 18 Incubation times and treatment conditions used for this study.....	59
Table 19 Used combinations of BIFC-constructs in this work.....	68
Table 20 Alteration of the marker proteins expression level in the smooth muscle cells during phenotype switch and/or diseases.....	100

### III. Abbreviations

<b><math>\alpha</math>SMA</b>	Smooth muscle $\alpha$ -actin
<b><math>\Delta</math>C-YFP</b>	Yellow Fluorescent Protein aa 1-158
<b><math>\Delta</math>N-YFP</b>	Yellow Fluorescent Protein aa 159-238
<b><math>\mu</math>l</b>	Microliter
<b>ABPs</b>	Actin binding proteins
<b>ADP</b>	Adenosine diphosphate
<b>APS</b>	Ammonium persulfate
<b>Arp2/3 Complex</b>	Actin-Related Proteins ARP2 and ARP3
<b>ATP</b>	Adenosine triphosphate
<b>BIFC</b>	Bimolecular fluorescence complementation
<b>BLAST</b>	Basic Local Alignment Search Tool
<b>BSA</b>	Bovine serum albumin
<b>CalP</b>	Calponin
<b>CaMKII</b>	Ca <sup>2+</sup> -Calmodulin dependent kinase II
<b>Cc</b>	Critical concentration
<b>CCD</b>	Cytochalasin D
<b>CD90</b>	Cluster differentiation 90, Thy-1
<b>cDNA</b>	Complementary DNA
<b>CFP</b>	Cyan fluorescent protein
<b>CHAP</b>	Cytoskeletal heart-enriched actin-associated protein
<b>dNTP</b>	Deoxyribonucleotide triphosphate
<b>DTT</b>	Dithiothreitol
<b>EDTA</b>	Ethylenediaminetetraacetic acid
<b>EtBr</b>	Ethidium bromide
<b>FACS</b>	Fluorescence Activated Cell Sorting Assay
<b>FBS</b>	Fetal bovine serum
<b>FRET</b>	Förster resonance energy transfer
<b>GFP</b>	Green fluorescent protein
<b>HBSS</b>	HEPES-buffered saline solution
<b>hCaD</b>	High Caldesmon
<b>HEK</b>	Human embryonic kidney
<b>IF</b>	Immunofluorescence
<b>IPTG</b>	Isopropyl-thio- $\beta$ -d-galactoside
<b>JASP</b>	jasplakinolide
<b>kb</b>	Kilo base
<b>kDa</b>	kilodalton
<b>LB</b>	Lysogeny broth
<b>lCaD</b>	Low Caldesmon
<b>MLC20</b>	Myosin light chain 20
<b>MLCK</b>	Myosin light chain kinase
<b>MLCP</b>	Myosin light chain phosphatase
<b>ml</b>	Milliliter

<b>mRNA</b>	Messenger RNA
<b>NEB</b>	New England Biolabs
<b>PAGE</b>	Polyacrylamide gel electrophoresis
<b>PBS</b>	Phosphate-buffered saline
<b>PCR</b>	Polymerase chain reaction
<b>PFA</b>	Paraformaldehyde
<b>PIC</b>	Protease inhibitor cocktail
<b>PMSF</b>	Phenylmethylsulfonyl fluoride
<b>PP1</b>	Protein phosphatase 1
<b>PP2A</b>	Protein phosphatase 2A
<b>RNA</b>	Ribonucleic acid
<b>ROCK</b>	Rho-associated protein kinase
<b>RT</b>	Room temperature
<b>SDS</b>	Sodium dodecyl sulfate
<b>SEM</b>	Standard error of the mean
<b>SMC</b>	Smooth muscle Cell
<b>smMHC</b>	Smooth muscle myosin heavy chain
<b>Smtn</b>	Smoothelin
<b>SYNPO</b>	Synaptopodin
<b>SYNPO2</b>	Synaptopodin 2
<b>SYNPO2L</b>	Synaptopodin 2-like
<b>TAE</b>	Tris-acetate-EDTA
<b>TBS</b>	Tris-buffered saline
<b>TEMED</b>	N,N,N',N'-tetramethylethylenediamine
<b>Tm</b>	Melting temperature
<b>Tris</b>	Tris (hydroxymethyl) aminomethane
<b>UV</b>	Ultraviolet
<b>V</b>	Volts
<b>VSMCs</b>	Vascular Smooth Muscle Cells
<b>Vim</b>	Vimentin
<b>WB</b>	Western blot
<b>WT</b>	Wild-type

#### IV. Zusammenfassung

In eukaryotischen Zellen stellt Aktin das Protein mit der höchsten Abundanz dar, besitzt diverse Funktionen und ist Hauptbestandteil des Zytoskeletts. Daher spielt Aktin eine wichtige Rolle für die Entstehung und Erhaltung der Zell Form, der Zellmotilität, der Zelladhäsion, der Muskelkontraktion und der Zytokinese. Die Struktur des Aktinnetzwerks und seine zellulären Funktionen werden von Proteinen reguliert, welche allgemein als Aktin bindende Proteine (ABP) bekannt sind.

Gegenstand dieser Arbeit war die Analyse eines neuen ABPs Synaptopodin 2 (SYNPO2) und seine Relevanz für die Phänotyp Modulation in vaskulären Glattmuskelzellen (vascular smooth muscle cell; VSMC). SYNPO2 ist maßgeblich an der Regulation von Aktin Nukleation und dem Umbau des Aktin Zytoskeletts beteiligt. SYNPO2 ist ein Dual-Kompartiment Protein, welches seine subzelluläre Lokalisation zwischen dem Nukleus und dem Zytoplasma in Herz- und Skelettmuskelzellen ändert. Dieser Prozess geschieht in Abhängigkeit einer cyclischen Adenosinmonophosphats (cAMP)-abhängigen Phosphorylierung des SYNPO2 durch Protein kinase A (PKA) und Calcium/calmodulin-dependent protein kinase II (CaMKII). Die unterschiedliche SYNPO2 Lokalisation spielt in vielen Prozessen, wie der Zelldifferenzierung, der Antwort auf Hitzeschock und unter pathophysiologischen Bedingungen, wie z. B. Blasen- und Prostatakrebs eine bedeutende Rolle. SYNPO2 wird abundant in VSMCs exprimiert, wobei seine Rolle in diesen Zellen jedoch bis jetzt unbekannt ist.

In der vorliegenden Arbeit zeigen wir, dass der cAMP-abhängige PKA Signalweg am Pendeln von endogenem SYNPO2 zwischen Zellkern und Zytoplasma in beiden Richtungen beteiligt ist. Wie bereits beschrieben, konnten in Folge von erhöhtem cAMP eine Akkumulation von SYNPO2 im Zellkern detektieren werden. Des Weiteren legen wir dar, dass die Inhibierung der Protein Phosphatase 1 (PP1), der Protein Phosphatase 2A (PP2A) und/oder der Inhibierung von Phosphodiesterasen (PDEs) einen Einfluss auf die Anreicherung von SYNPO2 im Zellkern hat. Im Gegensatz zu Weins et al. 2001, die eine nukleäre Lokalisation von SYNPO2 in Folge eines Hitzeschocks zeigten, konnten wir nach einem Hitzeschock keine Veränderung in der Lokalisation des endogenen SYNPO2

feststellen. Zudem verursacht die Phänotypänderung der VSMCs nicht nur eine subzelluläre Lokalisationsänderung des endogenen SYNPO2, sondern beeinflusst auch dessen Expressionsrate. Kontraktile VSMCs (Tag 1) weisen eine starke Akkumulation von SYNPO2 im Zytoplasma auf, während nicht kontraktile (proliferative) VSMCs aus Passage 3 eine starke Reduktion von zytoplasmatischem SYNPO2 und einen Anstieg von nukleärem SYNPO2 aufweisen. Wir konnten feststellen, dass die Aussaat von VSMCs (Passage 3) auf einer lamininbeschichteten Matrix zu einer Umkehrung des Phänotyps von nicht-kontraktile zu kontraktile und somit zu einer Akkumulation von SYNPO2 im Zytoplasma führt. Im Vergleich dazu, verbleiben VSMCs nach Aussaat auf Collagen I Beschichtung, im nicht-kontraktilen Zustand und weisen eine Akkumulation von SYNPO2 im Nukleus auf. Interessanterweise wurde darüber hinaus eine Hochregulation von SYNPO2 im kontraktilen Phänotyp bei frisch isolierten VSMCs (Tag 1), als auch bei VSMCs, die auf Laminin kultiviert wurden, nachgewiesen. Um die subzelluläre Lokalisation von SYNPO2 und dessen Interaktion mit potentiellen Bindungspartnern zu analysieren wurde ein bimolekularer fluoreszenzkomplementations (bimolecular fluorescence complementation; BIFC) Ansatz etabliert. Es konnte eine Interaktion zwischen SYNPO2, 14-3-3 $\beta$  und Importin $\alpha$  im Nukleus beobachtet werden, während SYNPO2 mit 14-3-3 $\beta$  ausschließlich im Zytoplasma interagiert. Diese Interaktion von SYNPO2 mit 14-3-3 $\beta$  wurde in Form von ‚nuclear bodies‘-ähnlichen Strukturen, welche nicht für den SYNPO2-Importin $\alpha$  Komplex festgestellt werden konnte. Interessanterweise, formen beide Komplexe SYNPO2-14-3-3 $\beta$  und SYNPO2-Importin $\alpha$  ringförmige Strukturen. Zuletzt konnten wir zeigen, dass SYNPO2 Homodimere bildet, die hauptsächlich im Zytoplasma vorkommen.

Zusammenfassend ist zu sagen, dass das neue Aktin bindende Protein SYNPO2 eine potentiell wichtige Rolle in mindestens drei Prozessen spielt, die mit einer Phänotypänderung einhergehen. Zum Ersten, während der Zelldifferenzierung und der vaskulären Entwicklung, des Weiteren für die Reparatur nach Gefäßverletzung und zuletzt unter pathologischen Umständen wie Arteriosklerose oder Krebs. Abschließend können wir sagen, dass SYNPO2, durch Aktin selbst und durch das Aktinnetzwerk vermittelte

Transkription, einen wesentlichen Teil zu der frühen und späten Differenzierung von VSMCs beiträgt.

**Abstract**

In eukaryotic cells actin is the most abundant protein, forming different cytoskeletal structures and having different functions. Thus, actin plays a crucial role in processes such as the establishment of cellular shape, cell motility, cell adhesion, muscle contraction and cytokinesis. The structures of actin networks and their cellular functions are regulated by other proteins, generally known as actin binding proteins (ABPs).

Subject of this work was the investigation of the novel ABP synaptopodin 2 (SYNPO2) and its relevance in vascular smooth muscle cell phenotype modulation. SYNPO2 is involved in the regulation of actin nucleation and remodeling of actin cytoskeleton. SYNPO2 is a dual compartment protein that alters its subcellular localization or shuttles between the cell nucleus and cytoplasm in cardiac and skeletal muscle cells depending on cAMP dependent kinases like protein kinase A (PKA), and calcium/Calmodulin- dependent kinase II (CaMKII). SYNPO2 shuttling occurs in several processes like differentiation, heat shock response, as well as under pathophysiological conditions, such as bladder and prostate cancer. SYNPO2 is abundantly expressed in VSMCs, whereas its functional role in these cells remains elusive.

Our results demonstrate that the cAMP-mediated PKA pathway is involved in the shuttling of endogenous SYNPO2 between the cell nucleus and the cytoplasm in both directions. As described before, we detected that increased cAMP causes nuclear accumulation of SYNPO2 in VSMCs. Additionally, we show that inhibition of phosphatases like protein phosphatases 1 and 2A (PP1 and PP2A) and/or inhibition of phosphodiesterases (PDEs) affected the accumulation of SYNPO2 in the cytoplasm. Contrary to Weins et al. 2001, reporting a nuclear localization of GFP-myopodin upon heat shock, we did not detect any changes in the localization of endogenous SYNPO2 due to heat shock. Furthermore, the phenotype switch of VSMCs not only causes an alteration of subcellular localization of endogenous SYNPO2 but it also affects its expression level. Contractile VSMCs (day one) showed a strong accumulation of SYNPO2 in the cytoplasm, while non-contractile (proliferative) VSMCs from passage 3 displayed a strong reduction of cytoplasmic SYNPO2 and an increase in the number of cells with nuclear-localized SYNPO2. We observed that plating of VSMCs (passage 3) on laminin-

coated matrices led to a back-switch from a synthetic phenotype to a contractile phenotype, which subsequently induces an accumulation of SYNPO2 in the cytoplasm. In contrast VSMCs plated on collagen I remain non-contractile, displaying nuclear accumulation of SYNPO2. Interestingly, we found an upregulation of SYNPO2 in the contractile phenotype of fresh isolated VSMCs (day one), as well as VSMCs (passage 3) grown on laminin. A new bimolecular fluorescence complementation (BIFC) based assay was established in order to analyze the subcellular localization and the interaction of SYNPO2 with its binding partners. An interaction between the SYNPO2, 14-3-3 $\beta$ , and importin $\alpha$  was detected in the nucleus, while SYNPO2 interacts with 14-3-3 $\gamma$  exclusively in the cytoplasm. The nuclear interaction of SYNPO2 with 14-3-3 $\beta$  was detected in form of nuclear bodies-like structures, which were not observed for the SYNPO2-importin $\alpha$  complexes. Interestingly, both SYNPO2-14-3-3 $\beta$  and SYNPO2-importin $\alpha$  complexes formed a loop-like structure. Finally, we show a self-association of SYNPO2 in the form homo-dimers mainly in the cytoplasm.

Taken together, our findings indicate that the novel actin binding protein SYNPO2 plays a potential role in at least three different processes in which phenotype switch is essential, like during cell differentiation and vascular development, after vascular injury (vascular repair) and under pathological conditions like atherosclerosis, cancer. In summary, we may conclude that SYNPO2 is essential for early and late differentiation of VSMCs via mechanisms involving actin and actin-mediated transcription networks.

# 1 Introduction

## 1.1 Muscle

There are three types of muscle tissues in human and other vertebrates: skeletal, cardiac and smooth muscle. Skeletal muscles are the most abundant muscles in the body, which control and regulate positioning, and moving the skeleton, while cardiac muscle is only present in the heart and is responsible for blood streaming in the vascular system. Smooth muscles are found in various internal organs like stomach, urethra, and blood vessels.

### 1.1.1 Vascular smooth muscle

By using light microscopy, we are able to see differences between smooth muscle cells (SMCs) and skeletal muscles. In skeletal muscle, the arrangement of actin and myosin filaments cause a myofibrillar striated structure while in smooth muscle cells appear homogeneous. This difference can be explained by morphological differences of the individual muscle fibers between the skeletal muscle and SMCs. In the muscle fibers of skeletal muscle, the contractile elements like myofibrils are arranged in parallel, which showing a longitudinal view of bundles. However, in smooth muscle, the myofilaments form a cross-linked structure within the cells. Furthermore, SMCs contain actin as much as skeletal muscle cells per unit of cell volume, but five times less myosin<sup>1-3</sup>. The SMCs are spindle-shaped with a factor of 20 smaller than skeletal muscle cells (Fig. 1).

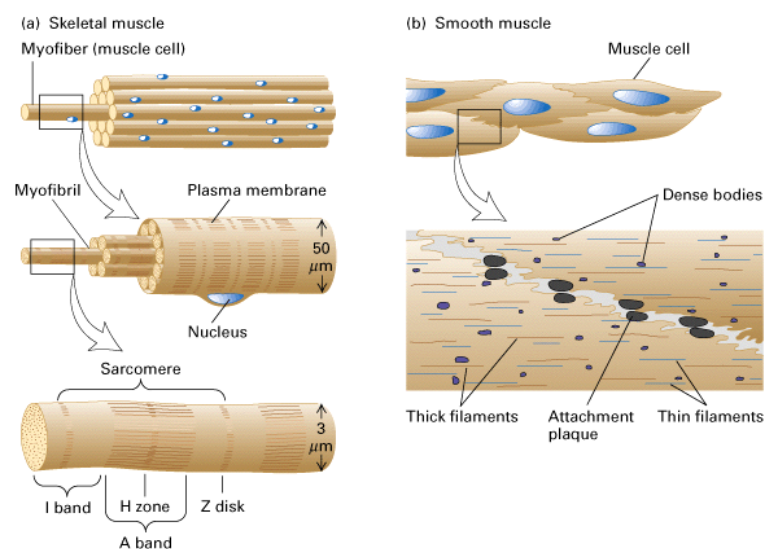


Fig. 1 Schematic illustration of (A) skeletal and (B) smooth muscles (according to Lodish 4th Ed).

The single nucleus of SMCs is centrally located in the cell, while in the multinucleated skeletal muscle cells, the nucleus are located directly at the periphery of the cell (Fig. 1).

In smooth muscle, the actin filaments are anchored to the cell membrane by the dense plaques and intracellular to the dense bodies via an actin binding protein known as  $\alpha$ -actinin. Dense plaques and dense bodies contain  $\alpha$ -actinin and vinculin, and they are therefore considered to be equivalent to the Z-discs of skeletal muscle. Based on the size of the protein structures, three types of filaments can be distinguished in the smooth muscles as follows: (A) The thin filaments having a diameter of  $\varnothing$  5-8 nm consist mainly of filamentous actin, tropomyosin and actin-binding proteins, for example, caldesmon. These thin filaments form together with (B) the thick myosin filaments ( $\varnothing$  16 nm) the contractile apparatus of SMCs. Furthermore, actin filaments are connected with (C) intermediate filaments ( $\varnothing$  10 nm) by adapter proteins. Intermediate filaments are a part of the cytoskeleton, which are not involved in the contraction of muscles, but have structural functions. Desmin and vimentin are two abundant intermediate filaments proteins in smooth muscle<sup>4</sup>.

SMCs can be functionally divided into two types, which in turn can perform different functions.

- ✚ The "multi-unit" type, which is usually stimulated vegetatively, and this type is without spontaneous activity. They mainly occur in blood vessels with a larger diameter and the bronchi.
- ✚ The "single-unit" type is of the hollow organs of the gastrointestinal tract (GI track), in which the SMCs are connected via gap junctions. They can almost simultaneously contract together and demonstrate a rhythmic activity of spontaneously active pacemaker cells.

Smooth muscles can be further distinguished in phasic and tonic contractile smooth muscle. Phasic contraction underlies the rhythmic contractions of for instance, the intestine, the portal vein and the ureter. Tonic contractions occur in most blood vessels, the trachea, and in the sphincters of the gastrointestinal tract<sup>5</sup>. The vascular smooth muscle cells are a main component of the vascular system like blood vessels, which regulate vessel tone, blood pressure and distribution of blood flow in the vascular system

like arteries, veins and capillaries<sup>6, 7</sup>. The vascular smooth muscle cells control and/or regulate blood stream through the vessels by contraction and relaxation, and therefore changes in the vessel volume<sup>8, 9</sup>. In the mature vessels, smooth muscle cells are mainly in the contractile state (also known as differentiated) and have an extremely low non-contractile phenotype<sup>8, 10</sup>. However, unlike skeletal muscle and cardiac cells, SMCs retain remarkable plasticity and can therefore change their phenotype during different pathophysiological conditions<sup>6, 10-13</sup>.

### 1.1.2 Molecular basis of contraction and relaxation

To analyze and to comprehend the function of smooth muscle cells in normal physiological conditions and in diseases, it is not easy without a complex study about cellular events, extracellular matrix components and their interactions together and with membrane components. The general principle of contractility of SMCs is the same as that described for skeletal muscle depends on ATP/ADP exchanges. Each myosin protein head possesses ATPase activity and controls its binding to actin in a cyclical manner that couples ATP binding and its hydrolysis into ADP and inorganic phosphate (Pi) to a conformational change in the myosin head<sup>14, 15</sup>.

In absence of ATP, the head of the heavy chains of myosin binds tightly to actin. Briefly, after binding of ATP, the myosin head can detach from the actin whereas the ATP is hydrolytically cleaved into ADP and Pi. The cleavage products initially remain on myosin, while myosin is weakly bound to actin. Only the sequential release of Pi and ADP leads to the formation of strongly bound myosin to actin, force-generating cross-bridges, conformational changes in the area of myosin heads and therefore the so-called "Power stroke", which finally causes the shortening of sarcomeres and thus the whole muscle<sup>14, 15</sup>.

Fig. 2 illustrates a general signaling that regulates the smooth muscle contractile machinery depending on both  $\text{Ca}^{2+}$  and GTPase protein signaling<sup>16</sup>. Regulation of smooth muscle cell tone is mainly depends on calcium concentration and  $\text{Ca}^{2+}$  sensitization and desensitization, which in turn are regulated by various agonists bind to the specific receptors and in the subsequent activation of the SMCs contraction mechanism<sup>17, 18</sup>. An

increase in the intracellular  $\text{Ca}^{2+}$  concentration, in response to a wide spectrum of extracellular signals, activates  $\text{Ca}^{2+}$ -Calmodulin dependent myosin light chain kinase (MLCK), and subsequent phosphorylation of the regulatory light chain of myosin ( $\text{MLC}_{20}$ ) at serine 19, which is the main regulatory mechanism in activating smooth muscle cell contraction<sup>18-20</sup>. In contrast to contraction, relaxation is initiated by dephosphorylation of  $\text{MLC}_{20}$  by myosin light chain phosphatases (MLCP). MLCP belongs to the family of hydrolases and is a heterotrimer of three subunits: a PP1c catalytic subunit, a 20-kDa subunit of unknown function, and a regulatory subunit, myosin phosphatase type 1 (MYPT1), which targets MLCP to myosin<sup>18</sup> (Fig. 2).

In addition, G proteins increase  $\text{Ca}^{2+}$  sensitivity and therefore contractility in the smooth muscle cells due to the inhibition of MLCP<sup>21-23</sup>. Further studies demonstrated that this inhibition is controlled by the phosphorylation state of MYPT1<sup>24, 25</sup>. Moreover, several groups reported that GTPase-induced  $\text{Ca}^{2+}$ -sensitivity and therefore contractility of SMCs is based on the activation of Rho and Rho-associated protein kinase (ROCK) signaling pathways, in which ROCK inhibits MLCP by phosphorylation<sup>26-31</sup>.

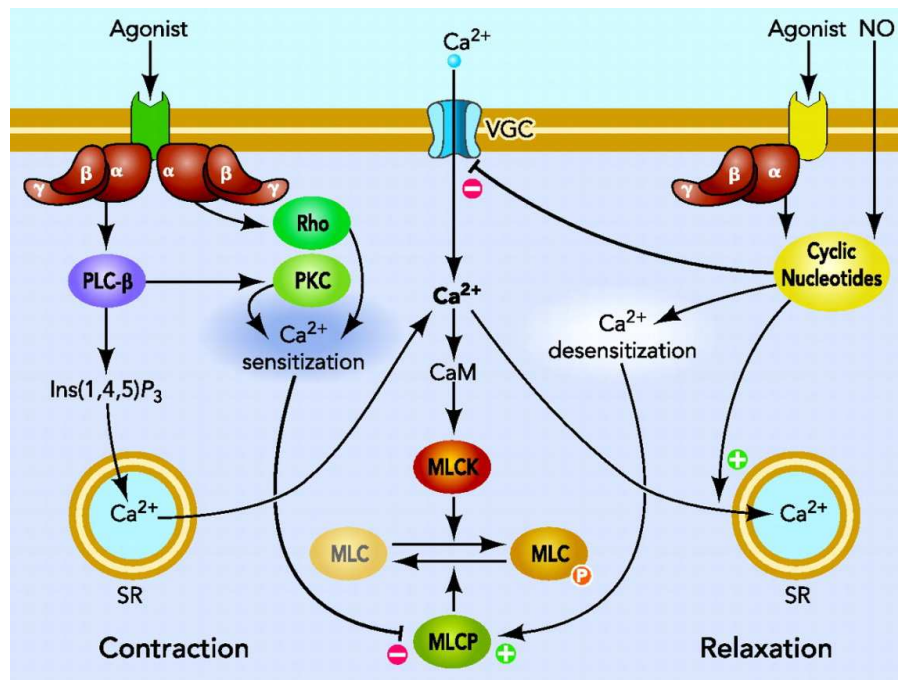


Fig. 2 Schematic illustration of the signals that regulate and control the smooth muscle cell contraction and relaxation (according to Puetz et al 2009)<sup>16</sup>.

### 1.1.3 Smooth muscle cells phenotype plasticity and disease

SMCs in the vascular system and other systems in adult animals are differentiated cells, whose principal function are the contraction and regulation of blood vessel tone, blood pressure, and blood flow<sup>7, 8, 10, 32</sup>. Notably, unlike other cells that are terminally differentiated, smooth muscle cells retain their ability to change their phenotype from a contractile to a non-contractile phenotype (synthetic phenotype) and vice versa according to the physiological and pathophysiological conditions<sup>10, 11, 13, 33</sup>. The phenotype plasticity of SMCs (also known as phenotype modulation) plays a crucial role during vascular development, regulation of the vascular system (vascular remodeling) during blood flow, blood pressure, and also during diseases such as injuries, atherosclerosis, cancer, and diabetes<sup>10-12, 34-39</sup>. SMCs in a differentiated state express a variety of contractile proteins and contractile-associated marker proteins that regulate and control the correct function of these cells. In other words, in mature vessels contractile or differentiated SMCs are characterized by the expression of marker proteins such as smooth muscle  $\alpha$ -actin ( $\alpha$ SMA), smooth muscle myosin heavy chain (smMHC), calponin, h-caldesmon, SM22<sup>40, 41</sup>, and smoothelin<sup>42-44</sup>. Consequently, many studies have also shown that up and/or down regulation of these proteins are correlated by phenotype modulation of VSMCs and diseases<sup>45-47</sup>. For instance, upon injury, VSMCs dedifferentiate into non-contractile smooth muscle cells, with an increased rate of proliferation, migration and also synthesis of extra cellular matrix components<sup>13, 48</sup>, while at the same time VSMCs showed a reduction in expression levels of marker proteins<sup>12, 41</sup>.

Many groups reported specific factors and regulatory pathways, which directly or indirectly promote and control SMCs phenotype modulation during cellular processes and diseases<sup>8, 10, 11, 32</sup>. Tacking together, these results suggested that the phenotype modulation plays a crucial role in vascular development<sup>10, 49</sup> and repair of vascular diseases like injury<sup>36, 37</sup>. Furthermore, the model that has evolved in the last years for the regulation and controlling of VSMCs phenotype modulation is extremely complex. It depends on environmental cues, signaling pathways that control expression of genes characteristic for VSMCs. Therefore, we are just beginning to understand some of the

molecular mechanisms that control phenotype modulation of VSMCs during pathophysiological conditions.

#### **1.1.4 Actin cytoskeleton**

##### **1.1.4.1 Actin and actin filaments**

Actin is the most abundant protein in eukaryotic cells (up to 20% of the total protein)<sup>50, 51</sup>. It is a highly conserved protein family with six different actin proteins that is divided into three isoforms: 3  $\alpha$ -, 1  $\beta$ -, 2  $\gamma$ , which are tissue specific<sup>52</sup>. Alpha actins are found in muscle ( $\alpha$ -skeletal,  $\alpha$ -aortic smooth,  $\alpha$ -cardiac), and  $\gamma$ 2-enteric smooth, whereas  $\beta$  and  $\gamma$  isoforms are dominant in non-muscle cells. Smooth muscle  $\alpha$ -actin is mainly expressed in vascular smooth muscle<sup>53</sup>, whereas in visceral smooth muscle, a high proportion of  $\gamma$ -actin is found. The  $\beta$ -isoform of actin is expressed in all smooth muscle tissues and appears to be a component of the cytoskeleton<sup>54</sup>. Actin, as a major component in cytoskeleton, is the best investigated protein in motility systems, and regulation of mechanical and biomechanical signals through the cells. However, its exact functions in different pathophysiological conditions, development, aging and diseases are not completely understood. Actin exists in two forms, monomeric, G-actin with a molecular mass of 42 kDa and filamentous, F-actin.

Actin, as an involved protein in the cell movements, controls contraction/relaxation mechanism by two actions: A) actin polymerization and depolymerization and B) interaction with motor proteins like myosin family. The average length of actin filaments in the contractile state of VSMCs is about 4.5  $\mu\text{m}$ , whereas myosin filament length is only 1.6  $\mu\text{m}$ <sup>1, 54, 55</sup>. Actin filaments, Actin binding proteins (ABPs), myosin and other proteins that interact with the actin cytoskeleton, make stress fibers in the cells<sup>50, 56, 57</sup>, which are dominant in cell culture conditions<sup>57</sup>. The actin cytoskeleton contains two types of filaments, cross-linked filaments and cortical actin filaments<sup>50</sup>. Cross-linked filaments control cytoskeletal deformation, transmit forces and stabilize subcellular localization of cellular organelles, while cortical filaments stabilize the form of cells during different physiological conditions, cellular development and inhibit lateral movement of organelles in the cells<sup>50, 56</sup>.

Actin filaments extend when ATP-G-actin monomers bind to the barbed end, while actin filaments disassemble when ADP-G-actin monomers lose from the pointed end<sup>58-60</sup> (Fig. 3). Actin filaments are highly dynamic and their elongation involves both polymerization and depolymerization<sup>61-63</sup>. The polymerization of actin filaments occurs in three sequential steps: (A) nucleation step, (B) elongation step, and (C) steady state step<sup>61, 64</sup>. The first step (A) initiates with the formation of a trimer of G-actin monomers that is also known as a polymerization nucleus, which in the second step (B) will be used to elongate a filament by the addition of actin monomers to both of its ends. Finally, as actin filaments grow, (C) the concentration of G-actin monomers decreases until it reaches a steady state with the F-actin filaments (critical concentration) that are important to control assembly and disassembly of actin monomers<sup>56, 64, 65</sup>. With this notion that both the formation of a stable actin trimer as the initial point for polymerization and elongation are dependent on the critical concentration of monomers, dynamics of this concentration play a major role in assembly and disassembly processes. Actin nucleation and  $C_c$  therefore require additional proteins known as 'actin binding proteins' that control and/or regulate the formation of a stable actin nucleus and  $C_c$  in the cells. Beside actin, actin binding proteins are the other abundant protein super family, which account for 10% of total cellular protein<sup>56</sup>. For instance, the Arp2/3 complex<sup>66</sup>, formins<sup>67, 68</sup>, and synaptopodin 2 (SYNPO2) as a novel actin protein regulate nucleation of actin and ADF/cofilin<sup>69, 70</sup> disassembles actin filaments. While the function of actin nucleators such as the Arp2/3 complex<sup>65, 71</sup>, and formins has been extensively studied in cells, the role of SYNPO2 is not completely clear. The detailed biochemistry and function of the synaptopodin family on the actin dynamics is under investigation. Further detail about the synaptopodin family is discussed in the next section.

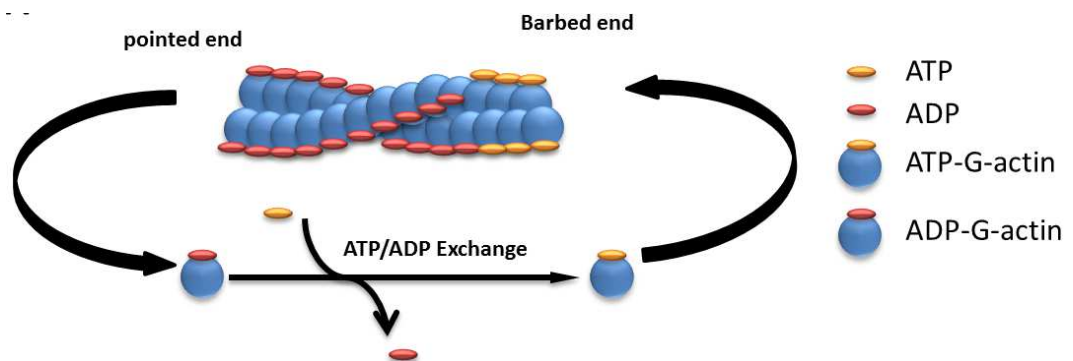


Fig. 3 Schematic illustration of actin polymerization/depolymerization. ADP binds with  $\sim 10$ -fold lower affinity to the nucleotide binding site of Mg-G-actin and  $\sim 200$ -fold weaker to the Ca-G-actin monomers as compared to the ATP and ADP-P<sub>i</sub>, which is crucial for actin polymerization and depolymerization<sup>60</sup>.

## 1.2 Synaptopodin family

As described above, the functions of actin and the actin cytoskeleton are regulated or/and controlled during a variety of cellular processes which are involved in different pathophysiological conditions by ABPs<sup>50, 56, 72</sup>. The synaptopodin family comprises a conserved family of proteins that fall into three different members; Synaptopodin, Synaptopodin 2 (SYNPO2), and Synaptopodin 2 like proteins (SYNPO2L), which are also divided by different splicing in various isoforms<sup>73</sup>. The main feature of the synaptopodin family seems to be the natively unfolded form of these proteins, which is supposed to be necessary for their potential functions in the cells. Accordingly, the synaptopodin family may have different binding partners<sup>73</sup>. Although different genes, located on different chromosomes, express synaptopodin proteins they show a high similarity<sup>73</sup>. The intrinsically unfolded structure of the synaptopodin family members depends on position and/or the high proline content.

Since their discovery, the synaptopodin family members have been studied in different cell types. The synaptopodin family members play various roles in spine motility<sup>74</sup>, actin organization<sup>75, 76</sup>, cell differentiation<sup>77</sup>, cancer<sup>78-80</sup>, and heart development and somitogenesis<sup>81, 82</sup>. The detailed biochemistry and function of synaptopodin family is discussed in the following sections.

### 1.2.1 Synaptopodin

Synaptopodin (SYNPO) as the first member of the synaptopodin family was reported by Mundel et al. in 1997 as a novel actin binding protein which expresses in both differentiated kidney podocytes, associated with the actin cytoskeleton of postsynaptic densities, and in telencephalic synapses of the brain, associated with dendritic spines<sup>74, 83</sup>. Synaptopodin is expressed by the gene SYNPO, located on chromosome 5 (human). Synaptopodin binds either directly to F-actin and  $\alpha$ -actinin on several independent binding sites<sup>84</sup> or indirectly to F-actin via binding to  $\alpha$ -actinin<sup>85</sup>. At this time, the published human protein sequence included a 685-aa polypeptide with a calculated molecular mass of 73.7 kDa and an isoelectric point of 9.38. The appropriate murine homolog showed a 690-aa protein with a calculated molecular mass of 74.0 kDa and an isoelectric point of 9.27. In SDS-PAGEs SYNPO2 migrated with an app. molecular mass of 100 kDa. A sequence analysis showed a 84% sequence similarity between the human and murine synaptopodin. Furthermore, 2005 the Mundel group reported<sup>85</sup>, that murine synaptopodin includes three splice variants that are tissue-specific, short-variant (685 amino acids) neuronal, long-variant (903 amino acids) and variant T (181 amino acids) renal. Functional analysis demonstrated that synaptopodin caused a connection between the actin cytoskeleton and spine apparatuses of telencephalic neurons<sup>86</sup>, which may suggest a crucial role for synaptopodin in case of regulation of long-term potentiation (LTP). Further analysis showed that the lack of synpatopodin in synpo-/- mice caused a complete lack of spine apparatuses and in turn a loss of LTP and learning impairments<sup>87</sup>.

### 1.2.2 Synaptopodin 2

The novel actin binding protein synaptopodin 2<sup>73, 75</sup> (known as myopodin<sup>77</sup> or fesselin<sup>88</sup>) regulates actin nucleation and polymerization in a  $\text{Ca}^{2+}$ -Calmodulin manner<sup>89-91</sup>. SYNPO2 is expressed by the gene SYNPO2, located on chromosome 4 (human). Sequence analysis of SYNPO2 demonstrated a 47% amino acid similarity to synaptopodin. De Gank reported in 2008 three different isoforms which seem to be a result of different splicing events<sup>79</sup>, however Chalovich and Schroeter reported in 2010, 5 isoforms of SYNPO2 (Fig. 4 ). SYNPO2 binds directly to F-actin and  $\alpha$ -actinin at several binding sites<sup>92, 93</sup>.

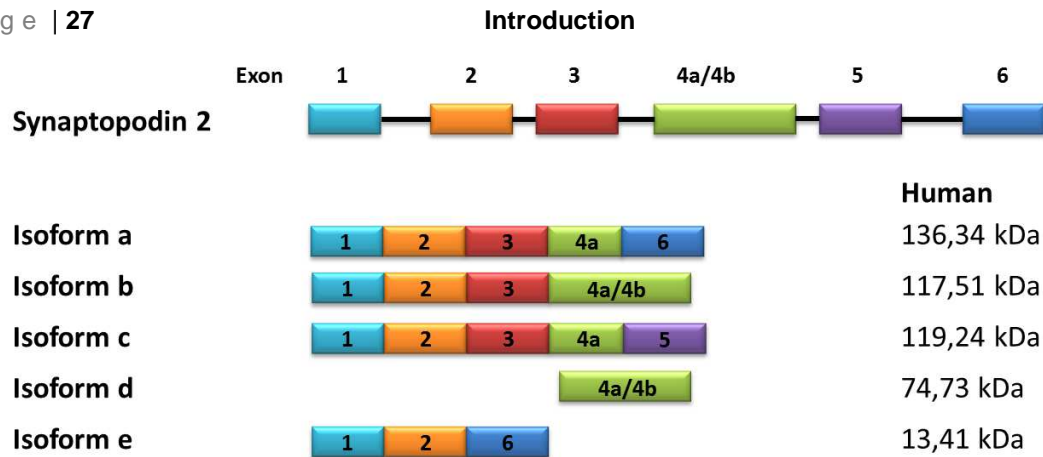


Fig. 4 Schematic illustration of synaptopodin 2 isoforms in human.

SYNPO2 is a tumor suppressor protein<sup>80, 94, 95</sup> and shuttles between the nucleus and the cytoplasm during differentiation and under stress such as heat shock<sup>77, 96</sup>. The suppressor activity of synaptopodin 2 on cell growth and cell motility seems to be dependent on phosphorylation and interaction of myopodin by/with integrin-linked kinases<sup>95</sup>. It has been shown that the differentiation of myoblasts to myotubes affects translocation of SYNPO2 from the nucleus to the cytoplasm<sup>77</sup>. In smooth muscle cells SYNPO2 is expressed in the cytoplasm where it is localized in dense bodies<sup>97</sup> (and Z-disc in striated muscle<sup>77, 93</sup>). Additionally it has been observed that SYNPO2 accumulated in the cell cytoplasm during tumor development and metastases<sup>79, 80, 94</sup>. Notably, loss of nuclear myopodin is connected to the clinical outcome<sup>94</sup>. However, its exact function is still unclear and under intensive investigation.

Detailed analyses of the biochemical and biophysical properties of SYNPO2 from turkey gizzards showed that it can control critical functions of actin, such as nucleation and elongation of monomeric G-actin as well as bundling and crosslinking of F-actin filaments<sup>73, 75, 90, 98</sup>. A further link to the actin cytoskeleton is established by the ability of SYNPO2 to bind to myosin<sup>76</sup>,  $\alpha$ -actinin<sup>93, 99</sup>, and filamin<sup>93</sup>. The binding to  $\alpha$ -actinin is important for the regulation of the transport of SYNPO2 to the nucleus, which was observed in C2C12 cells and cardiac myocytes<sup>93, 100</sup>. This shuttle has been observed after the application of heat shock<sup>77, 96</sup>, upon which murine SYNPO2 is phosphorylated by protein kinase A (PKA) and  $\text{Ca}^{2+}$ -calmodulin dependent kinase II (CaMK II)<sup>100</sup>. This posttranslational phosphorylation releases SYNPO2 from  $\alpha$ -actinin and induces the

binding of SYNPO2 to the 14-3-3 protein<sup>100-102</sup>. Binding of SYNPO2 to 14-3-3 requires the presence of two 14-3-3 binding motifs<sup>73, 100, 101</sup>. Afterwards the 14-3-3-SYNPO2-complex binds to the protein importin- $\alpha$ , and shuttles to the nucleus<sup>96, 100-102</sup>.

Interestingly, the human SYNPO2 provides only one 14-3-3 binding motif, the required second motif is missing. Therefore, the mechanism by which SYNPO2 is translocated to the nucleus of human cells is still unclear.

### 1.2.3 Synaptopodin 2-like

The synaptopodin 2-like protein also known as cytoskeletal heart-enriched actin-associated protein (CHAP) or tritopodin is the third member of the synaptopodin family<sup>81, 103</sup>. A gene (SYNPO2L) located on chromosome 10 in human expresses CHAP protein. CHAP is a new Z-disc protein that is expressed in differentiated heart, skeletal muscle during embryonic development<sup>81</sup> and in adult aorta, carotid and coronary arteries in vascular smooth muscle cells, but not during embryonic development<sup>82</sup>. This protein exhibits approximately 31% similarity to SYNPO2 and 30% to synaptopodin. This sequence similarity may suggest similar features for CHAPs<sup>81, 82</sup>. Beqqali reported two isoforms of murine CHAP (mCHAP) that are produced by alternative splicing. CHAPa resulted from exons 1, 2, 3, and 5 and has a molecular weight about 140 kDa, while CHAPb started with a start-codon in exon 4 and produced a protein with 110 kDa. A sequence analysis of both isoforms showed a classical NLS sequence (KKRR) for both CHAPa and CHAPb and a PDZ domain for CHAPa. However, this NLS was not crucial for nuclear import of mCHAP. A protein expression analysis of different isoforms showed that CHAPb was only expressed during early skeletal muscle and heart development, while the long isoform CHAPa was expressed around day E 17.5 and a high level of CHAPa protein was detected in adult heart and skeletal muscle, whereas CHAPb protein was undetectable. Immunofluorescence studies demonstrated a low nuclear localization and a strong colocalization of mCHAP proteins and  $\alpha$ -actinin within the Z-discs in the sarcomers of embryonic cardio myocytes. Although, CHAP contains a C-terminal actin-binding domain, it interacts with actin via binding to  $\alpha$ -actinin. Zebra fish studies using antisense morpholino oligonucleotides demonstrated a crucial role of CHAP during heart

development and somitogenesis. Downregulation of CHAP in zebra fish caused dysfunction of cardiac contractility, myofibrillar disarray, disruption of somite boundaries, sarcomeric integrity and notably muscle defects in case of the contraction.

### 1.3 Protein-Protein interaction

All cellular processes, including development, pathophysiological conditions and diseases are controlled by signaling pathways, which in turn are based on protein-protein interactions. Correct localization of proteins, protein-protein interactions and their dynamic at the plasma membrane and along the signaling cascade play important roles in cell signal transductions<sup>49, 104, 105</sup>. Although, many biochemical techniques like immunoprecipitation, pull-down assay, yeast two-hybrid and other *in vitro* assays elucidated many details about protein-protein interactions, the existence of protein complexes and their physiological roles in living cells is of greater interest, especially in cases of diseases and development studies<sup>106, 107</sup>. Despite the evidences and results from biochemical methods, there are many details about the exact roles and functions of proteins that remain unclear.

To investigate the existence of protein complexes and in turn also their physiological roles in cells, the methods often rely on Fluorescent tagged proteins and therefore conventional fluorescence imaging methods to detect the distribution and/or protein-protein interaction in a cellular context<sup>108-110</sup>. Due to their sensitivity and selectivity, fluorescence imaging techniques like fluorescence and confocal microscopy stand out among the other optical techniques used in characterization of structures, detection and quantification of processes like protein-protein interaction<sup>109-112</sup>. Notably, these techniques provide useful information on diversity of process and involved proteins that can be related to their physiological functions. Regarding to these evidences, Förster resonance energy transfer (FRET) and more recently bimolecular fluorescence complementation assay, BIFC, are two powerful assays that facilitate and realize live imaging of protein interactions in the cellular context. It has been recently reported that 14-3-3 proteins as chaperone-like adaptor proteins are able to bind a specific sequence of SYNPO2<sup>101</sup>, which in turn is crucial for the interaction of importin $\alpha$  with NLSs of SYNPO2

and its shuttling from the cell cytoplasm to the nucleus<sup>96, 101</sup>. This synergy strongly depends on the phosphorylation form of SYNPO2 as shown by *in vitro* experiments<sup>100</sup>. Nevertheless, this evidence waited for more physiological information about these proteins in the cellular context.

We will use specific techniques that should allow us to analyze the interaction between SYNPO2, 14-3-3 and importin $\alpha$  in a cellular context. In this way we will be able to increase our understanding of both the basic mechanisms of interaction between SYNPO2, 14-3-3 and importin $\alpha$  in cells and also how this interaction controls subcellular distribution of SYNPO2.

### 1.3.1 Förster resonance energy transfer

FRET is a commonly used method to investigate molecular dynamics in biochemistry<sup>113</sup>, protein-DNA interactions<sup>114</sup>, protein-protein interactions, and protein conformation changes<sup>115</sup> in both *in vitro* and *in vivo*<sup>116-118</sup>. It is describing an energy transfer between two fluorescent (fluorophores) that are tagged to proteins of interest. Notably, the introduction of fluorescent proteins like GFP and GFP variants revolutionized one more time the use of this method for protein-protein interaction studies and the study of protein conformational changes in cellular context<sup>116, 119</sup>. In principle, FRET occurs when emission and absorption spectra of two different chromophores, usually two green fluorescent protein variants, overlapped. However, this is only achieved if two chromophores fused to two different proteins or two different sites of one protein, which it becomes a distance range between 10-80 Å according to the conformational changes of protein or the interaction of two proteins (Fig. 5). Combination of fluorescent conjugated proteins and FRET assay offer a unique chance to visualize and to monitor a real-time protein-protein interaction, conformational changes, and localization studies of proteins in living cells<sup>117, 118, 120, 121</sup>.

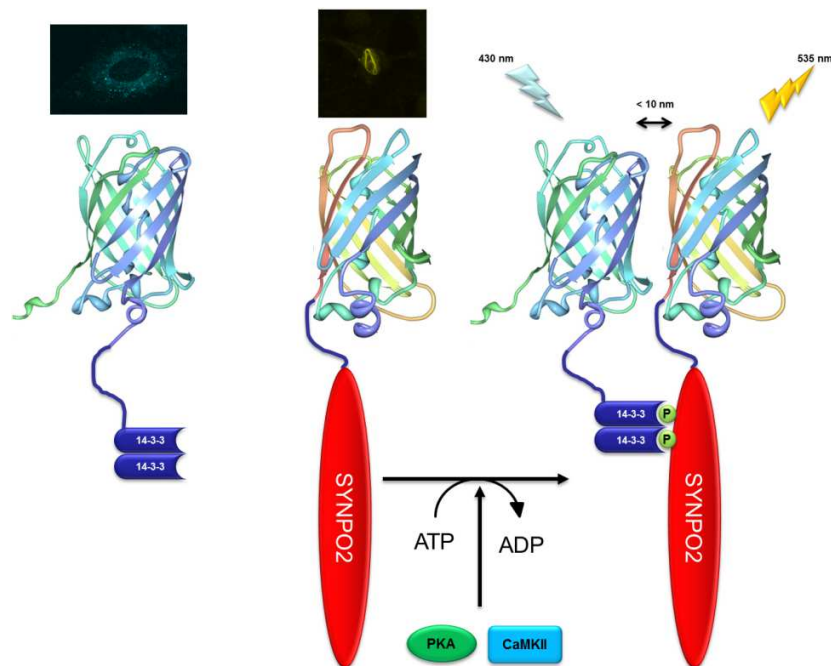


Fig. 5 Principle of FRET assay used in vivo. Two fluorescent fusion proteins were used to perform FRET measurements with CFP as a donor and YFP as an acceptor. FRET occurs as a non-radioactive energy transfer between two fluorophores, in which the excitation of the donor induces an energy transfer from the donor to the acceptor resulting in the reduction of the donor and an increase of acceptor fluorescence. The critical point is 10 nm distance.

### 1.3.2 Bimolecular fluorescence complementation (BIFC)

Although, FRET is a powerful method for colocalization and protein-protein interaction studies of the fluorescent conjugated proteins, its limitations include the crucial distance  $\sim 10\text{ nm}$ , and choice of the best sites for ligation of fluorescent proteins (chromophores) that may lead to false-positive or -negative, remains a significant challenge<sup>117, 122</sup>. For instance, false-negative can occur when the distance between two fluorescent labeled components in large protein complexes is too far. Therefore optimizing and characterizing the best FRET constructs can be time-consuming. The second technique, known as bimolecular fluorescence complementation (BIFC), is an alternative method that eliminates these limitations in case of distance and false negative<sup>123, 124</sup>. Notably, this method offers a simultaneous visualization of multiple protein interaction in living cells<sup>125, 126</sup>. It is based on fluorescence development, according to complementation of two non-fluorescent fragments when they associate together by the interaction between interested proteins fused to each fragment<sup>123, 127</sup>. Therefore, the reconstitution of the

fluorescent protein is activated by the direct interaction between the two target proteins. Since BIFC introduction, different BIFC-based assays have been developed and used in a cellular context. For instance, BIFC was used to visualize the molecular mechanism of protein-protein interaction in living cells<sup>128</sup>, protein dimerization/oligomerization, protein ternary complex formation<sup>129</sup>.

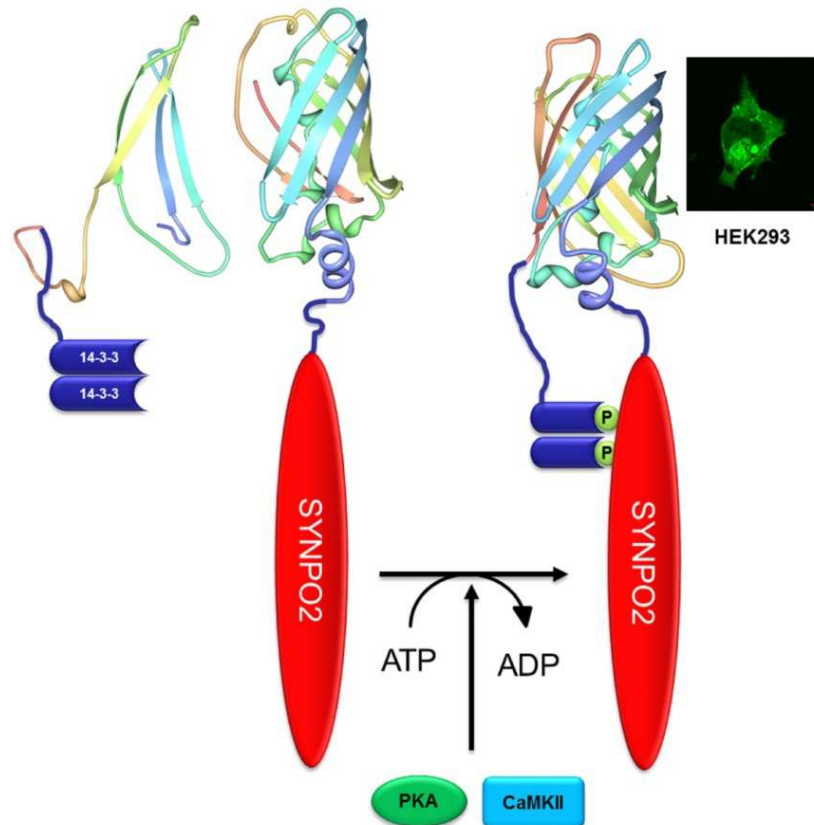


Fig. 6 Schematic illustration of the BIFC assay used in this work according to Hu, CD. et al. 2003<sup>130</sup>. BIFC fluorescence development is based on the interaction between protein A (14-3-3) and protein B (SYNPO2) in a cellular context.

#### 1.4 Aim of the project

Vascular smooth muscle cell (VSMC) modulation is essential during vascular development, contributes to the vascular lesion formation and plays an essential role in diseases such as atherosclerosis, post-angioplasty restenosis and also during vascular repair. The mechanisms regulating the modulation of this cell type are therefore of great interest. Several studies have shown that alterations in the function and/or expression level of contractile and cytoskeletal proteins are associated with VSMCs modulation. Moreover, several studies have revealed that actin is associated with phenotype modulation of VSMCs. The structures of actin networks and their cellular functions are regulated by other proteins, generally known as actin binding proteins (ABPs). One novel class of such proteins is synaptopodin 2 (SYNPO2), of which there are at least five isoforms.

The functional features and significant roles of SYNPO2 in VSMCs, characterized by an abundant expression of SYNPO2, are so far unknown.

The purpose of this work is to find out **(A)** the consequences of the VSMCs phenotype switch on the subcellular distribution of SYNPO2, **(B)** whether SYNPO2 plays an active role in this process, **(C)** whether cAMP dependent signaling pathways like PKA, are required for SYNPO2 trafficking in VSMCs, and finally **(D)** to investigate the molecular mechanism of SYNPO2's shuttling by using biophysical techniques such BIFC and FACS-BIFC assay in a cellular context.

## 2 Materials and Methods

### 2.1 General materials

In this work, the materials and reagents were purchased from Qiagen, New England Bio-Lab, Sigma Aldrich, Merck, Invitrogen, and Roth. Sequencing of DNA fragments were performed by MWG. Primers were designed with snap-gene viewer software and ordered from Invitrogen and MWG.

#### CHEMICALS

Table 1 All chemicals used in this work.

NAME	PROVIDER
3-Isobutyl-1-methylxanthin (IBMX)	Sigma-Aldrich
Acrylamide/Bisacrylamide	AppliChem
Agarose	Sigma-Aldrich
Ammonium peroxodisulfate (APS)	Serva
Ammonium sulfate	AppliChem
Ampicillin	AppliChem
$\beta$ -mercaptoethanole	Serva
Bacto-agar	Roth
Bacto-tryptone	Sigma-Aldrich
BCA reagents	Pierce
Bradford reagent	BioRad
Chloramphenicol	Roth
Collagenase I, II	Worthington
Collagen I	Upstate
Complete protease inhibitor cocktail	Roche
Coomassie Brilliant Blue	BioMol Feinchem. GmbH
Cover Slip Mounting Medium	Poly Science
Dimethyl sulfoxide (DMSO)	Sigma-Aldrich

Dried milk powder (fat free)	AppliChem
Dithiothreitol (DTT)	AppliChem
ECL Cell Attachment Matrix	Millipore
Ethylenediaminetetraacetic acid disodium salt Dehydrate (EDTA)	Sigma-Aldrich
Ethanol (absolute p.a.)	J.T. Baker
Fetal Bovin Serum	Sigma-Aldrich
Formaldehyde	Sigma-Aldrich
Forskolin	Tocris
Fungicide	Gibco
Glutathione	Roth
Glycerol	Sigma-Aldrich
H89	Tocris
Hank's Balanced Salt Solution (HBSS)	Gibco
HCl	J.T. Baker
HEPES	Gerbu Biotechnik GmbH
Hoechst 33342	Sigma
Isopropyl-thio- $\beta$ -d-galactoside (IPTG)	Roth
Isopropanol	Roth
Kanamycin	Gerbu
Leptomycin B (LMB)	Santa Cruz
LB-Agar	Roth
LB-Medium	Roth
L-Glutamine 200mM	Gibco
Kanamycin	AppliChem
KCl	Sigma-Aldrich
KH <sub>2</sub> PO <sub>4</sub>	Sigma-Aldrich
K <sub>2</sub> HPO <sub>4</sub>	Sigma-Aldrich

Laminin I	Sigma-Aldrich, L2020
Methanol (absolute p.a.)	J.T. Baker
MgCl <sub>2</sub>	Sigma-Aldrich
N <sub>2</sub> (liquid)	Air Liquid
NaCl	J.T. Baker
NaHCO <sub>3</sub>	Sigma-Aldrich
NaH <sub>2</sub> PO <sub>4</sub>	Sigma-Aldrich
Na <sub>2</sub> HPO <sub>4</sub>	Sigma-Aldrich
NaN <sub>3</sub>	Sigma-Aldrich
NaOH	J.T. Baker
NP-40	AppliChem
Paraformaldehyde (PFA)	Sigma
Penicillin Streptomycin (Pen Strep)	Invitrogen
Phalloidin	Invitrogen
Phosphate buffered saline (PBS)	Invitrogen
Phenylmethylsulfonyl fluoride (PMSF)	Sigma-Aldrich
Polyacrylamide	Roth
Ponceau S	Sigma
Sodium dodecyl sulfate (SDS)	AppliChem
Tetramethylethylen di amine (TEMED)	Serva
Trypsin-EDTA Solution (1x) 0.05%	Gibco
Tryptone	MP Biomedicals
Tris	Roth
Triton-X100	Sigma-Aldrich
Tween-20	Calbiochem
Trypan blue	Sigma-Aldrich

## KITS AND MATERIALS

Table 2 List of Kits and Materials

KIT	PROVIDER
10 cm dishes for Agar Plates	BD Biosciences
BCA Protein Assay Kit	Pierce/Thermo Scientific
Cell culture dishes (10 cm)	BD Biosciences
Cell culture dishes (6 cm)	BD Biosciences
Cell culture dishes (24-well)	BD Biosciences
Cell culture dishes (12-well)	BD Biosciences
Cell culture dishes (6-well)	BD Biosciences
Cover glass 10 mm	VWR
Cover glass 12 mm	VWR
G-Actin/F-actin In Vivo Assay Biochem Kit	Cytoskeleton
Gel Purification Kit	Qiagen
GoTaq® qPCR MasterMix	Promega
Maxwell Simply RNA	Promega
Micro-Amp Fast 96-Well Reaction Plate (0.1 ml)	Invitrogen
Mini-Prep	PeqLab,Qiagen
Micro tubes (1.5 ml)	Eppendorf
Micro tubes (2 ml)	Eppendorf
PCR Purification Kit	Qiagen
PCR Soft-tubes 0.2 ml clear	Biozym
Stripettes 5, 10, 25 (ml)	Falcon
Tube 15, 50 (ml)	Falcon

## BUFFERS AND SOLUTIONS

Table 3 All buffers and solutions used in this PhD work

NAME	INGREDIENT	APPLICATION
Blocking Solution	5 % (w/v) non-fat milk powder in 1X TBS or TBST	Western Blot
Blocking Solution	5 % (w/v) BSA powder in 1X PBS	Immunofluorecence
CELL LYSIS BUFFER (RIPA)	25 mM Tris, pH 7.4, 137 mM NaCl, 50 $\mu$ M EDTA, 1% Triton X100, 0.5% sodium deoxycholol, 0.1% SDS, 1 mM PMSF, 1X PIC	Mammalian cell
Coomassie Stock Solution	755 mM $(\text{NH}_4)_2\text{SO}_4$ 2.55% (v/v) Phosphoric acid 0.1% (w/v) Coomassie brilliant blue G-250	SDS-PAGE (Protein analysis)
Coomassie Solution	80% Coomassie Stock Solution 20% (v/v) Methanol	SDS-PAGE (Protein analysis)
HEPES-buffered saline (HBS) 2X	50 mM HEPES 280 mM NaCl 1.5 mM $\text{Na}_2\text{HPO}_4$	Transfection
PFA FIXATION SOLUTION	4 % (w/v) Formaldehyde in 1X PBS pH 7.5	Immunofluorescence study
PBS	2.7 mM KCl 1.7 mM $\text{NaH}_2\text{PO}_4$ 10 mM $\text{Na}_2\text{HPO}_4$	Protein isolation, western blot, and cell culture

	137 mM NaCl, pH 7.5	
SDS-loading buffer (2X)	8 M Urea, 100 mM Tris-HCl, pH 6.8, 2% SDS (w/v), 0.2% bromophenol blue, 20 mM DTT, 1 mM PMSF, 1X PIC	Visualization of proteins by SDS-PAGE
SDS-Separation buffer (4X)	1.5 M Tris, pH 8.8 0.4% (w/v) SDS	SDS-PAGE
SDS-Running buffer (10X)	250 mM Tris, 1.92 M glycine, 1% SDS	SDS-PAGE
TAE buffer (1X)	40 mM Tris acetate, 2 mM EDTA, pH 8	
TBS	150 mM NaCl 10 mM Tris, pH 7.5	Western blot
TBST	150 mM NaCl 10 mM Tris, pH 7.5 0.01% Tween 20	Western blot
Western blot running buffer (1X)	25 mM Tris-HCl 192 mM Glycine 20 % (v/v) MeOH 0.01% SDS	Western blot

## MEDIA

All media used in this work are shown in the table. All media were autoclaved or sterile filtered before use.

Table 4 Bacterial and mammalian media

NAME	INGREDIENTS
Cell Culture Medium (A10, A7r5)	DMEM (Gibco) 10 % FBS (Sigma-Aldrich) 1% Penicillin (100 U) Streptomycin (100 µg) (Pen/Strep, Invitrogen)
Cell Culture Medium (HEK293)	DMEM/F12 1:1 (Gibco) 10 % FBS (Sigma-Aldrich) 1% Penicillin (100 U) Streptomycin (100 µg) (Pen/Strep, Invitrogen)
Cell Culture Medium (raVSMCs)	DMEM/F12 1:1 (Gibco) 10 % FBS (Sigma-Aldrich) 1% Penicillin (100 U) Streptomycin (100 µg) (Pen/Strep, Invitrogen)
LB media for 1 L	25 g LB-dry powder, ddH <sub>2</sub> O to 1 L, pH 7.0
LB agar plates	15 g/l bacto agar 50 mg/l ampicillin or 35 mg/l Kanamycin

## INSTRUMENTS

Table 5 list of used instruments during this work.

INSTRUMENT	PROVIDER
10, 20, 100, 200, 1000 µl, pipette	Eppendorf
Autoclave	Varioklav
Avanti Centrifuge G-52 I	Beckman Coulter

Cell Culture Hood	Airclean-Telstar
Centrifuge 5412 (refrigerated)	Eppendorf
Centrifuge Micro 200	Hettich
Confocal laser microscope	Olympus
Electrophoresis Chamber	Hoefer
FACS	Applied Bioscience
High Voltage Power Pack P30	Biometra
High-speed centrifuge (refrigerated) RC-5C plus	Sorvall
Incubator shaker innova 4000	New Runswick Scientific
Incubator shaker innova 4300	New Runswick Scientific
Incubator	Heraeus
Infrared Imaging System Odyssey	LI-COR
Inverted Microscope	Leica
Nanodrop Spectrophotometer 1000	PeqLab
Operating Scissor	World Precision Instruments
PCR Thrmocycler 5436	MJ Research
Real-Time PCR System (One-Step)	Life Technology
Thermomixer 5436	Eppendorf
Ultra-centrifuge rotor (TLA-55)	Beckman
Ultrasound water bath (2200)	Branson
Vortex Mixer (MS525-20)	Heidolph (Reax)
Western Blot Chamber	Bio-Rad
Water Bath	Grant
Water Bath	Shel-Lab

## BACTERIA STRAINS AND MAMMALIAN CELLS

Table 6 List of used bacterial for cloning and sub-cloning process.

NAME	SOURCE
BL21 Rosetta (DE3)	Institute of physiology
<i>E. Coli</i> XI-1 blue	Institute of physiology
A10	Institute of physiology
A7r5	Institute of physiology
HEK293	Institute of physiology
raVSMC	Primary isolated

## VECTORS AND PLASMIDS

All vectors used in this work are listed in the table 7. All Fluorescent vectors used for SYNPO2, 14-3-3 $\gamma$ , 14-3-3 $\beta$ , Importin $\alpha$  (Table 7) were taken from the vector bank of the group of Prof. Dr. Papadopoulos. Splice vectors (YFP- $\Delta$ C, YFP- $\Delta$ N) used for BIFC assay were a kind gift from Prof. Dr. Beam, University of Colorado, USA. All Plasmids used to study SYNPO2 were prepared by me. Table 7 List of vectors and plasmids used in this work

NAME	GENE	ANTIBIOTIC RES.
pECFP-N1	14-3-3 $\gamma$	Kanamycin
pECFP-C1	14-3-3 $\gamma$	Kanamycin
pECFP-N1	14-3-3 $\beta$	Kanamycin
pECFP-C1	14-3-3 $\beta$	Kanamycin
pECFP-N1	Importin $\alpha$	Kanamycin
pECFP-C1	Importin $\alpha$	Kanamycin
pEYFP-N1	SYNPO2	Kanamycin
pEYFP-C1	SYNPO2	Kanamycin
pCDNA1-YFP- $\Delta$ C (YFP-1-158)	14-3-3 $\gamma$	Ampicillin
pCDNA1-YFP- $\Delta$ N (YFP-159-238)	14-3-3 $\gamma$	Ampicillin
pCDNA1-YFP- $\Delta$ C (YFP-1-158)	14-3-3 $\beta$	Ampicillin

pCDNA1-YFP-ΔN (YFP-159-238)	14-3-3β	Ampicillin
pCDNA1-YFP-ΔC (YFP-1-158)	SYNPO2	Ampicillin
pCDNA1-YFP-ΔN (YFP-159-238)	SYNPO2	Ampicillin
pCDNA1-YFP-ΔC (YFP-1-158)	Importinα	Ampicillin
pCDNA1-YFP-ΔN (YFP-159-238)	Importinα	Ampicillin
pcDNA3-mRuby2	14-3-3γ	Ampicillin
pcDNA3-mRuby2	14-3-3β	Ampicillin
pGEX4T-1	14-3-3γ	Ampicillin

### PRIMERS

All primers were designed by using NCBI and Snap-Gene program and NTI. The primers were purchased from both MWG-Biotech and Invitrogen.

Table 8 List of primers used in this work

PRIMER SEQUENCES	DIG. SITE	Add. INFORMATION
GAGAGAGGATCCATGGTGGACCGCGAGCAACTAGTGC	<u>BamHI</u>	14-3-3γ into pGEX4T-1
GAGAGAGAATTCTTAGTTGTTGCCTTCGCCCGCTC	<u>EcoRI</u>	14-3-3γ into pGEX4T-1
GAGAGAAGATCTATGGTGGACCGCGAGCAACTAG	<u>BglII</u>	14-3-3γ into pECFP-C1
GAGAGAGGATCCCTTAGTTGTTGCCTTCGCCGC	<u>BamHI</u>	14-3-3γ into pECFP-C1
GAGAGAAGATCTATGGTGGACCGCGAGCAAC	<u>BglII</u>	14-3-3γ into pECFP-N1
GAGAGAGGATCCcgGTTGTTGCCTTCGCCGCC	<u>BamHI</u>	14-3-3γ into pECFP-N1
GAGAGACTCGAGATGTTTAAGAAGCGGAGG	<u>BglII</u>	SYNPO2 into

		pEYFP-C1
GAGAGAGGATCCTCACTCTTCCACAACCTGAAGG	<u>BamHI</u>	SYNPO2 into pEYFP-C1
GAGAGAAGATCTATGTTTAAGAAGCGGAGGCG	<u>BglII</u>	SYNPO2 into pEYFP-N1
GAGAGAGGATCCTCTTCCACAACCTGAAGG	<u>BamHI</u>	SYNPO2 into pEYFP-N1
AGAGAGAGGCGGCCGCAATGGTGGACCGCGAGCAACT AGTGC	<u>NotI</u>	14-3-3 $\gamma$ into pCDNA1-YFP- $\Delta$ C (YFP-1-158) and pCDNA1-YFP- $\Delta$ C (YFP-158- 238)
AGAGAGAGTCTAGATTAGTTGTTGCCTTCGCCGCCGTC	<u>XbaI</u>	14-3-3 $\gamma$ into pCDNA1-YFP- $\Delta$ C (YFP-1-158) and pCDNA1-YFP- $\Delta$ C (YFP-158- 238)
GAGAGAGCGGCCGCAATGACCATGGACAAAAGTGAGC	<u>NotI</u>	14-3-3 $\beta$ into pCDNA1-YFP- $\Delta$ C (YFP-1-158) and pCDNA1-YFP- $\Delta$ C (YFP-158- 238)

GAGAGATCTAGATTAGTTCTCTCCCTCTCCAGCATC	<u>XbaI</u>	14-3-3 $\beta$ into pCDNA1-YFP- $\Delta$ C (YFP-1-158) and pCDNA1-YFP- $\Delta$ C (YFP-158-238)
GAGAGAGCGGCCGCAATGTCCACCAATGAGAATGC	<u>NotI</u>	Importin $\alpha$ into pCDNA1-YFP- $\Delta$ C (YFP-1-158) and pCDNA1-YFP- $\Delta$ C (YFP-158-238)
GAGAGATCTAGATTAGAAGTTAAAGGTCCCGGG	<u>XbaI</u>	Importin $\alpha$ into pCDNA1-YFP- $\Delta$ C (YFP-1-158) and pCDNA1-YFP- $\Delta$ C (YFP-158-238)
GAGAGAGCGGCCGCAATGTTTAAGAAGCGGAGGCGG	<u>NotI</u>	SYNPO2 into pCDNA1-YFP- $\Delta$ C (YFP-1-158) and pCDNA1-YFP- $\Delta$ C (YFP-158-238)

GAGAGATCTAGATCACTCTTCCACAACCTGAAGGTTTCC	<u>XbaI</u>	SYNPO2 into pCDNA1-YFP- ΔC (YFP-1-158) and pCDNA1-YFP- ΔC (YFP-158- 238)
AGAGAGAGGCGGCCGCCACCATGGTGGACCGCGAGCA ACTAGTGC	<u>NotI</u>	14-3-3γ into pcDNA3- mRuby2
GAGAGAGGATCCCGGTTGTTGCCTTCGCCGCC	<u>BamHI</u>	14-3-3γ into pcDNA3- mRuby2
GAGAGAGGATCCCGGTTCTCTCCCTCTCCAGCATC	<u>BamHI</u>	14-3-3β into pcDNA3- mRuby2
GAGAGAGCGGCCGCAATGACCATGGACAAAAGTGAGC	<u>NotI</u>	14-3-3β into pcDNA3- mRuby2
<b>Quantitative Real-Time PCR Analysis</b>		
CCATGGAGAAGGCTGGGG		GAPDH
CAAAGTTGTCATGGATGACC		
AGCCATGTACGTAGCCATCC		β-actin
CTCTCAGCTGTGGTGGTGAA		
CACCTATCCTCAGCCTCAGC		Sm22
TTCAAAGGACATTGGCTTCC		
CACCAGAAACCCAAGAGGAA		CalD1
CATCTTTTCCGATGGGCTA		
ACCGCTTCGCCAACTAC		Vimentin

GTTGTCCCTCTCCACCTC	
CCGCTGTCTGGTCCAGAA	Smoothelin
GGCTTTTTGCCATGATCA	
TTCTCCTGGCGAGTCATCT	14-3-3 Beta
CTGCATGGGTAGCATTGAGA	
GCCATGAAGAACGTGACAGA	14-3-3 Gamma
TCTTCTTCTCGTTGCCATCC	
GATCGGGAGGATCTGGTGTA	14-3-3 Epsilon
GCTCTTCTGGCTCCAATCAC	
AAACGTTGTAGGAGCCCGTA	14-3-3Zeta
AGACTTTGCTTTCTGGCTGC	
TTACTACCGCTACCTGGCAG	14-3-3eta
TCATCGAAGGCTTGTTGGC	
TAGAGACCGAGCTCAGAGGT	14-3-3 Sigma
CGATGATGCGCTTCTTGTC	
AAGACCGAGCTGATCCAGAA	14-3-3 Tetha (tau)
TGTCCGAGGTATCGGTCTTC	

## ANTIBODIES

Table 9 List of all used antibodies in this work.

NAME	APPLICATION	SUPPLIER	DILUTION	HOST
anti SYNPO2	WB, IF	Prof. Chalovich	1:100000, 1:5000	Rabbit
anti CD90	FACS	Miltenyi Biotec	1:100	Rabbit
anti Caldesmon	WB, IF	Prof. Pfitzer	1:1000, 1:1000	Rabbit
anti $\beta$ -actin	WB,	Sigma	1:500	Mouse
anti $\alpha$ -SMA	WB, IF	Sigma	1:1000, 1:1000	Mouse

anti GAPDH	WB	Sigma	1:25000	Rabbit
anti Lamin B1	WB	Prof. Noegel	1:4000	Rabbit
anti $\gamma$ Tubulin	WB	Prof. Noegel	1:100	Rabbit
anti GFP	WB	Cell signalling	1:1000	Rabbit
anti GFP	WB	Prof. Noegel	1:20	Mouse
anti smMHC	WB, IF	Sigma-Aldrich	1:500	Rabbit
anti Rabbit Dylight 800	WB	Thermo	1:10000	Goat or Monkey
anti Rabbit Dylight 680	WB	Thermo	1:10000	Goat or Monkey
anti Mouse Dylight 800	WB	Thermo	1:10000	Goat or Monkey
anti Mouse Dylight 680	WB	Thermo	1:10000	Goat or Monkey
Alexa Fluor <sup>®</sup> 488 anti- Rabbit IgG	IF	Invitrogen	1:1000	Goat
Alexa Fluor <sup>®</sup> 555 anti- Rabbit IgG	IF	Invitrogen	1:1000	Goat

## 2.2 Methods

### 2.2.1 Molecular biology methods

#### 2.2.1.1 Total RNA isolation and cDNA synthesis

Cells were trypsinized or were mechanically harvested and total RNA or/and DNA was isolated using the Maxwell® 16 LEV simply RNA tissue kit and/or the Maxwell® 16 LEV Blood DNA kit (Promega, Madison, WI) according to the manufacturer's instructions or by RNeasy Mini Kit (Qiagen).

##### 2.2.1.1.1 Total RNA isolation by MAXWELL machine

- Harvest the cells from a 10 cm cell culture plate at 80% confluent using 0.5% trypsin.
- Spin the cells at 1500 rpm using a table centrifuge.
- Remove the medium and wash the cells one time with cold PBS and spin one more time.
- Homogenize the cells in 200 µl of buffer A (1-thioglycerol/homogenization solution = 1:1) by pipette.
- Add 200 µl buffer B (Lysis buffer) into the mixture shortly before total RNA isolation.
- Place the RNA isolation cartridge on machine plate and add 5 µl of the DNase into the tube four.
- Add cell mixture to the tube 1 and mix briefly.
- Place a 500 µl tube in the elution place at cartridge and add 50 µl of elution buffer into the tube.
- Place the isolation plate in the machine and start appropriate program.
- Determine RNA concentration with Nanodrop 1000.
- Use RNA for cDNA synthesis.
- Freshly isolated RNA, must be used directly after isolation for further experiment or store at -80°C for long time used.

**2.2.1.1.2 cDNA synthesis**

The single strand cDNAs were synthesized from isolated total RNA with the Quantitect<sup>®</sup> Reverse Transcriptase Kit (Qiagen, Germany) using random primers following the manufacturer's protocol. In this work typically 1 µg of total RNA per 20 µl cDNA reaction mixture was used.

The reaction mixtures were prepared as follows:

1) Genomic DNA elimination reaction:

2 µl of gDNA Wipeout Buffer (7X)

1 µg total RNA (variable volume)

RNase-free water (variable) up to 14 µl

Incubation at 42°C for 2 min

2) Reverse-Transcription reaction:

1 µl Reverse transcriptase

4 µl reverse transcriptase buffer (5X)

1µl primer Mix

- Mix the reaction mixture 1 and 2 together and incubate at 42°C for 15 min
- Incubate the RT-reaction mixture at 95°C for 3 min to inactive the reaction

**2.2.1.2 Preparative PCR**

The PCR reaction mixtures were generally mixed as shown in table 10 in a 0.2 ml PCR tube. The PCR reaction was run in a thermo-cycler (PCT-100<sup>®</sup> Thermal Cycler, MJ Research) according to the listed program in table 11.

Table 10 General PCR Mixture used in this work

	Material	Volume (µl)	Concentration
1	PCR Buffer (5X)	10	1X
2	Primers (10 pmol/ µl)	5 (each primer)	0.5 µM
3	Template	0.1-05 µg	
4	dNTPs (each 2 mM)	5	200 µM
5	Polymerase*	0.5	1 unit

6	Water (DEPC)	Up to 50	
7	Total	50	

\*Phusion<sup>®</sup> High-Fidelity DNA Polymerase was used as standard polymerase in preparative PCR.

Table 11 PCR Programs used in this work

	Cycle	Temperature	Time
1	1X	98°C	2 min
2	30X	98°C	10 sec
3		Depending on used primer	20-30 sec
4		72°C	30 sec for 1 kb
5	1X	72°C	5 min
6	1X	4°C	

#### 2.2.1.2.1 Purification of PCR products

PCR products were purified depending on the size of the DNA fragments with different TAE agarose-gel concentration as listed in the table 12.

Table 12 Concentration of TAE agarose for DNA purification (taken from molecular cloning: a laboratory manual, Michael R. Green and Joseph Sambrook, 2nd Ed)

Amount of agarose (% [w/v])	Efficient of separation (KB)
0.3	5-60
0.6	1-20
0.7	0.8-10
0.9	0.5-7
1.2	0.4-6
1.5	0.2-3
2.0	0.1-2

Using protocol according to manufacturer's protocol:

1. Weight and dissolve desired amount of agarose in 1X TAE buffer by heating
2. Add 5  $\mu$ l EtBr to the gels
3. Mix PCR products with appropriate amount of 10X DNA loading buffer and load on TAE agarose-gel. Use 1kb marker as standard
4. Run the gel at 60 Volt in 1X TAE
5. Excise desired band and extract the DNA using a gel extraction kit from Qiagen according to the manufacture protocol.

#### 2.2.1.2.2 Sub-Cloning

##### ***Digestion of PCR products and vectors***

Both PCR products and vectors were digested by the same appropriate restriction enzymes as listed in table 6.7. Preparation of digestion mixtures and used time are listed in the table 13 according to the manufacturer's instructions.

Table 13 Digestion mixture and using times

	Components	Volumes ( $\mu$ l)	Volumes ( $\mu$ l)
1	10X Buffer (NEB or fermentas)	5	10
2	Vector (0.2 $\mu$ g/ $\mu$ l) or PCR product (1 $\mu$ g/ $\mu$ l)	10	55
3	Enzyme**	3	5
4	Enzyme**	3	5
5	Water	29	25
6	Total	50*	100

\* Digested vectors were treated by Alkaline Phosphatase, Calf Intestinal (CIP) for 1 h at 37°C (NEB).

\*\* 1 unit of enzyme can digest 1  $\mu$ g DNA.

##### ***Ligation of PCR products into the vectors***

Ligation was performed using a quick ligation Kit (New England Biolabs<sup>®</sup> Inc. Germany) according to the manufacture's protocol. After purification of digested products by using a PCR purification kit or by TAE agarose gel, products and appropriate vectors were

generally mixed together in a ratio of 8:1 as listed in table 14. The ligation reactions were incubated for 5 to 10 min at room temperature and deactivated as described in manufacture's protocols.

Table 14 Used ligation reaction mixture in this work

	Materials	Volume ( $\mu$ l)
1	Ligation buffer	10
2	T4-Ligase	1
3	Vector	1
4	Insert	8
5	Total	20

#### 2.2.1.2.3 Transformation

To get a large amount of plasmids, desired ligation reactions were transformed under heat stress into chemical competent *E. coli* XL-1 blue strain as described.

1. Add 5  $\mu$ l of ligation reaction mixture to 100  $\mu$ l of competent *E. coli* XL-1 blue and incubate the mixture on ice for 30 min.
2. Incubate the cells at 42°C for 45 Sec and briefly cool on ice.
3. Add 900  $\mu$ L LB medium to the cells.
4. Incubate the cells on a shaker at 37°C for 1 h.
5. Spin the cells at 3000 rpm for 30 Sec.
6. Spread 100  $\mu$ l of cells on LB-Agar plate with appropriate antibiotics.
7. Incubate the plate at 37°C, overnight.

#### 2.2.1.2.4 Colony PCR

On the following day, after transformation and plating the cells on LB-agar with appropriate antibiotic colonies were picked and analyzed by colony-PCR with appropriate primers.

1. Select and pick a single bacteria colony using a pipette tip.

2. Pick the tip in a PCR reaction tube and inoculate 3 ml of LB medium with appropriate antibody with the same pipette tip.
3. Incubate the LB medium at 37°C, overnight, 200 rpm.
4. Add PCR reaction mixture to the PCR reaction tube and run a PCR Table 15.
5. Analyze the PCR products by 1X TAE agarose-gel.

Table 15 Colony PCR reaction mixture

	Components	Volume ( $\mu$ l)	Concentration
1	Buffer (10x)	2.5	1x
2	Primer (10 pmol)	1.75	500 nM
3	dNTPs (each 2 mM)	2.5	200 $\mu$ M
4	Sample DNA	Bacterial colony	
5	MgCl <sub>2</sub>	1.5	
6	Taq DNA polymerase	0.25	1 unit
7	H <sub>2</sub> O	14.75	
8	Total	25	

#### 2.2.1.2.5 Preparation of plasmid DNA

##### **MINI PREP**

All plasmids prepared in this work were purified using a Qiagen Mini-Prep kit according to the manufacture's protocol.

1. The day after transformation, one single colony was picked and dissolved to 3 ml of LB-Medium containing the antibiotic.
2. The bacteria were grown at 37°C under shaking for over night.
3. The bacteria were harvested at 13 000 rpm by using a table centrifuge.
4. 250  $\mu$ l of buffer P1 was added to the cell pellet and mixed by a vortex.
5. 250  $\mu$ l of buffer P2 was added and mixed gently by inverting until the solution became clear.

6. 350  $\mu$ l of buffer N3 was added to the bacterial lysate and mixed by inverting to precipitate proteins, lipids and chromosomal DNA.
7. The mixture was centrifuged at 13 000 rpm for 10 min.
8. The resulted supernatant was added on a spin column and centrifuged at 13 000 rpm for 1 min.
9. The bound plasmid on the column was washed one time with buffer HB (500  $\mu$ l) and one more time with 750  $\mu$ l of wash buffer containing ethanol (13 000 rpm, 1 min).
10. Finally the column was placed in a 1.5 ml tube and the plasmid was eluted by 50  $\mu$ l elution buffer or water (13 000 rpm, 1 min).

#### **2.2.1.2.6 Test digest screening**

To prove the accuracy of ligation process, generated plasmids were digested by the appropriate restriction enzymes. After concentration estimation, 1  $\mu$ g of Plasmid was digested by the appropriate restriction enzymes and analyzed by using a 1X TAE agarose gel.

#### **2.2.1.2.7 DNA sequencing**

To check accuracy of ligated DNA into the vectors and analyze the sub-cloning, sequencing of yielded plasmids was performed by MWG Biotech according to the manufacture's protocols.

Preparation of Plasmid for sequencing:

- ✚ 50-100 ng of Plasmid in 15  $\mu$ l total volume in a 1.5 ml save-lock Eppendorf tube.

#### **2.2.1.3 Quantitative polymerase chain reaction (qRT-PCR)**

For analysis of gene expression levels, the RNA has to be transcribed into cDNA using a reverse transcriptase. In this work we used a tow step reaction. The RNA is first reverse transcribed into cDNA as described before with random oligomers (see 2.2.1.1.2). Finally, an aliquot of the reverse-transcription reaction is used for the real-time PCR. The gene specific primers were designed by Snap-Gen software 2.2.2 or Vector NTI Advance 10

and ordered by Invitrogen, science-technology or MWG Biotech (listed in Table 8). The Real-Time PCR reaction mixtures were generally mixed as shown in table 16 in a 0.1 ml MicroAmp Fast 96-well Reaction Plate (life Technologies, 4346907). The Real-time PCR was carried out with a GoTaq® qPCR Master Mix (Promega, Madison, WI) and was run in a thermo-cycler (StepOnePlus™ real-time PCR System, life Technologies) according to the listed program in table 17. Data analysis was achieved by StepOne Software v2.3.

Table 16 General Real-Time PCR Mixture in This Work

	Materials	Volume $\mu$ l	Concentration
1	GoTaq® qPCR Master Mix 2X	10	1X
2	Primers (10 pmol/ $\mu$ l)	2 each	1 $\mu$ M
3	Nuclease-Free Water	2	
4	cDNA (RNA 100 ng/20 $\mu$ l)	4	20 ng
5	Total	20	

Table 17 Real-Time PCR Program used in This Work

	Step	Cycle	Program
1	Activation	1	95°C, 10 min
2	Denaturation	40	95°C, 15 Sec
	Annealing/Extension		60°C, 1 min
3	Melt Curve	1	95°C, 15 Sec
			60°C, 1 min
			95°C, 15 Sec

#### 2.2.1.3.1 Analysis of qRT-PCR data

In this work, we calculated gene expression levels of our genes of interest by determining the ratio between the amount of a target gene and an endogenous reference gene that is equally expressed in all samples. Resulting raw data from Real-time PCR were analyzed by a free StepOne software V2.3 (Life Technologies). ROX dye was used as a passive reference for all analysis. The samples were run in triplicates, and the experiments were

repeated at least three times. The mRNA levels were normalized against the endogenous control (GAPDH) levels and calculated using the delta cycle threshold (Ct) method.

## 2.2.2 Cell biology methods

### 2.2.2.1 Isolation of vascular smooth muscle cells from rat aorta

rVSMCs were prepared by an enzymatic digestion published by Golovina et al. 2006<sup>131</sup> (Fig. 7).

- I. After anesthetizing, the aorta and vein were removed from the 6-8 weeks old rat under sterile conditions and transferred quickly in PBS, pH 7.4 (Gibco) that contains fungicide (Gibco, 0.2 mg/ml), and Pen/Strep (Gibco, 100 U/ml and 100 µg/ml) and stored for 15 min.
- II. Transfer tissues after 15 min in a sterile 6 cm cell plate with 1-2 ml HBSS (Gibco, with Ca<sup>2+</sup> and Mg<sup>2+</sup>) buffer with fungicide and antibiotics.
- III. Remove adherent fat and connective tissue from the aorta under a dissection microscope.
- IV. In order to avoid contamination, the same process was performed when removing the vein.
- V. Remove blood from the aorta and vein by injecting HBSS.
- VI. The further steps were performed under a laminar flow hood.
- VII. Transfer the tissues to a 3.5 cm plate containing the first enzyme solution (2 mg collagenase type 2 (Worthingen, #LS004194) in 1 ml HBSS (Gibco, without CaCl<sub>2</sub> and MgCl<sub>2</sub>)) and incubate for 45-60 min at 37°C and 5% CO<sub>2</sub>.
- VIII. Remove carefully the partially digested tissues from the enzyme solution and wash once in HBSS (with Ca<sup>2+</sup> and Mg<sup>2+</sup>).
- IX. Remove under a dissecting microscope, adventitia from the aorta
- X. Cut the aorta and vein tissues, that contain smooth muscle cells and endothelial, longitudinally with fine scissors.
- XI. Remove carefully the endothelial layer by using a fine scraper.
- XII. Transfer and incubate the aorta and vein in pre-warmed medium (DMEM, 10% FBS, Pen/Strep, 100 U/ml and 100 µg/ml) and incubate overnight at 37°C and 5% CO<sub>2</sub>.

- XIII. Remove the medium and wash the tissues twice by HBSS (without  $\text{CaCl}_2$  and  $\text{MgCl}_2$ ).
- XIV. Cut partially digested tissues with fine scissors in 1-2 mm pieces in the enzyme solution II (Collagenase type 2 and type 1 (2 mg/ml each, Worthingen) in HBSS buffer without  $\text{CaCl}_2$  and  $\text{MgCl}_2$ )
- XV. Incubate the mixture for 4 hours at  $37^\circ\text{C}$  and 5%  $\text{CO}_2$ .
- XVI. Stop the enzymatic reaction by adding 4 ml of culture medium and re-suspend the cells in DMEM medium.
- XVII. Spin the cells at 500 xg for 5 min.
- XVIII. After removing the supernatant, re-suspend the cells in 1 ml culture medium DMEM containing Pen/Strep (100 U/ml and 100  $\mu\text{g/ml}$ ).
- XIX. Use media without FBS at this step to avoid the growth of epithelial cells and fibroblasts.
- XX. Count the cells using trypan blue and determine the number of dead cells to compare the viability of cells at different days and in different cell types.
- XXI. For further characterization by immunofluorescence staining, plate  $2 \times 10^4$  cells on coverslips in a 24-well culture plate. Alternatively plate cells in a 10 cm culture dish for biochemical experiments.
- XXII. Change 80% of culture medium every 2 or 3 days.
- XXIII. In order to check the viability and growth ratio, cells were digested with 0.5% Trypsin-EDTA every second or third day.

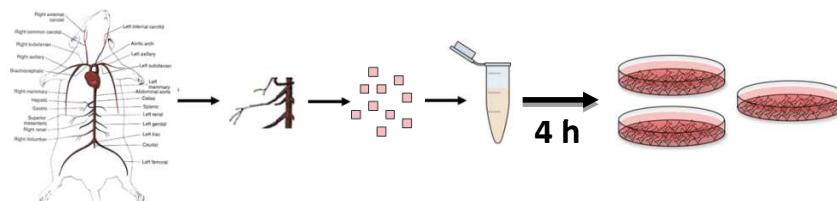


Fig. 7 Schematic illustration: Isolation of vascular smooth muscle cell from rat aorta using enzymatic method.

### 2.2.2.2 Cell culture and treatments

#### VSMCS

Rat vascular smooth muscle cells (rVSMCs) were seeded at a density of  $2.5 \times 10^4$  cells/cm<sup>2</sup> on coverslips, pre-coated with 0.1% gelatin, and left grown in DMEM supplemented with 10% FBS and 100 U/ml Pen and 100 µg/ml Strep in a humidified atmosphere at 37°C, 5% CO<sub>2</sub>. When the cells were 70% confluent, medium was replaced by serum free medium and cells were incubated for further 2 h prior to each experiment. Finally, cells were treated with different effectors, DMSO as vehicle control or not treated at all. The used concentrations of inhibitors and activators in this work and incubation times are listed in table 18. In case of heat shock studies and activation by PKA and CaMKII, experiments were performed with freshly isolated cells, where SYNPO2 is localized in the cell cytoplasm, while inhibitor studies were executed with cells from passage 2 to 4, where SYNPO2 accumulated in the cell nucleus.

Table 18 Used incubation times and treatment conditions for this study

Component	Concentration	Time	Inhibited	Activated	Company
urocortin	100 nM	1 h		cAMP signaling	Sigma-Aldrich
Sp-5.6-DCl-cBIMPS	10 µM	1 h		PKA	BioLog
forskolin	10, and 20 µM	1 h		cAMP signaling	ICN Biomedicals
KN93	10 µM	1 h	CaMK-II		Calbiochem
H89	10 µM	1 h	PKA		Sigma-Aldrich
Rp-8-PIP-cAMPS	100 µM	1 h	PKA		BioLog
Okadic acid	100 nM	1 h	PP2A and PP1		Sigma-Aldrich
Y-27632	10 µM	1 h	ROCK		Tocris
IBMX	10, 20 µM	1 h	PDEs		Sigma-Aldrich

In order to analyze whether the phenotype switch of VSMCs affects subcellular localization of SYNPO2, VSMCs from day 1 (contractile phenotype) and passage 2 (synthetic phenotype) at  $25 \times 10^3$  cells/cm<sup>2</sup> were seeded on coverslips for immunofluorescence studies or let grown in a 10 cm cell culture plate for biochemical studies. VSMCs at passage 3 were seeded on polyacrylamide matrices pre-coated with collagen type 1 (Upstate) or laminin (Sigma Aldrich) as extracellular matrix proteins, respectively, and let grown for 48 h prior to each experiment. Cells were grown in DMEM medium (high glucose), Life Technologies, supplemented with 100 U/ml Pen and 100 µg/ml Strep and 10% FBS in a humidified atmosphere at 37°C and 5% CO<sub>2</sub>. Cells on pre-coated polyacrylamide matrices (pre-coated by collagen I, and laminin) were used to study the effect of cytochalasin D and Jasplankloide on SYNPO2 distribution in the cells. Medium was replaced with serum free medium 2 h before each experiment. At least 150 cells (3 X 50) from four independent experiments were used for statistical analysis of subcellular localization of SYNPO2 in VSMCs.

#### **HEK293 Cells**

In order to investigate the subcellular localization and the interaction studies between SYNPO2, 14-3-3γ/β, and importinα, HEK293 cells were seeded on ECL (Entactin, CollagenIV, Laminin, MILLIPORE, 08-110) pre-coated coverslips placed in 6 wells cell culture plate, and let grown in DMEM supplemented with 10% FBS, 100 U/ml Pen, 100 µg/ml Strep at 37°C in a humidified atmosphere of 5% CO<sub>2</sub>. Cell were transiently co-transfected with 300 ng of constructs by the calcium phosphate method:

1. Prepare 2 M CaCl<sub>2</sub> solution in water, filter sterile and keep at room temperature.

2. Prepare the 2x HBS buffer:

50 mM HEPES

280 mM NaCl

1.5 mM Na<sub>2</sub>HPO<sub>4</sub>

Adjust pH to 7.0 using HCl. Filter sterilize. The solution can be frozen/thaw once for future use.

3. Incubate HEK-293 cells in DMEM medium with 10% FBS, 100 U/ml Pen, 100 µg/ml Strep at 37°C, 5% CO<sub>2</sub>.
4. 24 hours before transfection, trypsinized and reseed log-phase cells into 35 mm tissue culture dishes. Seeding density should be that the cells reach 60~70 % confluence for transfection.
5. 3 hours before transfection, replenish cells with fresh medium.
6. For each DNA transfection, prepare following mixtures in two separate tubes:  
**Solution-A:** 100 µl 2x HBS  
**Solution-B:** 0.3-0.5 µg DNA + 12.2 µl of 2 M CaCl<sub>2</sub> and ddH<sub>2</sub>O to bring volume up to 100 µl, pipet gently to mix.
7. Add the Solution-B slowly (drop-wise) into Solution-A while mixing Solution-A.
8. After mixing the two solutions, incubate at room temperature for 20-30 minutes. The solution will become opaque while precipitates form.
9. Gently tap the mixture. Add the mixture directly to cells by dripping slowly and evenly into medium (a good way is to let tip touch medium surface).
10. Gently tilt the plate back and forth a couple of times to allow evenly distribution of added precipitate on the cell surface.
11. Incubate the cells at 37°C with 5% CO<sub>2</sub> for 24 hours, replenish medium.

### 2.2.2.3 Immunofluorescence staining

#### Cell on coverslips

To visualize the subcellular localization and translocation of SYNPO2, seeded VSMCs were serum starved 2 h before each experiment. After treatment (see 2.2.2.2) cells were briefly fixed with 4% PFA in 1X PBS (10 mM sodium phosphate, 2.68 mM KCl, 140 mM NaCl, pH 7.4) for 15 minutes and permeabilized with 0.4% triton X-100 diluted in blocking buffer (5% BSA diluted in PBS) for 15 min at room temperature (RT). Cells were then washed three times with PBS, 5 min each, and blocked with blocking buffer for 45 min at RT. The cells were incubated with primary antibodies diluted in blocking buffer for 1 h at RT. Excessive antibodies were washed off with PBS and cells were incubated with secondary antibodies for one further hour followed by 3 washes with PBS. To visualize the nucleus

and the actin cytoskeleton, cells were incubated with Hoechst 33342 and Alexa-555 conjugated phalloidin (Life Technologies, Carlsbad, CA) diluted in blocking buffer for 1 h. Finally, cells were fixed on microscopic slides with PolyGlass coverslip mounting medium (Polysciences, Warrington, PA).

#### **Cells on coated polyacrylamide matrices**

Cells on pre-coated (Collagen I, Laminin) polyacrylamide matrices were fixed with 4% PFA for 30 min at room temperature. After permeabilization with triton X-100 for 15 minutes the cells were blocked for 1 h with blocking buffer. Incubation with primary and secondary antibodies as well as the staining of the actin cytoskeleton with Fluorescent labeled phalloidin and staining of the nucleus with Hoechst 33342 were performed as described above. Images were recorded with an Olympus Fluoview FV1000 confocal laser-scanning microscope using the appropriate filters.

#### **2.2.2.4 Confocal microscopy**

In this work an Olympus laser confocal microscopy was used to capture the images and to analyze localization, distribution and interaction of different immunostained and Fluorescent-fused proteins. In confocal images, Alexa-488 immunostained proteins were excited at 488 nm and observed from 505 to 525 nm. Alexa-555-Phalloidin (actin cytoskeleton) was excited at 515 nm and observed from 525 to 565 nm. The nucleus of cells was stained using Hoechst 33342 and excited at 350 nm, and the images were captured from 460-490 nm. Moreover, CFP fused proteins were detected at 458 nm and YFP fused proteins were detected at 465-495 nm. The images were 512 \* 512 pixels. The captured images were analyzed either by a commercially available program FV-10-ASW 2.0 Viewer or by using NIH-software ImageJ. For statistical analysis at least three independent experiments were performed where each time 150 cells were counted. The results were analyzed by Student's t-test.

## **2.2.3 Biochemical and analytical methods**

### **2.2.3.1 Characterization of isolated VSMCs**

Although, previous studies have shown that the cell populations isolated by enzymatic methods are almost smooth muscle cells, a minor contamination found using these methods are fibroblasts. With regard to this fact, we tested the purity of our isolated VSMCs by FACS analysis and Western blot using specific antibodies directed against VSMCs, like anti  $\alpha$ SMA, smMHC, and desmin or anti CD90 directed against fibroblast cells.

### **2.2.3.2 Fluorescence activated cell sorting assay (FACS)**

FACS, also known as Flow cytometer, is a laser-based, biophysical technology by which cells are counted and analyzed in a stream of fluid passing by an electronic detection device. FACS analysis was achieved by an attune acoustic focusing cytometer (Applied Bioscience), AG Saric (Institute of Neurophysiology). Isolated cells were characterized by using a fibroblast specific antibody against Cluster differentiation 90 (CD90)<sup>132</sup>. CD90 also known as Thy-1 is a 25- to 37-kD heavily N-glycosylated surface protein that anchored to the cell membrane of fibroblasts via a glycosylphosphatidylinositol (GPI) and is expressed on mesenchymal stem cells and fibroblasts<sup>133, 134</sup>. In order to analyze and to estimate the fibroblast contamination, freshly isolated VSMCs and as positive control STO fibroblasts (Mouse embryonic fibroblast cell line) were incubated with anti-CD90-FITC (Miltenyi Biotec, 1:100) diluted in 50  $\mu$ l PBS and 1% FBS or FCS for 1 h at 4°C. Untreated STO cells were used as a negative control. A mouse IgG-FITC labeled antibody was used as secondary antibody to exclude unspecific cross reactivity. Cells were washed three times with washing buffer (PBS, 1% FBS or FCS), each 5 min. Finally, cells were suspended in 500  $\mu$ l PBS containing 1% FBS or FCS. 10,000 events per sample were acquired at BL1 channel for green fluorescence on flow cytometer and the data were analyzed with Cell Quest Pro software (Beckton Dickinson).

### **2.2.3.3 Subcellular fractionation**

Cytoplasmic and nuclear fractions were prepared according to two methods: Neumann et al. 2010<sup>135</sup> and Thakar et al. 2013<sup>136</sup>, followed by Western blot analysis to quantify the

subcellular distribution of SYNPO2 in VSMCs. The methods are based on isolation of subcellular fractions using different buffers and centrifugal forces.

For subcellular fractionation and the following Western blot analysis, cells were seeded at  $5 \times 10^5$  on 10 cm cell culture plates and grown to 80% confluence. Cells were mechanically harvested on ice in medium and centrifuged at 110 xg, 4°C for 5 min (Eppendorf 5417).

**According to Neumann et al. 2010**

The cells were briefly washed (4-5 Sec.) with hypotonic buffer (10 mM HEPES, pH 7.9, 1.5 mM MgCl<sub>2</sub>, and 10 mM KCl containing protease inhibitor cocktail (PIC, Roche) and 1 mM PMSF) and directly centrifuged for 20 seconds at 110 xg, 4°C. The cell pellets were suspended in hypotonic buffer, incubated for 10 min on ice, and then completely disrupted by passing 10 times through a needle (26G x 2/4"). The cytoplasm was separated from the nuclear fraction by centrifugation (10 min, 110 xg, 4°C). The supernatant (cytoplasm) was stored on ice and the pellet, containing the nuclei, was washed 6 times with ice cold PBS containing 1 mM PMSF and PIC (Roche). The cytoplasm was clarified by centrifugation at 1500 xg for 20 minutes, and 4°C. Protein concentrations of the fractions were determined by the Bradford assay to ensure loading of equal protein amounts on the SDS-gels. The nuclear and cytoplasmic proteins were resolved on 10% SDS gels transferred to nitrocellulose membrane and probed with the appropriate antibodies as described in the section 2.2.3.4. The purity of the isolated fractions was tested by specific antibodies against GAPDH (cytoplasmic protein), and Lamin 1B (nuclear membrane protein).

**According to Thakar et al. 2013**

Subcellular fractionation was performed according to the protocol of Thakar et al. (2013)<sup>136</sup> with small modifications. After harvesting as described above, cells were briefly suspended in 400 µl buffer A (50 mM HEPES, pH 7.4, 150 mM NaCl, 1% triton X100, 1 mM PMSF and protease inhibitor cocktail (Roche)) and incubated on ice for 10 min. The mixtures were centrifuged for 10 min at 3000 xg, 4°C. The resulting supernatants represented the cytosolic fractions. The pellets were suspended in 400 µl buffer B (50 mM HEPES, pH 7.4, 150 mM NaCl, 1% Nonidet P-40, 1 mM PMSF and PIC (Roche)),

incubated for 30 min on ice, and then centrifuged at 7000 xg for 10 min. The supernatants contained the membrane-bound organelles and were stored on ice. The remaining pellets, containing the nuclear proteins, were suspended in 400 µl buffer C (50 mM HEPES, pH 7.4, 150 mM NaCl, 0.1% SDS, 0.5% sodium deoxycholate, 1 mM PMSF and PIC (Roche)), incubated on ice for 1 h, and centrifuged at 7000 xg for 10 min. The resulting supernatants, containing the nuclear proteins were stored on ice. Protein concentrations of the fractions were determined by the Bradford assay as already described and subjected to gel-electrophoresis.

#### **2.2.3.4 SDS-PAGE and Western blot analysis**

##### **Cells from cell culture plate**

For protein analysis, VSMCs that had reached 70% to 80% confluence were once washed with 1X PBS and incubated on ice. The cells were scratched on ice in 5 ml ice cold PBS and transferred in a 15 ml falcon tube. The cells were collected by centrifugation (110 xg, 5 min at 4°C). Cell pellets were suspended in SDS sample buffer (8 M Urea, 100 mM Tris-HCl, pH 6.8, 2% SDS (w/v), 0.2% bromophenol blue, 20 mM DTT, 1 mM PMSF, 1X PIC (Roche)) and incubated for 15 min at room temperature. Proteins were separated by gel electrophoresis on 10% SDS-polyacrilamid gels. Proteins were transferred to a nitrocellulose membrane using a Towbin buffer<sup>137</sup> (25 mM Tris, 192 mM Glycin, 20% MeOH, 0.01% SDS) in a tank blot (110 volt, 70 min) on ice or in a cold room. Membranes were blocked for 30 minutes at room temperature with 5% nonfat milk in Tris-buffered saline (TBS (10 mM Tris, 150 mM NaCl, pH 7.5)) followed by incubation with primary antibodies (diluted in blocking buffer) for 2 h at room temperature or overnight at 4°C under rotation. After intensive washing with TBS (5 min each time) the membranes were incubated with IRDye 680CW or 800CW (Thermo) secondary antibodies (1:12,000 diluted in blocking buffer) at room temperature for 45 min followed by intensive washing with 1X TBS. The protein bands were visualized by densitometry scanning using the Odyssey Infrared Imaging System (LI-COR).

### **Cells on polyacrylamide matrices**

Isolation of cells from polyacrylamide matrices was achieved as described before<sup>138</sup>. Cells were seeded at a density of  $2 \times 10^5$  cells/cm<sup>2</sup> on polyacrylamide matrices 48 h prior to each experiment and let grown to a 70% confluence. After removing the cell culture medium, cells were harvested by 200  $\mu$ l of RIPA buffer (25 mM Tris, pH 7.4, 137 mM NaCl, 50  $\mu$ M EDTA, 1% triton X100, 0.5% sodium deoxycholate, 0.1% SDS, 1 mM PMSF, protease inhibitor cocktail (Roche)), incubated on ice for 20 min and centrifuged at 15,000 rpm for 15 min, 4°C. 150  $\mu$ l of the supernatants was mixed with 150  $\mu$ l 2x SDS-Sample buffer (8 M Urea, 100 mM Tris-HCl, pH 6.8, 2% SDS (w/v), 0.2% bromophenol blue, 20 mM DTT, 1 mM PMSF, 1X PIC). The protein concentrations estimation and protein analysis were achieved as described above.

### **HEK293**

In order to analyze the expression levels of fluorescent fused proteins in transfected HEK293 cells, protein extracts from cells were prepared in RIPA buffer and characterized by 1D SDS-PAGE and Western blot as described above.

#### **2.2.3.5 Estimation of F/G-Actin ratio**

In order to investigate whether the alteration of F/G-actin ratio connected with the subcellular distribution of SYNPO2 during phenotype switch, cells from passage 2 were plated on acrylamide matrices pre-coated with collagen I and laminin and let grown for 24 h in a humidified atmosphere. On the following day, cells were treated with CCD, JASP or DMSO as control after 2 h serum starvation. F/G-actin ratio was measured using the F-actin/G-actin *in vivo* assay kit. Treated VSMCs were homogenized in 100  $\mu$ l LAS02 buffer (F-actin stabilization buffer, ATP, PIC) with a plastic pastel at RT, and centrifuged in a BioRad table-centrifuge at 350 xg for 5 min. Supernatants were collected and centrifuged at 100,000 xg (TLA-55) for 1 h at 37°C. The high-speed supernatant (G-Actin) was carefully removed, and 25  $\mu$ l of 5X SDS-gel sample buffer was added. The high-speed pellet (F-Actin) was resuspended in 100  $\mu$ l of F-actin destabilization buffer and incubated for 1 h on ice. 25  $\mu$ l of 5X SDS-gel sample buffer was added to the 100  $\mu$ l F-Actin. Samples were stored at -20°C before running the SDS-PAGE and Western blotting. F/G-actin ratio

analysis occurred by using 4%-15% SDS-PAGE. Experiments were performed three times as duplicate. The results were analyzed by Student's t-test using GraphPad Prism 4.

#### **2.2.4 Preparation of collagen I and laminin coated polyacrylamide matrices**

This experiment was performed by Dr. Carlos Omar Heras Bautista, Pfannkuche AG, Institute of Neurophysiology, Medical Faculty, University of Cologne. Polyacrylamide matrices were prepared as described before<sup>139</sup>. To prepare polyacrylamide matrices, polyacrylamide (PAA) solution was firstly mixed together as follow; 0.374 ml of 15% acrylamide (w/v), 0.150 ml of 0.3% N,N'-Methylenebisacrylamide (w/v), 0.010 ml of 1.5 M NaH<sub>2</sub>PO<sub>4</sub> and 0.465 ml of distilled water. The solution was briefly vortexed and degassed for 5 min. 12.5 mg of 2,5-Dioxopyrrolidin-1-yl 6-acrylamidohexanoate (linker) was added to 1 ml of PAA solution, briefly sonicated, and warmed to 40°C for 3 min until it was dissolved. Polymerization of PAA matrices were started by the addition of 0.015 ml of 200 mM potassium persulfate in distilled water (degassed) and 0.015 ml of TEMED (diluted 1 to 10 in distilled water) to each 0.250 ml aliquot of PAA solution. To control the size of prepared matrices, PAA matrices were polymerized in a closed poly-Tetrafluoroethylen (Teflon) casts for 2 min. Resulting PAA matrices had 7 mm diameter and 1 mm thickness. Finally, PAA gels were washed twice with 200 mM Hepes pH 8.5 and 0.070 ml of Collagen I (40 µg/ml) or laminin 1 (20 µg/ml) in 200 mM Hepes pH 8.5 was added to each gel. Activated PAA gels were left at 4°C overnight.

#### **2.2.5 Stiffness measurement of polyacrylamide by atomic force microscopy**

Atomic Force Microscopy (AFM) was performed by Dr. Sabine Diluweit from the Institute of Complex Systems (ICS), research center Jülich. Measurements were done for sample, 55 kPa, prepared according to the acrylamide/bis-acrylamide ratios used for each solution<sup>139</sup>. Each sample was polymerized to silanized microscope slides, with a thickness of 8 mm per sample. Measurements were performed in triplicates, and were performed twice, using solutions from different stocks, resulting in matrices prepared under various conditions. Each sample was measured several times on randomized locations. For each location, three cantilever displacements were performed and their resulting force-curve

was analyzed applying the extended Hertz model, obtaining the elastic modulus for the each analyzed sample<sup>140-143</sup>.

AFM experiments were performed using a commercial Atomic Force Microscope, Nanowizard (JPK, Berlin, Germany) in spectroscopy mode. The samples were measured in 1X PBS. The cantilever was pressed onto several points of the sample with a velocity of 1 $\mu$ m/s. Standard silicon tips were used with a nominal spring constant of  $k = 42$  N/m (Atomic Force, Mannheim, Germany) and  $k = 2.8$  N/m (Nanoandmore, Wetzlar, Germany). The tip shape was assumed as a cone with an opening angle of 20° respectively 18°. The lower spring constant was determined using thermal fluctuations in air<sup>144</sup> and the value of the higher spring constant is given from the company. The sensitivity was determined under PBS on glass.

### 2.2.6 Bimolecular fluorescence complementation assay (BIFC)

Moreover, smooth muscle SYNPO2, 14-3-3 $\gamma/\beta$ , and importin $\alpha$  protein interaction analysis was achieved by using BIFC technique, an early reported technique. For BIFC measurements, HEK293 cells were seeded at 50% to 60% confluent either on ECL pre-coated coverslips for the subcellular localization and the interaction studies or on a 12 well cell culture plate for FACS analysis (2.2.7). On the following day, cells were transfected as described before with equal amounts (300 ng) of BIFC constructs using the calcium phosphate method. Table 19 summarizes the used BIFC-constructs, and their application in this chapter.

Table 19 Used combinations of BIFC-constructs in this work.

Construct 1	Construct 2	Application
$\Delta$ N-YFP	$\Delta$ C-YFP	Control 1, whether $\Delta$ N-YFP interacts with other constructs and develops fluorescence
	$\Delta$ C-YFP-SYNPO2	
	$\Delta$ C-YFP-14-3-3 $\gamma$	
	$\Delta$ C-YFP-14-3-3 $\beta$	
	$\Delta$ C-YFP-importin $\alpha$	

$\Delta C$ -YFP	$\Delta N$ -YFP-SYNPO2	Control 2, whether $\Delta C$ -YFP interacts with other constructs and develops fluorescence
	$\Delta N$ -YFP-14-3-3 $\gamma$	
	$\Delta N$ -YFP-14-3-3 $\beta$	
	$\Delta N$ -YFP-importin $\alpha$	
$\Delta N$ -YFP-SYNPO2	$\Delta C$ -YFP-SYNPO2	Dimerization study of SYNPO2
	$\Delta C$ -YFP-14-3-3 $\gamma$	Localization and interaction study
	$\Delta C$ -YFP-14-3-3 $\beta$	
	$\Delta C$ -YFP-importin $\alpha$	
$\Delta C$ -YFP-SYNPO2	$\Delta N$ -YFP-14-3-3 $\gamma$	Localization and interaction study
	$\Delta N$ -YFP-14-3-3 $\beta$	
	$\Delta N$ -YFP-importin $\alpha$	
$\Delta N$ -YFP-14-3-3 $\gamma$	$\Delta C$ -YFP-14-3-3 $\gamma$	Dimerization study
	$\Delta C$ -YFP-14-3-3 $\beta$	Localization and interaction study
	$\Delta C$ -YFP-importin $\alpha$	
$\Delta N$ -YFP-14-3-3 $\beta$	$\Delta C$ -YFP-14-3-3 $\gamma$	Dimerization study
	$\Delta C$ -YFP-14-3-3 $\beta$	Localization and interaction study
	$\Delta C$ -YFP-importin $\alpha$	
$\Delta C$ -YFP-importin $\alpha$	$\Delta N$ -YFP-importin $\alpha$	Dimerization study

### 2.2.7 FACS-BIFC based assay

In order to quantify the BIFC-fluorescence development during protein-protein interaction, HEK293 cells were transfected at 70% confluent with different BIFC-constructs using calcium phosphate methods and let grown for 24 h at a humidified atmosphere at 37°C, 5% CO<sub>2</sub>. For the preparation of single cell suspensions, cells were washed with 1X PBS, trypsinized, pelleted, suspended in PBS plus 1% FCS or FBS. Cell preparation and analysis were carried out consecutively for every sample, alternating the experimental and control condition (three times in duplicate). Per sample, 10,000 cells were analyzed on attune acoustic focusing cytometer (Applied Bioscience) at the Institute

of Neurophysiology (AG Saric) with excitation at 488 nm and registration with the 515-545 nm filter. Cells were defined as BIFC positive if they fell in a rectangular gate that eliminates 99.9% of control condition cells (without constructs).

### **2.2.8 Statistics**

All results are presented as means  $\pm$  SEM from at least three independent experiments performed in triplicate. For comparison between specific groups of continuous variables, the Student's t-test was used. A p value  $< 0.05$  was considered statistically significant.

### 3 Results

#### 3.1 Over 95% of the isolated cells were vascular smooth muscle cells

Analysis of the isolated VMSCs by FACS assay using the fibroblast specific antibody anti-CD90 showed that at least 95% of the isolated cells are VSMCs. As Fig. 8 shows, the mouse embryonic fibroblasts (STO fibroblast) used as a positive control gave in over 90% a positive signal when stained with the anti-CD90 antibody (Fig. 8A), while isolated SMCs demonstrated less than 3% positive signal when treated with anti-CD90 antibody (Fig. 8B). Morphological studies showed that the majority of the isolated cells had a characteristic spindle-shaped morphology of smooth muscle cells. Some of the cells exhibited a flattened morphology (Fig. 8C, white arrow).

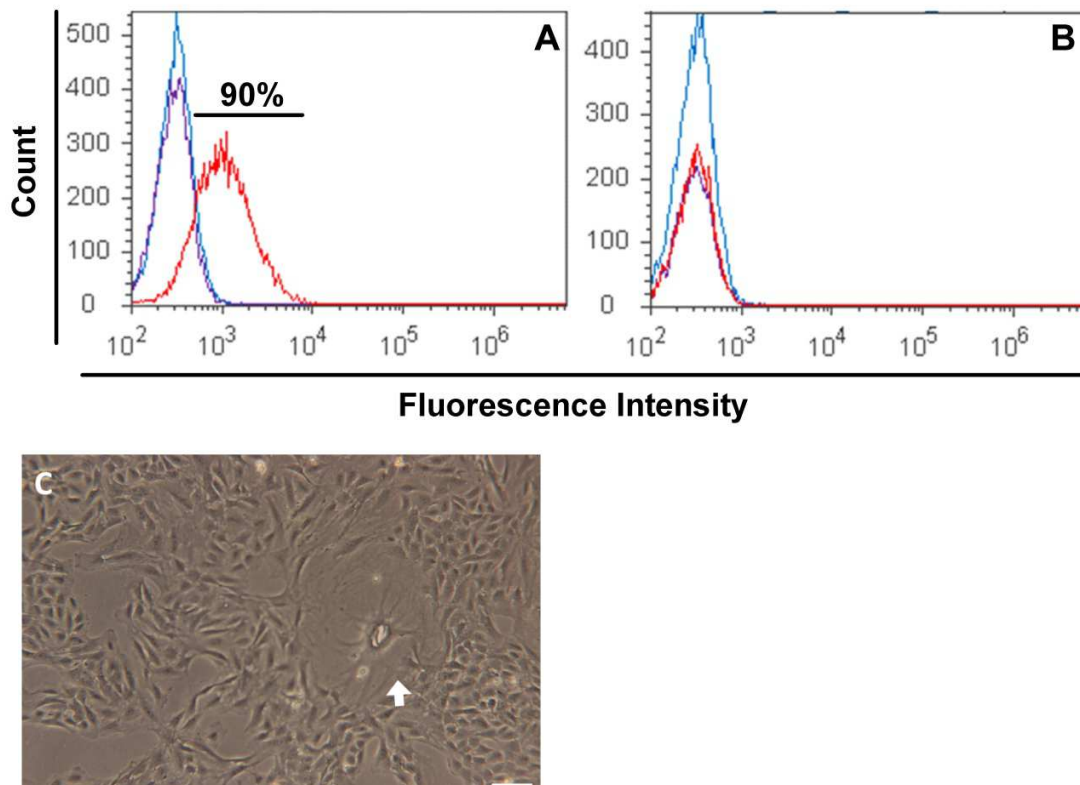


Fig. 8 Fluorescence-activated cell sorting (FACS) analysis of isolated rat aorta vascular smooth muscle cells versus fibroblasts. (A) STO-fibroblasts as positive control for CD90 and (B) isolated rat VSMCs were incubated with FITC conjugated anti-CD90 (1:100, 4°C, 1 h) before analyzing in a flow cytometer. 10,000 events were acquired for each sample on a histogram with blue laser canal (BL1-H) on the Y-axis. Cells that did not react with the anti-CD90 antibody were measured by light scattering. Differential interference contrast (DIC) image (C) of rat VSMCs. Curves represent incubated cells with anti-CD90 (red), with secondary antibody (violet), and cells without treatment (blue).

### 3.2 Isolated primary VSMCs expressed the smooth muscle marker proteins

As reported in previous studies, smooth muscle specific proteins like smMHC,  $\alpha$ SMA, desmin and calponin are commonly used as marker proteins to characterize isolated SMCs<sup>145</sup>. In order to determine the expression level of these marker proteins in the isolated cells, specific antibodies against those proteins were used for detection by immunofluorescence microscopy. The isolated cells showed a strong immuno-reaction with antibodies against desmin,  $\alpha$ -SMA and smMHC (Fig. 9A-C). As expected, antibodies against  $\alpha$ -SMA detected the protein in both smooth muscle cells and fibroblast as the latter one expresses  $\alpha$ -SMA as well.

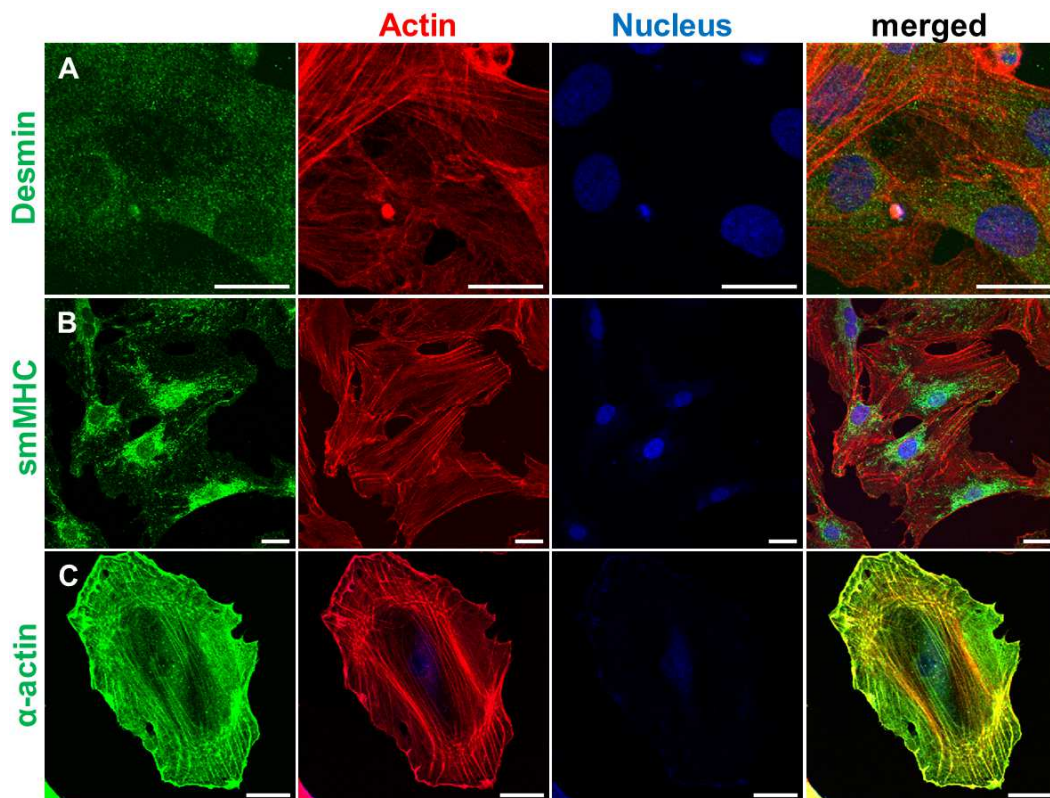


Fig. 9 Indirect immunofluorescence analysis of marker proteins of isolated VSMCs. Immunostaining of desmin (A), smMHC (B) and  $\alpha$ -SMA (C) in isolated cells. In order to characterize isolated cells by smooth muscle marker proteins, freshly isolated cells were seeded on 0.1% gelatin pre-coated coverslips overnight, and fixed with 0.4% PFA for 15 min. After permeabilization with 0.4% triton X100 (15 min), cells were immunostained against (A) desmin (1:500), (B) smMHC (1:500), and (C)  $\alpha$ -SMA (1:1000). The actin cytoskeleton and the cell nucleus were stained with Alexa-555 conjugated phalloidin (1:1000, red) and Hoechst 33342 (1:1000, blue). Scale bars represent 20  $\mu$ M.

### 3.3 Immunofluorescence studies demonstrated co-localization of SYNPO2, smMHC, and $\alpha$ -SMA

Furthermore, co-staining of VSMCs that were already treated with anti-SYNPO2 antibodies (2<sup>nd</sup> antibody anti-rabbit Alexa-555), with anti-smMHC, or with anti  $\alpha$ -SMA (2<sup>nd</sup> antibody anti-mouse Alexa-488), respectively, showed a high degree of colocalization of SYNPO2 &  $\alpha$ -SMA. In case of the co-staining with SYNPO2 and smMHC the staining was less intense and more diffuse (Fig. 10).

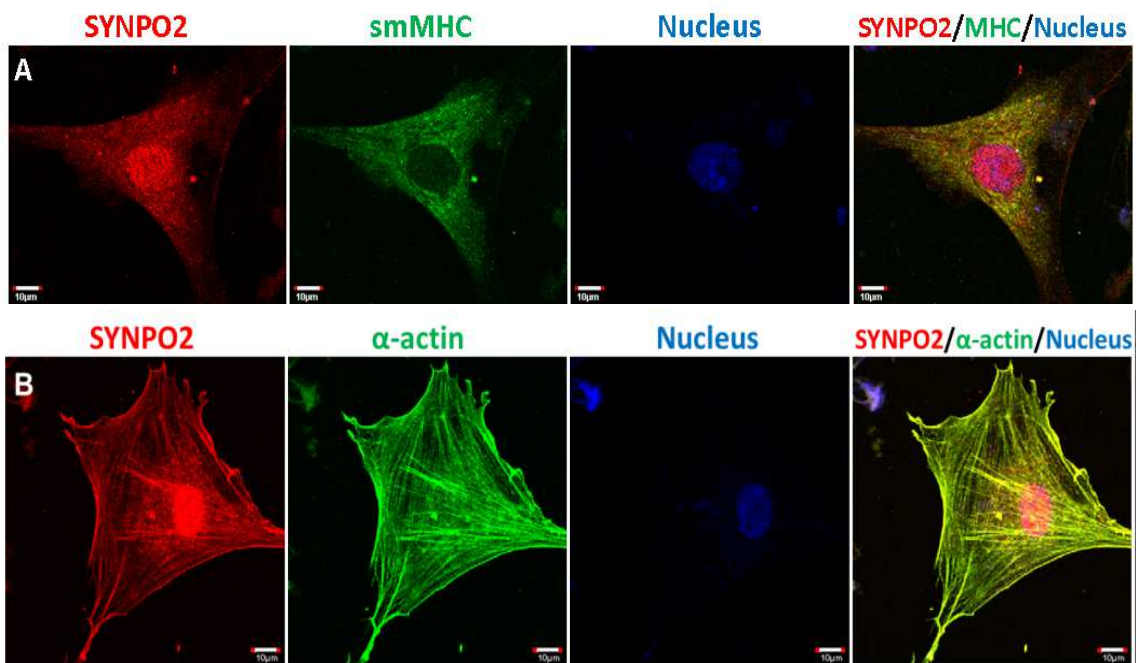


Fig. 10 Visualization of SYNPO2 and the contractile marker proteins, smMHC and  $\alpha$ -SMA. PFA (4%) fixed and Triton x100 (0.4%) permeabilized primary rat VSMCs (Passage 1) treated with rabbit anti-SYNPO2 antibodies (1:5000) and (A) monoclonal mouse anti-smMHC (1:500) or (B) anti- $\alpha$ -SMA (1:1000) antibodies. As secondary antibodies goat anti-rabbit IgG (1:1000), conjugated Alexa 555 and goat anti-mouse, conjugated to Alexa 488 (1:1000), antibodies were used. Scale bars represent 10  $\mu$ m.

### 3.4 Alteration of marker proteins during phenotype switch

The expression level of selected proteins typical for the differentiated smooth muscle cell phenotype was determined in two different ways. Firstly, the expression levels of further marker proteins were determined on mRNA level by using qRT-PCR. Additionally, Western blotting was used to determine expression levels of caldesmon and  $\beta$ -actin on the protein level. As shown in Fig. 11A, the mRNA of the smooth muscle specific proteins vimentin,

smoothelin, and sm22 were more abundant on the first day of isolation than at passage 3 (about day 20 after isolation). The significance level of vimentin expression was  $p < 0.001$  as determined by a two-tailed student's t-test. For smoothelin, caldesmon, and SM22 the significance was  $p < 0.0001$ . Expression of SYNPO2 has never before been investigated as a result of phenotypic switching of vascular smooth muscle cells. We found a down-regulation of SYNPO2 upon dedifferentiation of vascular smooth muscle cells with a significance level of  $p < 0.01$ .

The primers used for the amplification of caldesmon were selected in a way that both h- and l-caldesmon (*hCaD* and *lCaD*) would be amplified. Thus, the differentiation between h- and l-caldesmon was achieved by Western blot analysis.

While *lCaD* is scarcely found in native VSMCs, Western blot analysis during isolation and initial cultivation of VSMCs showed (Fig. 11B) that increasing cultivation time led to upregulation of *lCaD*, while at the same time *hCaD* levels declined in passage 1 (Fig. 11C). Although *hCaD* decreased, the onset of *hCaD* down-regulation was delayed and reached only its full extent when *lCaD* was thoroughly upregulated. Parallel to augmented *lCaD* levels  $\beta$ -actin expression increased. Normalization of these proteins to GAPDH showed, the typically in synthetic smooth muscle cells expressed proteins *lCaD* and  $\beta$ -actin were higher as early as passage 1. Low-caldesmon (Fig. 11E) was 12-fold higher in passage 1. In passage 2 the *lCaD* was higher by factor 10, and in passage 3 by the factor 8.5.  $\beta$ -actin (Fig. 11D) was upregulated 1.3-times on protein level in the first passage and did not undergo further changes at higher passages. The results on protein level for  $\beta$ -actin differed from those obtained by qRT-PCR demonstrating a downregulation between day 1 and the third passage of about 2.8 fold.

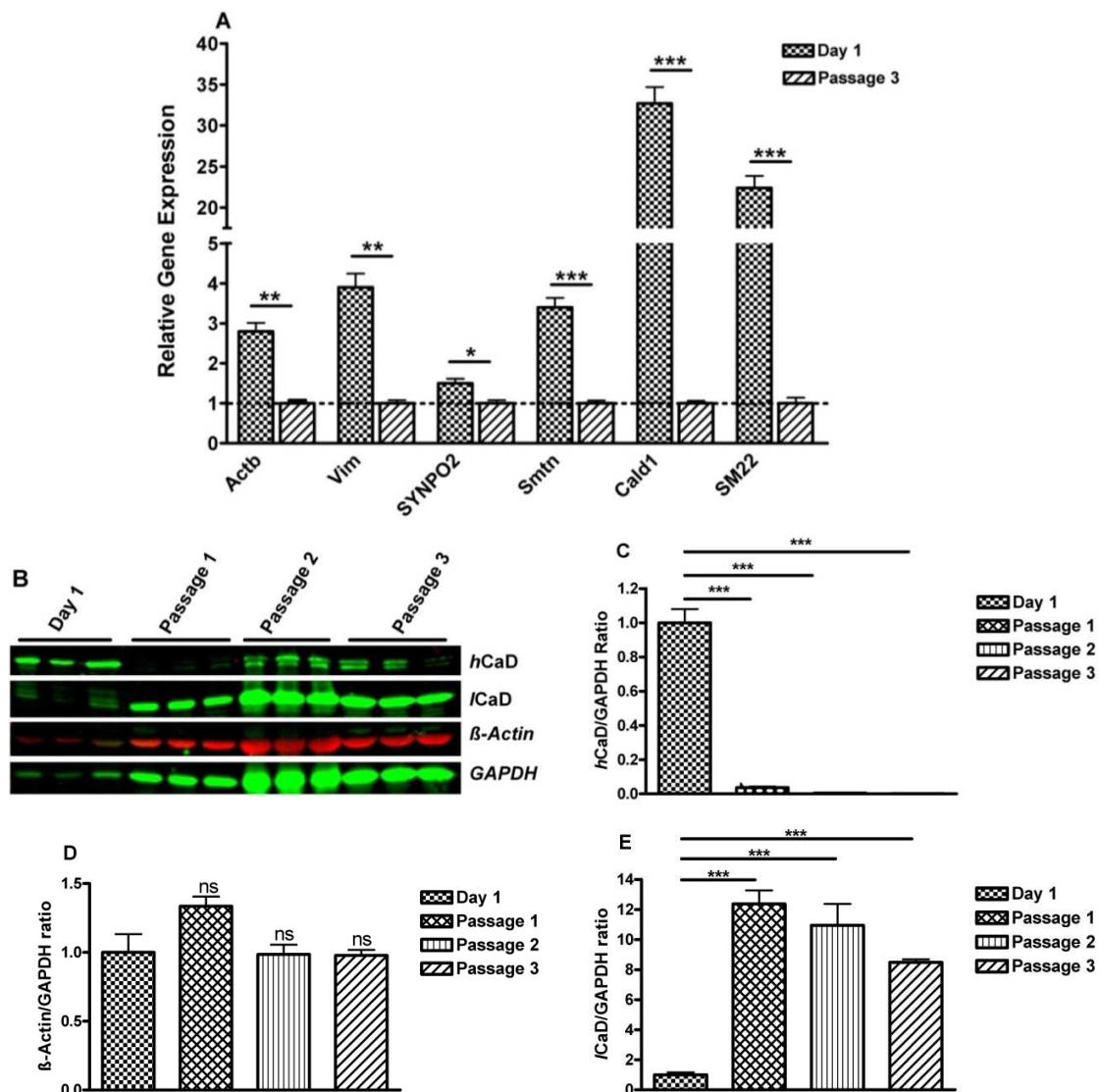


Fig. 11 Expression analysis of marker proteins in primary rat VSMCs. Quantitative RT-PCR from VSMCs from rat aorta on day 1 of isolation and passage 3 of cultivation. QRT-PCR was performed from three independent experiments in triplicates using 20 ng cDNA in each reaction. GAPDH was used as an endogenous control. Expressions levels are shown as the expression of target mRNA from cells of passage 3. Histograms show means  $\pm$  SEM (n=3), \*\*\*p< 0.0001; \*\*p<0.001; \*p<0.01 (A). Western blot analysis of whole cell extracts at day 1 of isolation, passage 1, passage 2, and passage 3 (B-E). Proteins were separated on a 10% SDS-PAGE, blotted on nitrocellulose membrane and probed with antibodies directed against hCaD, lCaD,  $\beta$ -actin, and GAPDH (B). Protein content as determined from IR Dye signals of the conjugated secondary antibodies: hCaD against GAPDH (C),  $\beta$ -actin versus GAPDH (D), and lCaD against GAPDH (E).

### 3.5 Phenotype switch of VSMCs alters subcellular distribution of SYNPO2

In striated muscle cells shuttling of SYNPO2 between the nucleus and cytoplasm depends on differentiation of the cells and exposure to stress like heat shock<sup>77, 101</sup>. Although

SYNPO2 is abundant in smooth muscle its subcellular localization during differentiation and dedifferentiation of smooth muscle cells is not known. As shown in Fig. 12, the subcellular localization of SYNPO2 is depends on vascular smooth muscle phenotype. On day 1 of isolation rat aorta smooth muscle cells present a differentiated smooth muscle phenotype. At this stage SYNPO2 was mainly found in the cytoplasm (Fig. 12A), where it seems to be uniformly spread. In the second passage, however, cells were already dedifferentiated presenting a synthetic phenotype. Dedifferentiation showed a serious impact on the localization of SYNPO2 (Fig. 12B). Most of the SYNPO2 was localized into the nucleus and nucleolemma. SYNPO2 that remained in the cytoplasm assembled as broad subcortical zone below the adhesion sites of the cells. The quantitative analysis of the subcellular localization of SYNPO2 based on immunofluorescence data (Fig. 12C) showed that upon (de)differentiation the distribution between the nucleus and the cytoplasm was nearly reversed. On day 1 of isolation SYNPO2 was found in 16.45% of the isolated VSMCs in the nucleus, but in the majority of the cells SYNPO2 was localized into the cytoplasm. In contrast, at passage 2 SYNPO2 showed a strong nuclear localization in 89.45% of the cells. Interestingly, the subcellular fractionation of VSMCs showed different distribution for SYNPO2 isoforms in the cytoplasm and the nucleus (Fig.12D).

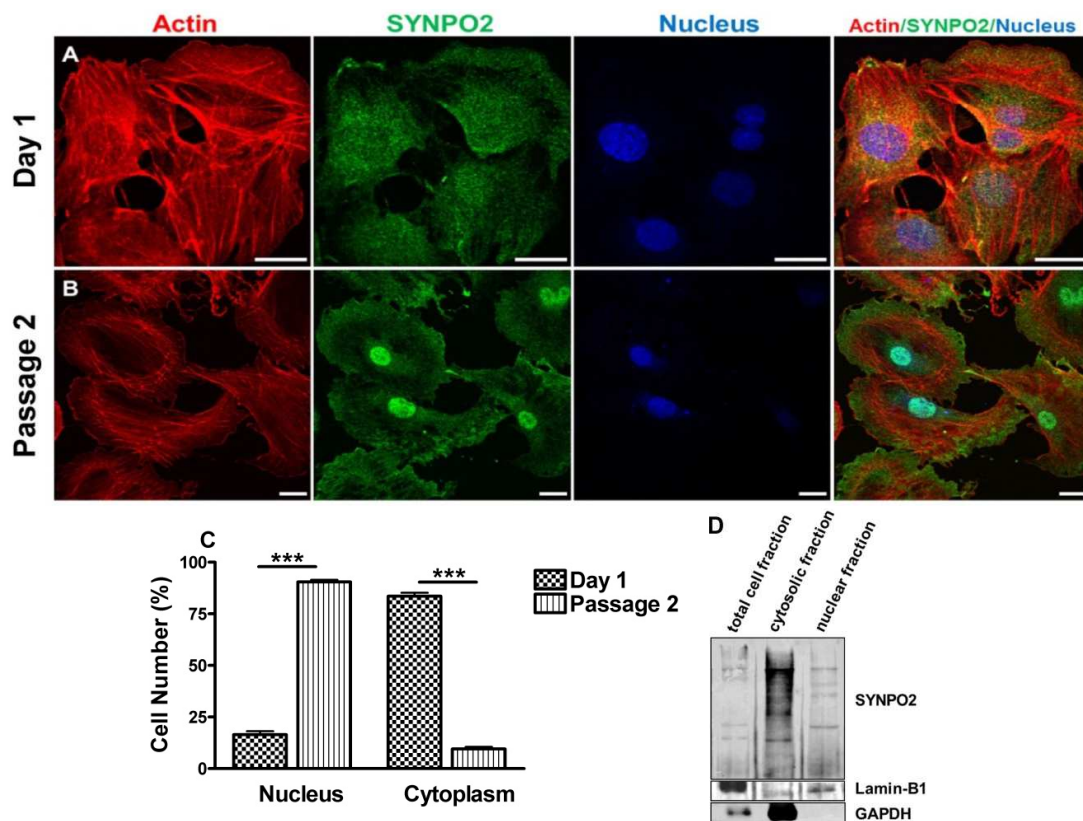


Fig. 12 Subcellular localization of synaptopodin 2 during isolation and cultivation of primary VSMCs. (A) Cells from day 1 (contractile phenotype) and (B) passage 2 (non-contractile phenotype) were grown on cover slips, fixed with 4% PFA, and permeabilized with 0.4% Triton X-100. Subcellular localization of SYNPO2 was detected with a polyclonal anti-SYNPO2 antibody and visualized using an anti-rabbit Alexa Fluor®488 antibody. The actin cytoskeleton and the cell nucleus were visualized by Alexa Fluor®555 phalloidin and Hoechst 33342, respectively. Scale bars represent 20  $\mu$ m. (C) Statistical analysis of SYNPO2 distribution in the nucleus versus the cytoplasm during isolation and cultivation. The histogram shows mean  $\pm$  SEM (n=4, 150 cells from each experiment) from four independent experiments performed in triplicate \*\*\* $p$ <0.0001. (D) SYNPO2 isoforms were analyzed using subcellular fractionation and Western blot assays (passage 3). Membrane was probed with anti LaminB1 (abcam, 1:4000) and GAPDH (Sigma-Aldrich, 1:25000) to characterize nucleus and cytoplasmic fractions. Distribution of SYNPO2 isoforms was detected by anti-SYNPO2 (1:50000).

### 3.6 Controlling of phenotype switch using ECM proteins

Previous studies reported, that the phenotypic switch in VSMCs is controlled by environmental conditions like extracellular matrix proteins<sup>8,10</sup>. In order to mimic stiffness as found under atherosclerotic conditions, a polyacrylamide matrix with stiffness of approximately 55 kPa was used<sup>139</sup> (The matrices were provided by Dr. Pfannkuche). The matrices were coated with the extracellular matrix proteins laminin 1 and collagen I,

respectively, in order to direct our isolated primary VSMCs to develop a differentiated or rather dedifferentiated phenotype. As a control, we used cells from the same passage that were cultivated on non-coated tissue culture dishes. The phenotypes were assigned according to the mRNA expression level and the expressed proteins, employing the same markers we used for our initial characterization (Fig. 13). On mRNA level, a slight, but non-significant upregulation of vimentin was detected, while  $\beta$ -actin, smoothelin, and SM22 were  $\sim 1.4$ ,  $\sim 1.8$ , and  $\sim 2$  fold, respectively, upregulated when VSMCs were cultured on laminin. In cells cultivated on laminin, *Cald1* and *SYNPO2* were markedly upregulated by the factors 6 and 3.2, respectively (Fig. 13A). Upregulation of  $\beta$ -actin, smoothelin, SM22, and *Cald1* indicated the presence of a contractile phenotype of VSMCs cultivated on laminin. Western blot analysis using antibodies directed against  $\beta$ -actin and caldesmon and GAPDH as internal control, confirmed the on laminin versus collagen I established phenotypes (Fig. 13B-E). In all cells, independent whether cultivated on laminin or collagen I coated matrices or on non-treated culture dishes, we found *hCaD* to be expressed, but reduced to a very low level in cells cultivated on non-treated dishes. The increase of *hCaD* is remarkable when cultured on pre-coated polyacrylamide matrices. While *hCaD* decreases to a minimum in uncoated dishes, it was highly upregulated by the factors 8 on collagen I, and 19 when cultivation took place on laminin coated matrices. *hCaD* presented itself as doublet when cells were grown on non-treated culture dishes. When calculating the expression of h-caldesmon, both bands were accounted for. Interestingly, *lCaD* was slightly, but not significantly upregulated in cells grown on laminin-coated matrices as compared to those VSMCs that were cultivated on non-treated dishes (Fig. 13E). In contrast, cells grown on collagen I coated matrices showed a significant ( $p < 0.001$ ) 3.2 fold upregulation of *lCaD*.

On protein level, a slightly higher expression of  $\beta$ -actin was detected in cells cultivated on laminin than what we expected from our previously determined mRNA-level of cells cultivated on laminin versus collagen I pre-coated polyacrylamide matrices (Fig. 13D). Expression of  $\beta$ -actin compared to our control cells was significantly ( $p < 0.0001$ ) increased in cells grown on laminin-coated matrices (factor 9.5) and those grown on collagen I (factor 5).

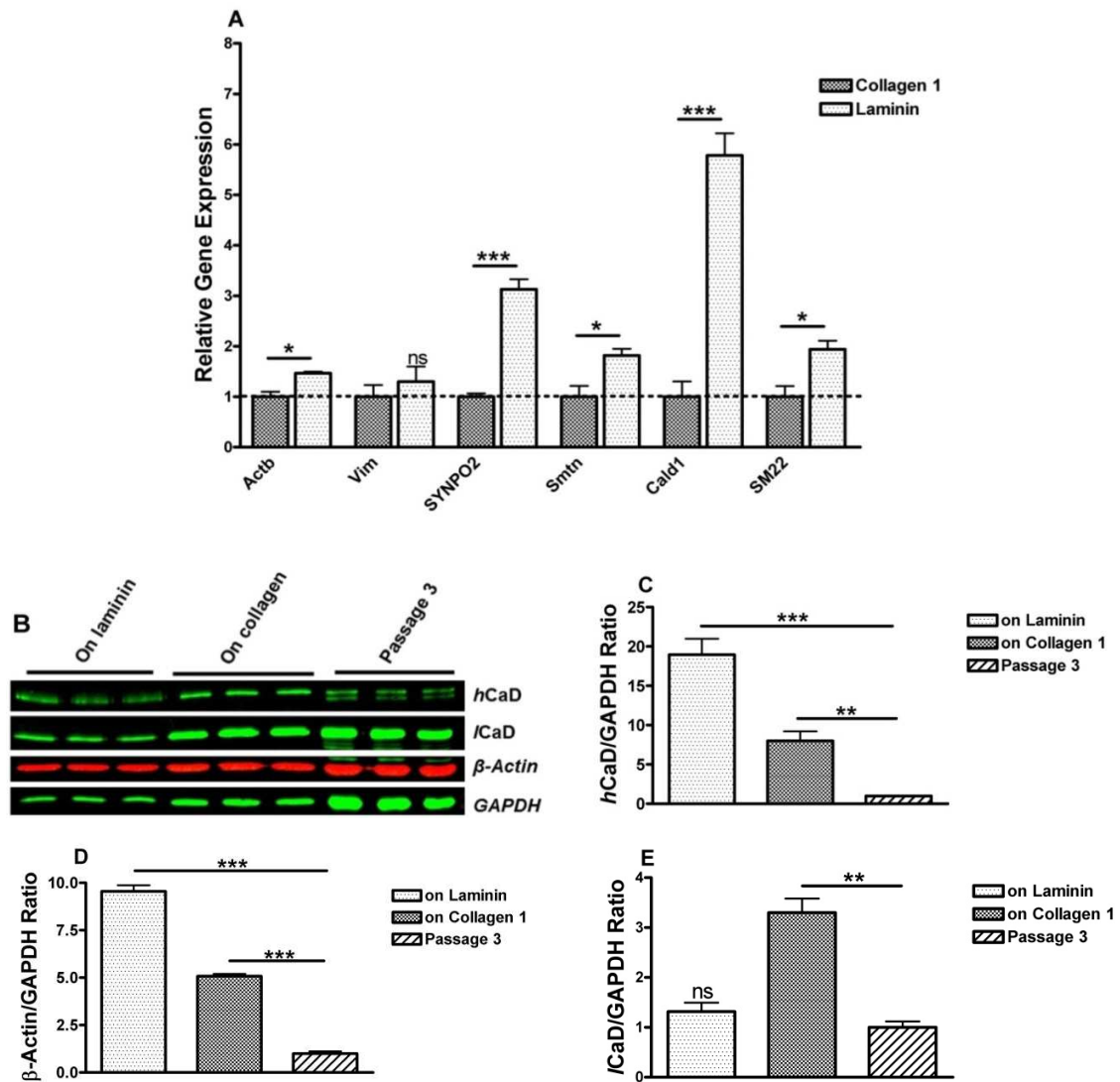


Fig. 13 Characterization of VSMCs cultivated on polyacrylamide matrices coated with extracellular matrix proteins. VSMCs from passage 2 were seeded on laminin or collagen I coated polyacrylamide matrices 48 h prior the experiments. For mRNA quantification, cells were harvested mechanically, total-RNA was isolated using a Maxwell 16 LEV RNA tissue kit, and cDNA was synthesized with a QuantiTect Reverse Transcription Kit. Real-time PCR was carried out from three independent experiments in triplicate, using GAPDH as an endogenous control. Expression levels are measured as an expression of target mRNA in on collagen I cultivated cells (gray bars) relative to that of on laminin grown cells (black bars) (A). For semi-quantitative Western blots (B) cells were disconnected using RIPA buffer. The proteins were separated on 10% SDS polyacrylamide gels, transferred in a tank blot apparatus to nitrocellulose and probed with anti-β-actin, anti-caldesmon and anti-GAPDH antibodies. The statistical results of these analyses are shown in the following: hCaD-GAPDH ratio (C), β-actin-GAPDH ratio (D), and ICaD-GAPDH ratio (E). For all experiments control cells of the same passage were grown in untreated culture dishes. Histograms show means ± SEM (n=3), \*\*\*p < 0.0001; \*\*p < 0.001; \*p < 0.01.

### 3.7 Cultivation the cells on ECM proteins pre-coated matrices alter subcellular localization of SYNPO2

The phenotype of VSMCs was determined using qRT-PCR and Western blotting, when cultivated on laminin or collagen I coated polyacrylamide matrices. In the following we focused on the shape of the cells grown under these conditions and the subcellular localization SYNPO2 occupies in the established phenotypes. In agreement with the literature<sup>146</sup>, we observed spindle form, elongated VSMCs upon cultivation on laminin coated matrices (Fig. 14B). In contrast, cells grown on collagen I had a flattened, widespread appearance typical for dedifferentiated VSMCs (Fig. 14A).

Using a polyclonal antibody against SYNPO2, combined with a Fluorescent labeled secondary antibody, we detected endogenous SYNPO2 in the cytoplasm and around the nucleus of VSMCs with the characteristics of differentiated smooth muscle cells. In contrast, most of the cells grown under conditions promoting a dedifferentiated phenotype exhibited the endogenous SYNPO2 in the nucleus (Fig. 14A). The difference of the SYNPO2 distributions between both phenotypes was highly significant ( $p < 0.0001$ ).

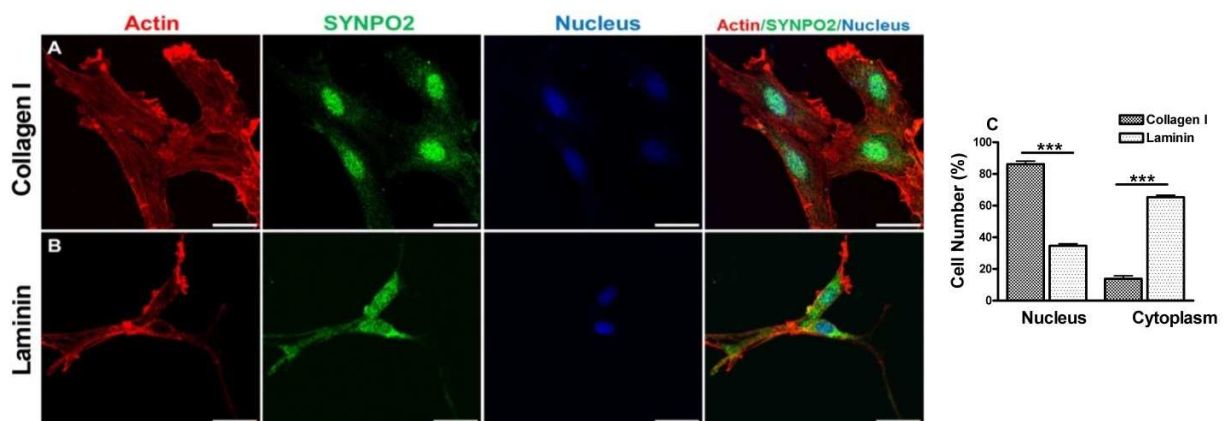


Fig. 14 On laminin coated polyacrylamide matrices cultivated VSMCs develop a contractile phenotype. VSMCs passage 2 was seeded on collagen I (A) or laminin (B) coated polyacrylamide matrices with a stiffness of 55 kPa 48 h prior experiments. Cells were fixed with 4% PFA, permeabilized with Triton-X100, and blocked with 5% BSA in PBS for 1h prior incubation with antibodies. Synaptopodin 2 was detected with a polyclonal anti-SYNPO2 antibody (1:5000) and visualized using an Alexa<sup>®</sup>488 conjugated secondary antibody (1:1000). F-actin was visualized using Alexa<sup>®</sup>555 conjugated phalloidin (0.2 U/ml), the nucleus was stained with Hoechst 33342 (10  $\mu$ g/ml). Quantitative analysis shows a significant reduction in the number of nuclear synaptopodin 2 displaying cells grown on laminin, while those grown on collagen I show a nuclear distribution (C). Means  $\pm$  SEM, n=4 (150 cells from each experiment), \*\*\* $p < 0.0001$ . Scale bars represent 20  $\mu$ m.

### 3.8 Actin cytoskeleton turnover affects subcellular distribution of SYNPO2

In order to investigate whether actin cytoskeleton turnover affects subcellular localization of SYNPO2, VSMCs were treated with 0.5  $\mu$ M cytochalasin D (CCD) and 0.1  $\mu$ M jasplakinolide (JASP), or with DMSO (0.04%) as vehicle control, respectively. Cells cultivated on collagen I coated matrices showed a strong accumulation of SYNPO2 in the nucleus and a diffuse staining in the cytoplasm (Fig. 15A). When cells were grown on collagen I coated polyacrylamide matrices and treated with either CCD or JASP, the most of the stress fibers were disrupted. The majority of SYNPO2 localized in the nucleus, regardless whether the actin cytoskeleton was treated with CCD or JASP (Fig. 15B-C). In contrast, when the actin cytoskeleton was not completely impaired, SYNPO2 staining was also found in the cytoplasm where it co-localized with the remaining F-actin structures (Fig. 15B & C, insets). F/G-actin ratio was measured, in order to quantify and to compare the F/G-actin ratio from the cells treated with CCD, JASP and also vehicle control. Cells seeded on collagen I coated matrices demonstrated a significant reduction of G-actin, when the cells were treated with JASP, while cells treated with CCD did not demonstrate significant changes in the F/G-actin ratio as compared to vehicle control (Fig. 15D).

Fig. 15E-G shows the distribution of SYNPO2 in cells grown on a laminin coated polyacrylamide matrix under control conditions (E) and after treatment with CCD (F) or JASP (G). The vehicle control with DMSO (E) showed the same cytoplasmic distribution, we observed earlier. Manipulating the actin cytoskeleton by application of CCD (F) or JASP (G) caused a disruption of stress fibers as shown by IF, which in turn accompanied by a strong enrichment of SYNPO2 around the nucleus. However, quantification of F/G-actin ratio demonstrated a significant increase of F-actin, when the cells were treated with JASP as compared to the vehicle control (Fig. 15H). In cells that had still some actin fibers we observed a colocalization of SYNPO2 with F-actin in the cytoplasm (see inset Fig. 15F & G).

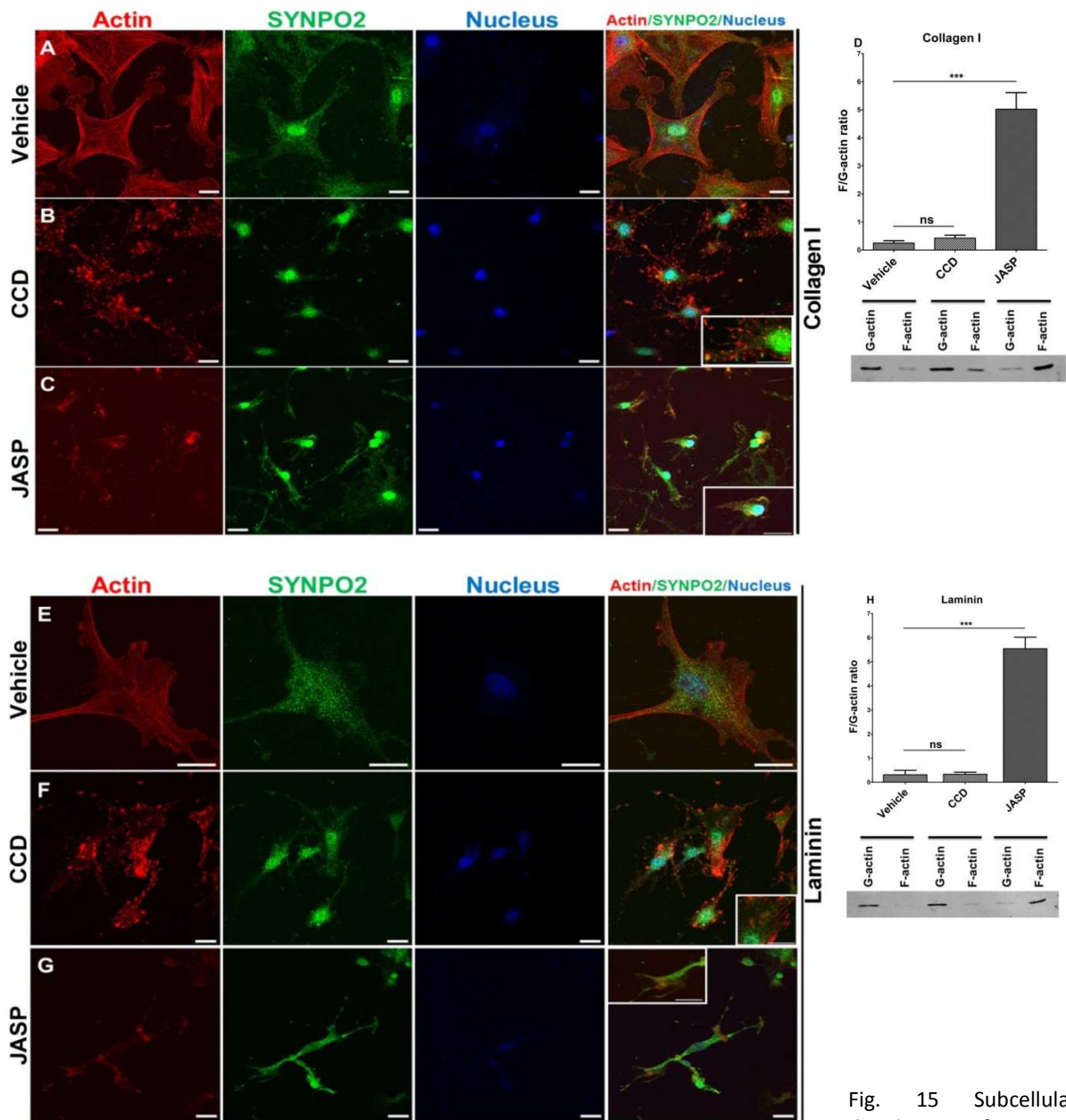


Fig. 15 Subcellular distribution of SYNPO2

during actin cytoskeleton turnover. VSMCs passage 2 (non-contractile) seeded on laminin or collagen I precoated polyacrylamide were treated with 0.04% DMSO as vehicle control (A & E) or in addition with 0.5  $\mu$ M CCD (B & F) or 0.1  $\mu$ M JASP (C & G) and incubated for 1 h at 37°C, 5% CO<sub>2</sub>. Cells were used to analyze F/G-actin ratio (D & H) or fixed with 4% PFA, permeabilized with 0.4% Triton-X100, and blocked with 5% BSA in PBS for 1h prior incubation with antibodies. SYNPO2 was detected with a polyclonal anti-SYNPO2 antibody (1:5000) and visualized using an Alexa<sup>®</sup>488 conjugated secondary antibody (life technology, 1:1000). F-actin was visualized using Alexa<sup>®</sup>555 conjugated phalloidin (life technology, 1:1000), the nucleus was stained with Hoechst 33342 (1:1000). F/G-actin ratio experiment was performed by F/Actin kit (Cytoskeleton) and the results are presented as means  $\pm$  SEM from three independent experiments performed in triplicate, performed in triplicate (D & H). Scale bars represent 20  $\mu$ m.

### 3.9 Heat Shock Stress did not affect the Subcellular Localization of SYNPO2 in VSMCs

Previous reports showed that heat shock induces nuclear accumulation of GFP-SYNPO2 (murine) in C2C12 myoblasts<sup>77</sup>. In order to test whether heat shock causes the same subcellular accumulation of SYNPO2 in VSMCs, in three independent experiments, heat shock at 43°C was applied for 90, 120, and 150 min respectively. With exception of heat exposure for an elongated time of 150 min, no change of the endogenous SYNPO2 distribution was observed (Fig. 16). This means, that the majority of the SYNPO2 protein was still in the cytoplasm of the VSMCs. Elongated exposure to high temperature (150 min at 43°C) resulted in a more punctuated distribution of SYNPO2.

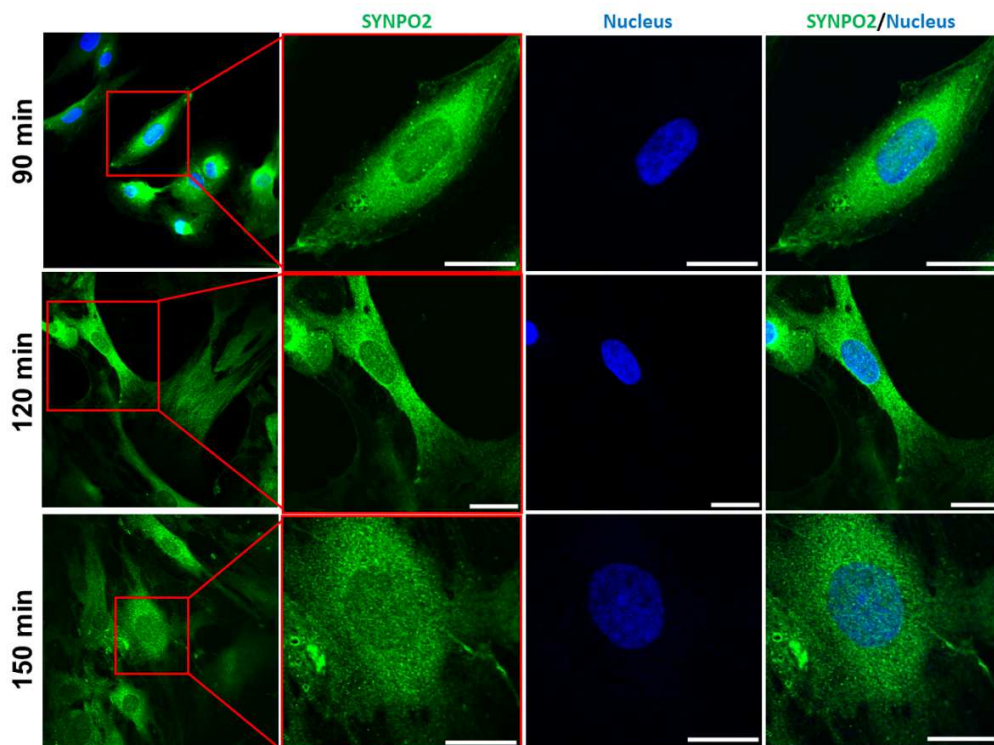


Fig. 16 Distribution of smooth muscle cells SYNPO2 is independent of heat stress. Isolated VSMCs were seeded on coverslips (precoated with 0.1% gelatin), and grown for 12 h before heat stress was applied. Cells were incubated at 43°C for 90, 120, and 150 min in a pre-warmed water bath. Cells were immunostained with anti SYNPO2 antibody (1:5000) as first antibody and Alexa-488 conjugated goat anti-rabbit IgG (1:1000) for 1h at RT. The cell nucleus was visualized by using Hoechst 33342 (1:1000). Scale bar represents 20  $\mu\text{m}$ .

### 3.10 Subcellular distribution of SYNPO2 is controlled by cAMP

Although, in the past years, several studies on GFP-SYNPO2 (murine) showed that an increased cAMP level in striated muscles is essential for phosphorylation and in turn its subcellular distribution in cardiac myocytes<sup>100, 101</sup>, this mechanism in VSMCs has never been investigated before.

In order to study the effect of cAMP dependent signaling pathways on trafficking of SYNPO2, cells were treated with agonist, which activate adenylyl cyclase and therefore raise the level of cAMP in the cells. While under control conditions (0.01% DMSO) SYNPO2 was found in the cell cytoplasm and around the nucleus (Fig. 17A), urocortin (Fig. 17B), and forskolin (Fig. 17D) treated cells demonstrated a strong accumulation of SYNPO2 to the nucleus. Cells treated with the cAMP analogue Sp-5,6-DCI-cBIMPS (5, 6-Dichloro-1-β-D-ribofuranosylbenzimidazole-3', 5'-cyclic monophosphorothioate, Sp-isomer) also increased SYNPO2 accumulation to the nucleus (Fig. 17C). Treatment of the cells with a combination of forskolin and IBMX (phosphodiesterase inhibitor) resulted in a diffuse distribution of SYNPO2 in the cells, with a markedly derogated concentration at the cell boundaries/leading edge and an accumulation in and around the cell nucleus (Fig. 17). Statistical analyses demonstrated a significant increase in the number of nuclear SYNPO2-displaying VSMCs after upregulation of cAMP by urocortin, forskolin, and Sp-5,6-DCI-cBIMPS. However, in the case of cells, treated with both forskolin and IBMX, the number of nuclear SYNPO2-displaying cells was significantly decreased (Fig. 17F).

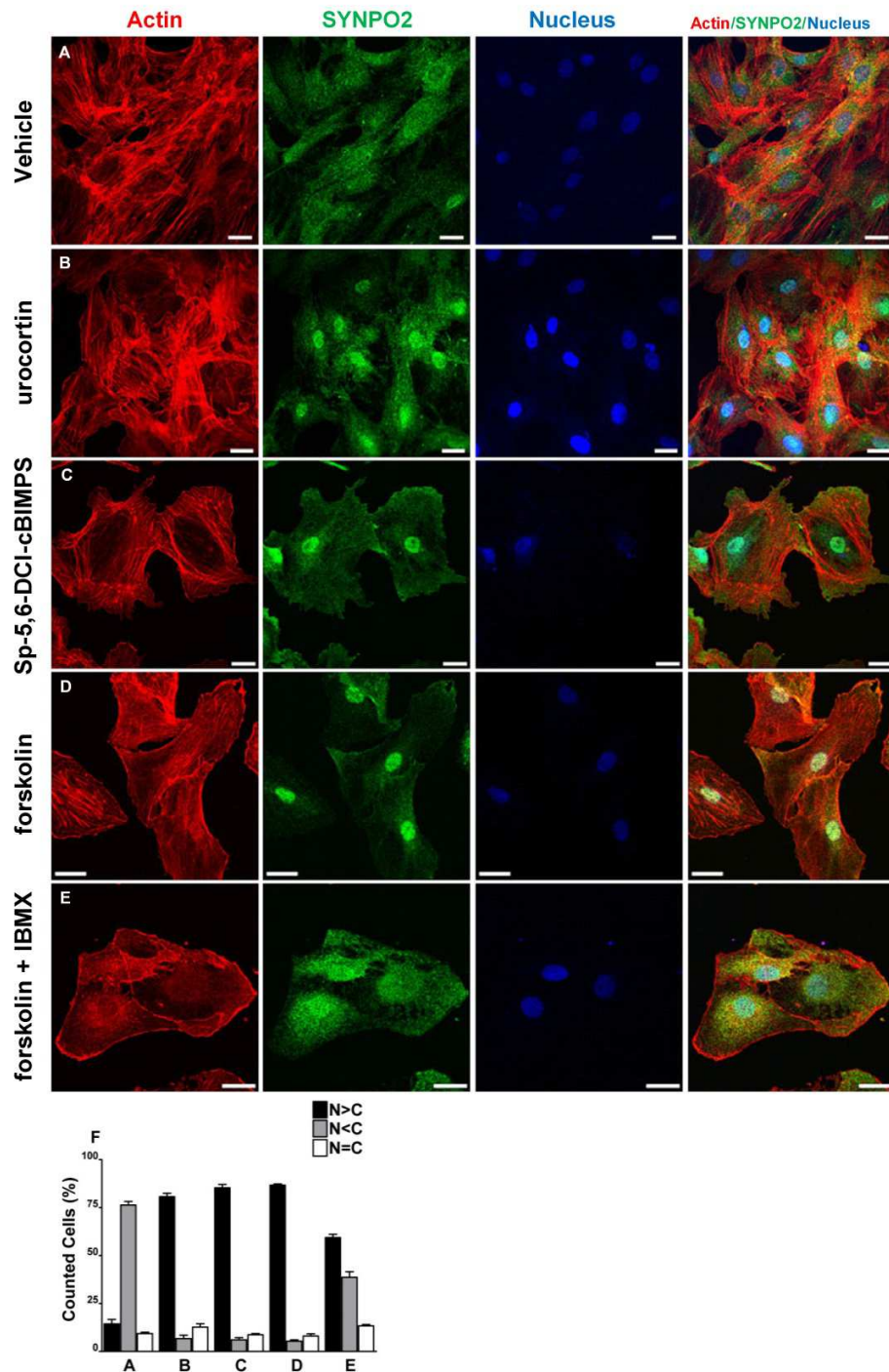


Fig. 17 cAMP-induced shuttling of SYNPO2 in VSMCs. VSMCs were treated with 0.01% DMSO as vehicle control (A), 100 nM urocortin (B), 10  $\mu$ M Sp-5,6-DCI-cBIMPS (C), 10  $\mu$ M forskolin (D), or 10  $\mu$ M forskolin-IBMX (E) for 1 h and immunostained with anti-SYNPO2 (1:5000, green). Cell nucleus (blue) and the actin cytoskeleton (red) were visualized with Hoechst 33342 (1:1000) and Alexa-555 conjugated phalloidin (1:1000). Statistical analysis was performed using two-sample Student's t test (F). Results are shown as the means  $\pm$  SEM from four independent experiments performed in triplicate (150 cells from each experiment). Scale bars represent 20  $\mu$ m. N>C, N<C and N=C represent nuclear, cytoplasmic, and equally distributed SYNPO2-displaying cells, respectively.

### 3.11 Inhibition of PKA and CaMK-II reduced the accumulation of SYNPO2 in the nucleus of VSMCs

In passages 2-4, where SYNPO2 mainly localized to the nucleus (Fig. 18A), inhibition of PKA by Rp-8-PIP-cAMPs (8-Piperidinoadenosine-3',5'-cyclic monophosphorothioate, Rp-isomer sodium salt) reduced the amount of nuclear SYNPO2, and demonstrated a diffuse localization around the cell nucleus (Fig. 18B). Similarly to the Rp-8-PIP-cAMPs, H89 (*N*-[2-[[3-(4-Bromophenyl)-2-propenyl]amino]ethyl]-5-isoquinolinesulfonamide dihydrochloride) treated cells demonstrated a reduction in nuclear SYNPO2, whereas cytoplasmic distribution of SYNPO2 was more consistent (Fig. 18C). Inhibition of CaMKII with a commercially available inhibitor KN93 (*N*-[2-[[[3-(4-Chlorophenyl)-2-propenyl]methylamino]methyl]phenyl]-*N*-(2-hydroxyethyl)-4-methoxybenzenesulphonamide) resulted in a slight reduction of nuclear SYNPO2 as compared to the PKA inhibition (Fig. 18D). Further quantitative analysis of treated cells with inhibitors as compared to the vehicle controls indicated a significant reduction of the number of nuclear SYNPO2-displaying cells (Fig. 18E).

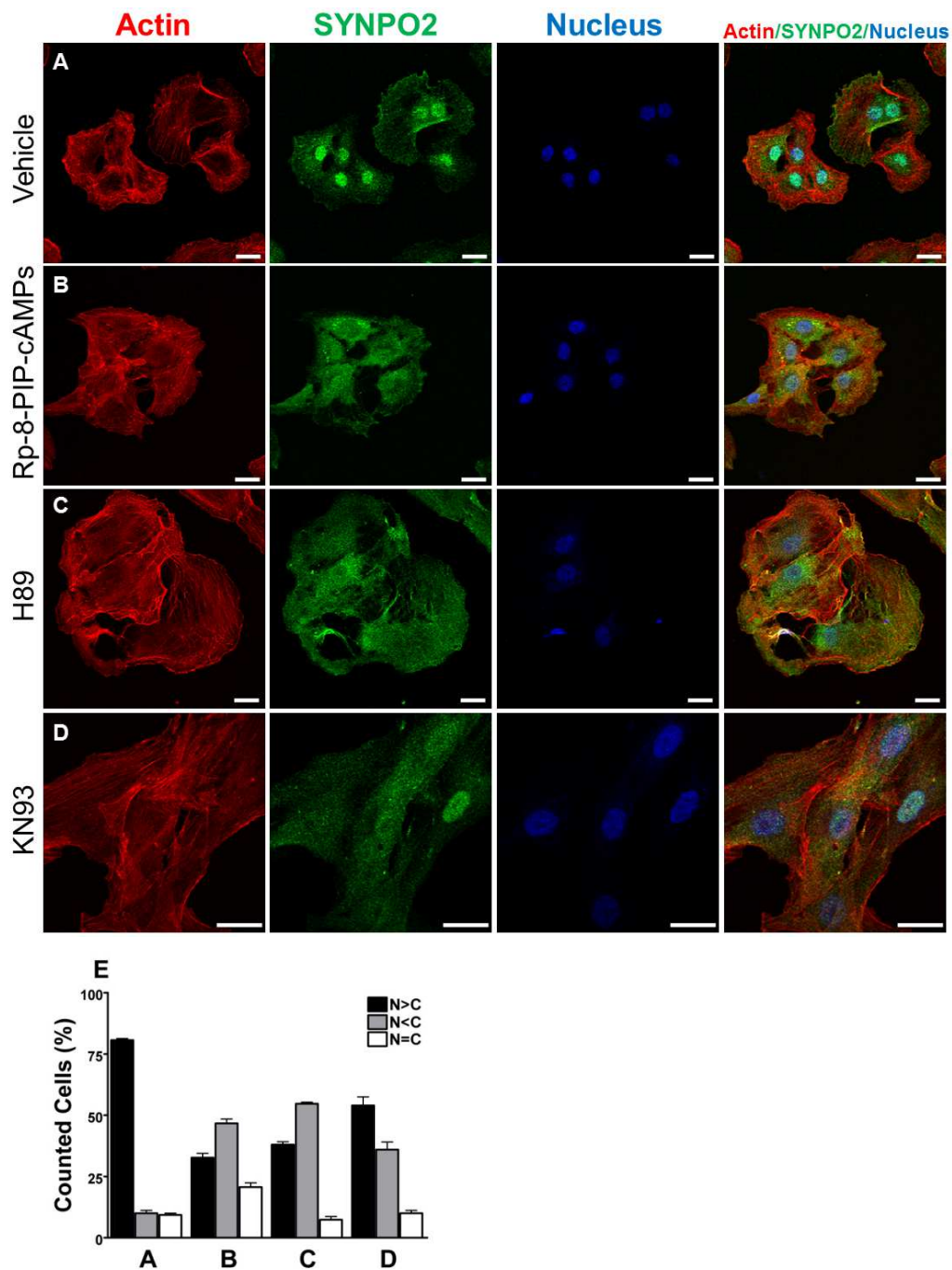


Fig. 18 Inhibition of both PKA and CaMKII reduced nuclear accumulation of SYNPO2 in the isolated VSMCs. VSMCs from passage 2 to 4 were treated with 0.01 % DMSO (A) as vehicle control, 100  $\mu$ M Rp-8-PIP-cAMPs (B) and 10  $\mu$ M H89 (C) as PKA inhibitors or 10  $\mu$ M KN93 (D) as a CaMKII inhibitor for 1 h. Statistical analysis (E) demonstrated at least four independent experiments performed in triplicate (150 cells from each experiment). Means  $\pm$  SEM are shown. Scale bars represent 20  $\mu$ m. N>C, N<C and N=C represent nuclear, cytoplasmic, and equally distributed SYNPO2-displaying cells, respectively.

### 3.12 ROCK signaling does not affect subcellular localization of SYNPO2

Treatment of VSMCs, passage 2-4, with the ROCK inhibitor, Y-27632 (10  $\mu$ M) caused disruption of stress fibers (Fig. 19B), while vehicle controls showed the characteristic actin cytoskeleton (Fig. 19A). However, this disruption of actin fibers was not accompanied by a change of the subcellular SYNPO2 distribution. Statistical analysis using Student's t-test did not show any significant alteration in subcellular localization of SYNPO2 in Y-27632 treated cells compared to the control.

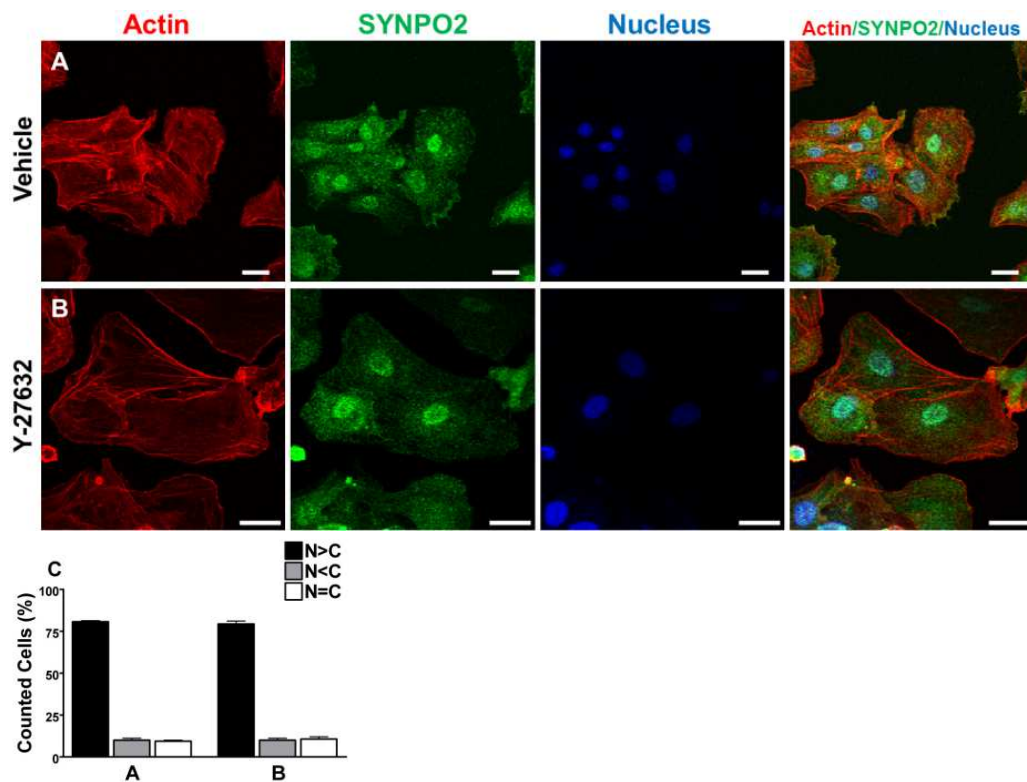


Fig. 19 Inhibition of ROCK had no effects on the subcellular localization of SYNPO2. Cells from passage 3, seeded on 0.1% gelatin pre-coated coverslips, and incubated in serum free medium (2 h) were grown without treatment (A) as vehicle control or were treated with 10  $\mu$ M Y-27632 (B) as a ROCK inhibitor for 1 h. For statistical comparison between Y-27632 treated cells and vehicle (C), two-sample Student's t test was used. A p value < 0.05 was considered statistically significant. Scale bars represent 20  $\mu$ m and results are shown as means  $\pm$  SEM (n=4), for 150 cells from each experiment. N>C, N<C and N=C represent nuclear, cytoplasmic, and equally distributed myopodin-displaying cells, respectively.

### 3.13 Treatment with okadaic acid resulted in a reduction of nuclear SYNPO2-displaying cells

In order to investigate whether protein phosphatases (PP1 and PP2A) affect the distribution of SYNPO2, VSMCs were incubated with okadaic acid (OA) to provide a complete inhibition of both phosphatases. Inhibition of phosphatases reduced significantly the number of nuclear SYNPO2-displaying cells (Fig. 20B). As expected from the results (Fig. 17 and 18), phosphorylation seems to be crucial for nuclear import and export of SYNPO2. Quantitative analysis of cells displaying nuclear SYNPO2 demonstrated a significant accumulation of SYNPO2 in the cytoplasm upon the treatment with OA (Fig. 20C).

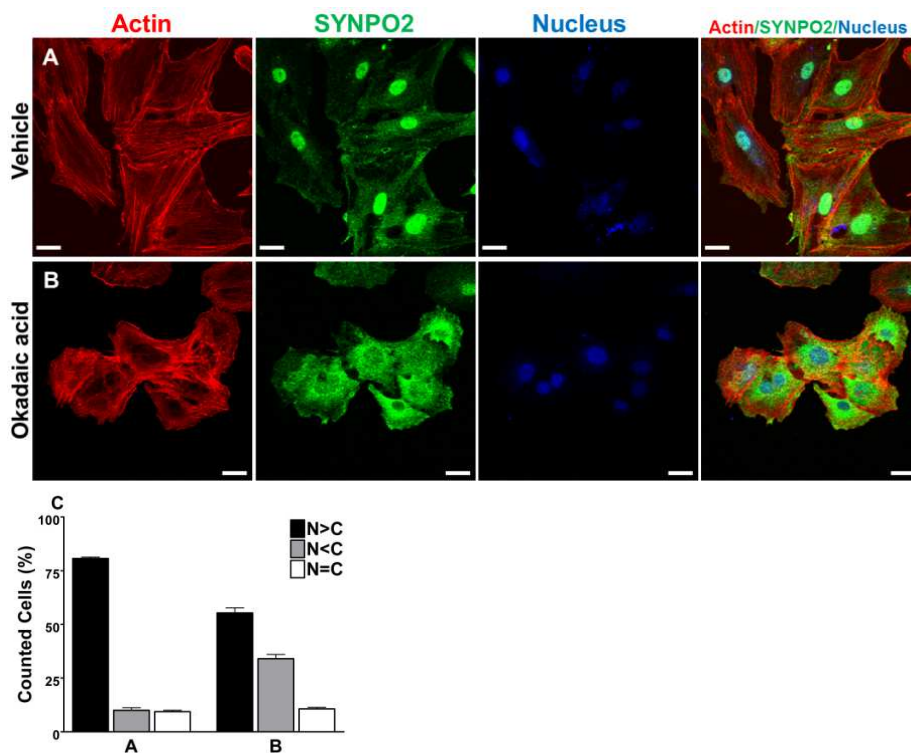


Fig. 20 Okadaic acid induced accumulation of SYNPO2 in the cytoplasm. After serum depletion for 2 h, untreated cells (A) or cells incubated with the phosphatase inhibitor okadaic acid (100 nM) for 1 h (B) were fixed, permeabilized, and treated with anti-SYNPO2, Phalloidin-Alexa555, and Hoechst 33342 as described before. Scale bars represent 20  $\mu$ m. Quantitative statistical analysis (C), was performed with the two-sample Student's t-test. At least four independent experiments were performed in triplicate. Results are shown as means  $\pm$  SEM. N>C, N<C and N=C represent nuclear, cytoplasmic, and equally distributed myopodin-displaying cells, respectively.

### 3.14 Characterization of expression level of 14-3-3 isoforms in VSMCs

Previous works already showed that 14-3-3 proteins are an important player at the subcellular shuttling of SYNPO2 in the cell<sup>100, 101</sup>. This could of course also imply a functional relevance of its isoforms at the differentiation states of VSMCs and in turn also at the trafficking of SYNPO2. However, no reports are currently available to test the functionality of the 14-3-3 isoforms experimentally in this term. Accordingly, we next tested the hypothesis that 14-3-3 isoforms change their expression level during phenotype switch of VSMCS and therefore they regulate different step of this shuttling. To test this, expression level of seven 14-3-3 isoforms were analyzed using quantitative real-time PCR. As shown in Fig. 21, the mRNA level of the 14-3-3 $\tau$ ,  $\eta$ , and  $\zeta$  were more abundant on the first day of isolation than at passage 3, while the mRNA level of isoform  $\sigma$  was higher at passage 3. The significance level of 14-3-3 $\eta$  expression was  $p < 0.02$  as determined by a two-tailed student's t-test. For 14-3-3 $\tau$ , and  $\zeta$  the significance was  $p < 0.001$ . We found a higher expression of 14-3-3 $\sigma$  upon dedifferentiation of VSMCs with a significance level of  $p < 0.005$ . Interestingly, no significant changes in mRNA level of the isoforms  $\beta$ ,  $\gamma$ ,  $\epsilon$  was detected at passage 3 in VSMCs compared to cells from day 1.

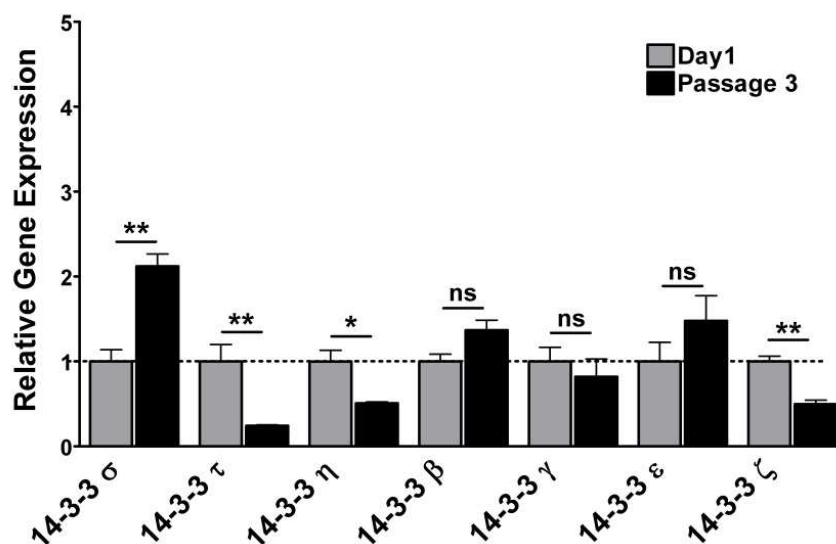


Fig. 21 Expression analysis of 14-3-3 isoforms in primary rat VSMCs. Quantitative RT-PCR from VSMCs from rat aorta on day 1 of isolation and passage 3 of cultivation. qRT-PCR was performed from three independent experiments in triplicates using 20 ng cDNA in each reaction. GAPDH was used as an endogenous control. Expression levels are shown as the expression of target mRNA from cells of day 1. Histograms show means  $\pm$  SEM ( $n=3$ ), \*\*\* $p < 0.0001$ ; \*\* $p < 0.001$ ; \* $p < 0.01$  (A).

### 3.15 Analysis of subcellular localization of SYNPO2 and its interaction with 14-3-3 $\beta/\gamma$ , and importin $\alpha$ using fluorescent fused proteins and BIFC assay

In 2005 and 2007, Faul et al. showed that interaction of SYNPO2 with 14-3-3 $\beta$  and importin $\alpha$  leads to its accumulation in the nucleus of C2C12 cells<sup>100, 101</sup>. Moreover, it is already reported that of the seven isoforms comprising this family, 14-3-3 $\gamma$  and  $\beta$  have been shown to be expressed in VSMCs<sup>147-150</sup>. Accordingly, we next investigated the subcellular localization of SYNPO2, 14-3-3 $\gamma/\beta$ , and importin $\alpha$  and their interaction together in living cells by designing and combining different fluorescent proteins (Fig. 22 A and B).

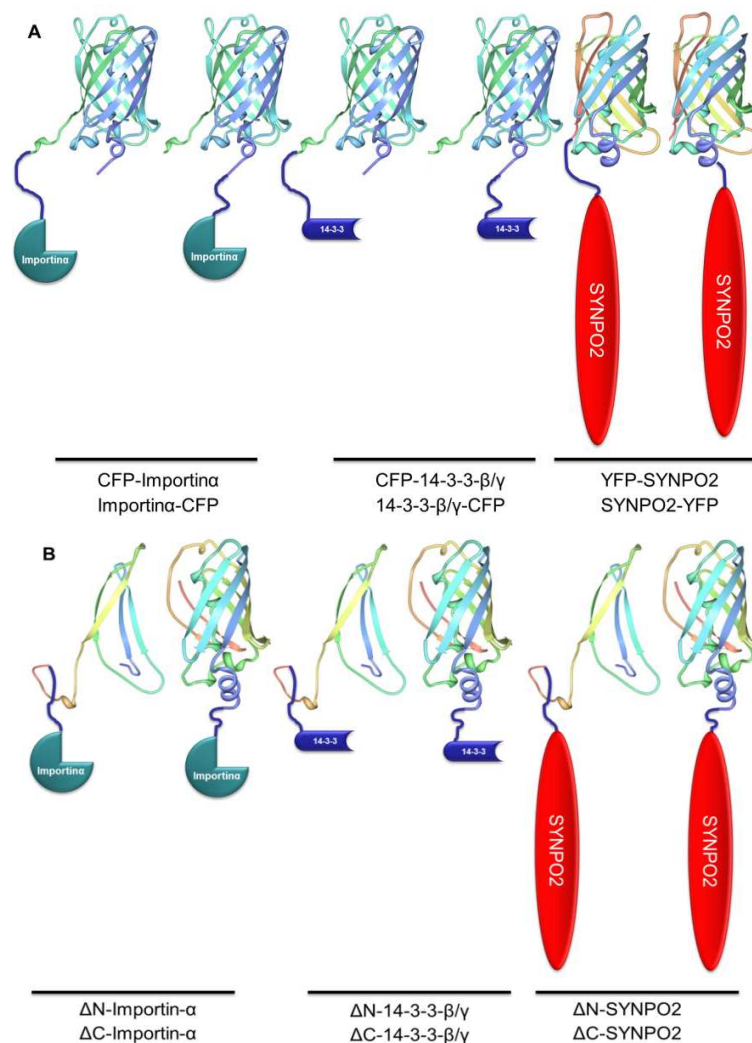


Fig. 22 Schematic illustration of constructs used for SYNPO2, 14-3-3 $\gamma/\beta$  & importin $\alpha$  interaction and localization analysis by BIFC and a FACS-BIFC based assays. (A) Schematic representation of SYNPO2, 14-3-3 $\beta/\gamma$  and importin $\alpha$  proteins fused to YFP, CFP, and (B) Non-fluorescent fragments of YFP ( $\Delta$ C-YFP-1-158,  $\Delta$ N-YFP-159-238) fused to N-terminus of SYNPO2, 14-3-3 $\beta/\gamma$  and importin $\alpha$  proteins.

In order to validate the accuracy and the expression level of the fluorescent fused proteins, designed vectors were transiently transfected in HEK293 cells by the calcium phosphate method and in each case Western blotting was used to demonstrate the results. The fluorescent fused proteins were detected by probing the membrane with rabbit anti-YFP/CFP antibody. Detected bounds on membrane demonstrated calculated molecular mass for both N-or C-terminus fluorescent fused SYNPO2, 14-3-3 $\gamma$  (Fig. 23A) and for 14-3-3 $\beta$ , and importin $\alpha$  (Fig. 23B). BIFC constructs were detected using a mouse polyclonal anti-GFP antibody (Fig. 23C).

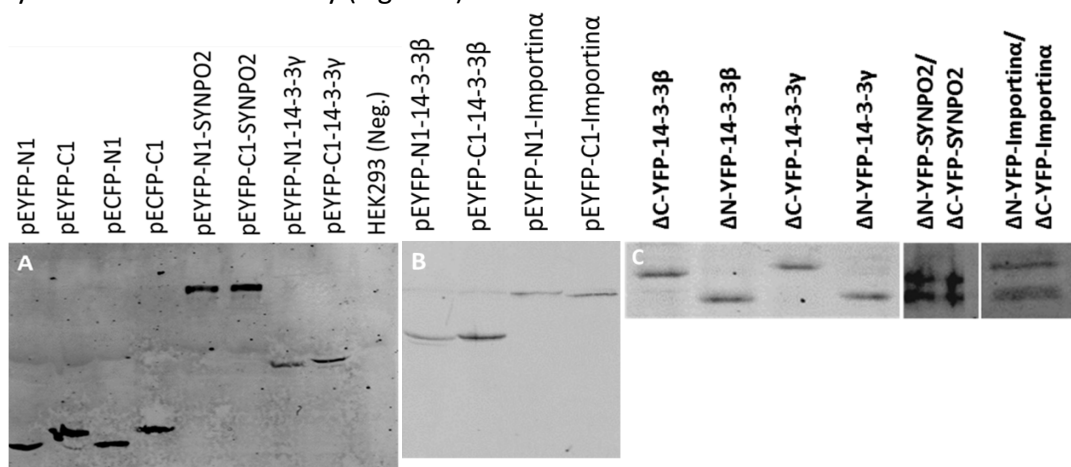


Fig. 23 Expression analysis of fluorescent fused proteins. Samples of (A) N- and C-terminus CFP fused 14-3-3 $\gamma$  around 55 kDa (calculated MW= 55610 Da), N- and C-terminus YFP fused SYNPO2 at around 102 kDa (Calculated MW= 102553 Da) and, (B) N- and C-terminus CFP fused importin $\alpha$  around (calculated MW=55669 Da) and 14-3-3 $\beta$  around (calculated MW=55669 Da) were subjected to SDS-PAGE and Western blotting. C) Protein expression analysis of  $\Delta$ N-,  $\Delta$ C-YFP fused SYNPO2, 14-3-3 $\gamma$ / $\beta$ , and Importin $\alpha$  showed also MW of each protein as same as we calculated for each by ExPASy website.

### 3.16 Subcellular localization of YFP-fused SYNPO2 & CFP-fused 14-3-3 $\gamma$ / $\beta$ , importin $\alpha$

Fluorescent fused proteins allowed subcellular localization, colocalization and interaction studies, between SYNPO2, 14-3-3 $\gamma$ / $\beta$  and importin $\alpha$  in the cellular context. In order to perform the localization studies, N- and C-terminus YFP fused SYNPO2, N- and C-terminus CFP-fused-14-3-3 $\gamma$  or  $\beta$  and N- and C-terminus CFP-fused importin $\alpha$  were used. YFP-SYNPO2 was strongly accumulated in the nucleus of HEK293 cells, either in form of a loop structure (Fig. 24A, white arrow), which seems to be an actin loop as described before<sup>77</sup>

and/or in forms similar to nuclear bodies as reported earlier<sup>151</sup> (Fig. 24A', arrowhead). However, cells transfected with SYNPO2-YFP, C-terminal fused YFP, mostly showed a diffuse distribution of SYNPO2 in both cell nucleus and cytoplasm of HEK293 cells. Notably, it did not detect definable structure in this case (Fig. 24B & B'). CFP-14-3-3 $\gamma$  was mainly accumulated in the cytoplasm of HEK293 cells (Fig. 24C & C'), which in turn was also detected for 14-3-3 $\gamma$ -CFP, respectively (Fig. 24D & D'). CFP-14-3-3 $\beta$  (Fig. 24E & E') and 14-3-3 $\beta$ -CFP (Fig. 24F & F') were mainly localized in the cytoplasm of transfected cells. HEK293 cells transfected with CFP-importin $\alpha$  (Fig. 24G & G') and importin $\alpha$ -CFP (Fig. 24H & H') showed a strong accumulation of importin $\alpha$  in the cell nucleus and a slight distribution in the cytoplasm. Interestingly, cells transfected with both constructs of importin $\alpha$  demonstrated also a nucleolar or nuclear bodies similar localization of importin $\alpha$  in both cases (Fig. 24G to H', white arrows).

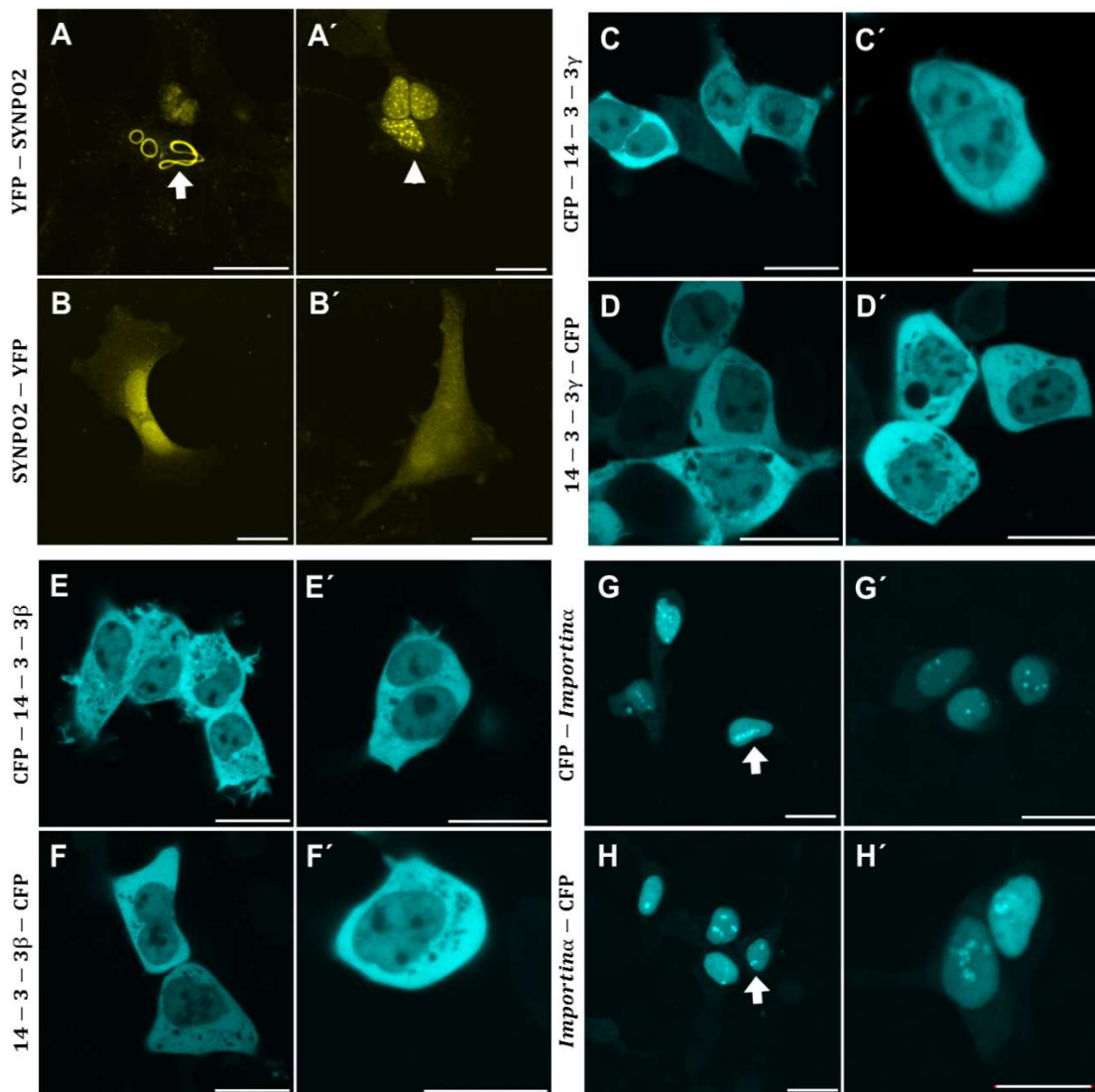


Fig. 24 Subcellular distribution of fluorescent fusion proteins in living cells detected by confocal laser scanning microscopy. Confocal fluorescence images of HEK293 cells transiently transfected with 300 ng of plasmids expressing the indicated YFP fused SYNPO2 (A & B) and CFP fused 14-3-3 $\gamma$  (C & D), 14-3-3 $\beta$  (E & F), and importin $\alpha$  (G & H) by the calcium phosphate method. CFP-fluorescent emission of transfected cells is shown in blue (excitation 458 nm, emission 465–495 nm) and YFP-fluorescent emission is shown in yellow (excitation 514 nm, emission 525–565 nm). At least three independent experiments were performed in triplicate. Scale bars present 20  $\mu$ m.

### 3.17 Analysis of SYNPO2, 14-3-3 $\gamma/\beta$ and importin $\alpha$ interaction by using BIFC

In order to investigate the physical interaction between SYNPO2, 14-3-3 $\beta/\gamma$ , and importin $\alpha$  in the living cell, it was tested whether both  $\Delta$ N-YFP-SYNPO2 and  $\Delta$ C-YFP-SYNPO2 interact with  $\Delta$ N-,  $\Delta$ C-YFP fused 14-3-3 $\beta/\gamma$  and importin $\alpha$  based on fluorescence development according to BIFC principle<sup>125</sup>.

#### 3.17.1 SYNPO2 interacts with 14-3-3 $\gamma$ in the cytoplasm and not in the nucleus

To analyze the interaction between SYNPO2 and 14-3-3 $\gamma$ , cells were transiently cotransfected with equal amounts (300 ng) of the constructs and incubated for 24 to 48 h at a humidified atmosphere. Fig. 25 shows representative images of both the control and the interaction experiments. Control experiments (Fig. 25A & D) did not show any fluorescence development between non-fluorescent fragments ( $\Delta$ C-YFP-1-158 and  $\Delta$ N-YFP-159-238) with  $\Delta$ N-YFP-14-3-3 $\gamma$  and/or  $\Delta$ C-YFP-14-3-3 $\gamma$  fragments. Interaction between both  $\Delta$ N- and  $\Delta$ C-YFP fused SYNPO2 with 14-3-3 $\gamma$  was shown as fluorescence development that is shown in Fig. 25B and E. Interaction between 14-3-3 $\gamma$  and SYNPO2 was mainly detected in the cytoplasm and not in the nucleus. However, HEK293 cells cotransfected with  $\Delta$ N-YFP-14-3-3 $\gamma$  and  $\Delta$ C-YFP-SYNPO2 demonstrated pointed structures in the cytoplasm (Fig. 25E, white arrow), while the interaction between  $\Delta$ C-YFP-14-3-3 $\gamma$  and  $\Delta$ N-YFP-SYNPO2 was diffuse in the cytoplasm (Fig. 25B).

A FACS-BIFC based analysis confirmed the results from confocal imaging (Fig. 25C, F). Around 11% of HEK293 cells cotransfected with  $\Delta$ C-YFP-14-3-3 $\gamma$  and  $\Delta$ N-YFP-SYNPO2 (Fig. 25C) demonstrated a positive fluorescence development as compared to the negative control ( $\Delta$ N-YFP &  $\Delta$ C-YFP), while cells cotransfected with  $\Delta$ N-YFP-14-3-3 $\gamma$  and  $\Delta$ C-YFP-SYNPO2 showed a population of around 12% with positive fluorescence (Fig. 25F).

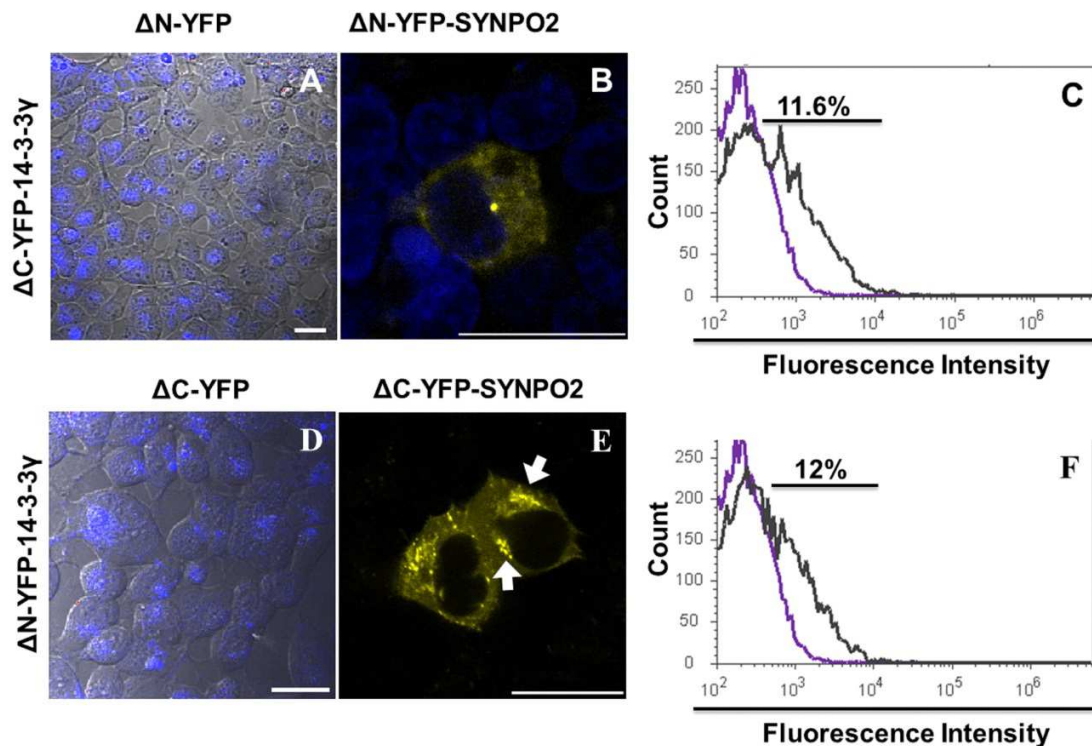


Fig. 25 Interaction between SYNPO2 and 14-3-3 $\gamma$  takes place in the cytoplasm of HEK293 cells. Transiently cotransfected HEK293 cells, seeded on ECL precoated coverslips with 300 ng of non-fluorescent plasmids using the calcium phosphate method. Confocal fluorescence images of control cells, cotransfected with  $\Delta C$ -YFP-14-3-3 $\gamma$ / $\Delta N$ -YFP (A),  $\Delta N$ -YFP-14-3-3 $\gamma$ / $\Delta C$ -YFP (D) and cells cotransfected with  $\Delta C$ -YFP-14-3-3 $\gamma$ / $\Delta N$ -YFP-SYNPO2 (B),  $\Delta N$ -YFP-14-3-3 $\gamma$ / $\Delta C$ -YFP-SYNPO2 (E). YFP-fluorescent emission is shown in yellow (excitation 514 nm, emission 525–565 nm). FACS-BIFC results from 10,000 events for  $\Delta C$ -YFP-14-3-3 $\gamma$ / $\Delta N$ -YFP-SYNPO2 (C),  $\Delta N$ -YFP-14-3-3 $\gamma$ / $\Delta C$ -YFP-SYNPO2 (F) as histogram.  $\Delta C$ -YFP/ $\Delta N$ -YFP cotransfected HEK293 cells was used as a control for FACS analysis (violet curve). At least three independent experiments were performed in triplicate. Scale bars present 20  $\mu$ m.

### 3.17.2 SYNPO 2 and 14-3-3 $\beta$ accumulate and form loop-like complexes in the nucleus

In order to analyze the interaction between SYNPO2 and 14-3-3 $\beta$ , transiently cotransfected HEK293 cells were used for both confocal imaging and FACS-BIFC based assay as described. Cells cotransfected with  $\Delta N$ -YFP-SYNPO2 and  $\Delta C$ -YFP-14-3-3 $\beta$  (Fig. 26B) demonstrated an interaction between SYNPO2 and 14-3-3 $\beta$  due to the fluorescence development as compared to the control cells cotransfected with  $\Delta C$ -YFP-14-3-3 $\beta$ / $\Delta N$ -YFP (Fig. 26A). Interestingly, confocal fluorescence images demonstrated a nuclear accumulation of SYNPO2-14-3-3 $\beta$  complex and protein aggregate in the cell (Fig. 26B, white arrow). Validation of the results by FACS-BIFC based assay (Fig. 26C) showed a population of around 10% positive cells as compared to the negative control ( $\Delta N$ -YFP &

$\Delta$ C-YFP). In HEK293 cells cotransfected with  $\Delta$ C-YFP-SYNPO2 and  $\Delta$ N-YFP-14-3-3 $\beta$  using calcium phosphate method, a nuclear localization of SYNPO2 and 14-3-3 $\beta$  was detected (Fig. 26E). Interestingly,  $\Delta$ C-YFP-SYNPO2/ $\Delta$ N-YFP-14-3-3 $\beta$  transfected cells demonstrated an accumulation and/or colocalization of SYNPO2-14-3-3 $\beta$  complex in the nucleus in form of a loop (Fig. 26E, white arrows) as we detected before (see Fig. 24A). Quantitative analysis of transfected HEK293 cells with  $\Delta$ C-YFP-SYNPO2/ $\Delta$ N-YFP-14-3-3 $\beta$  by FACS demonstrated 12% positive cell population of 10,000 events (Fig. 26F).

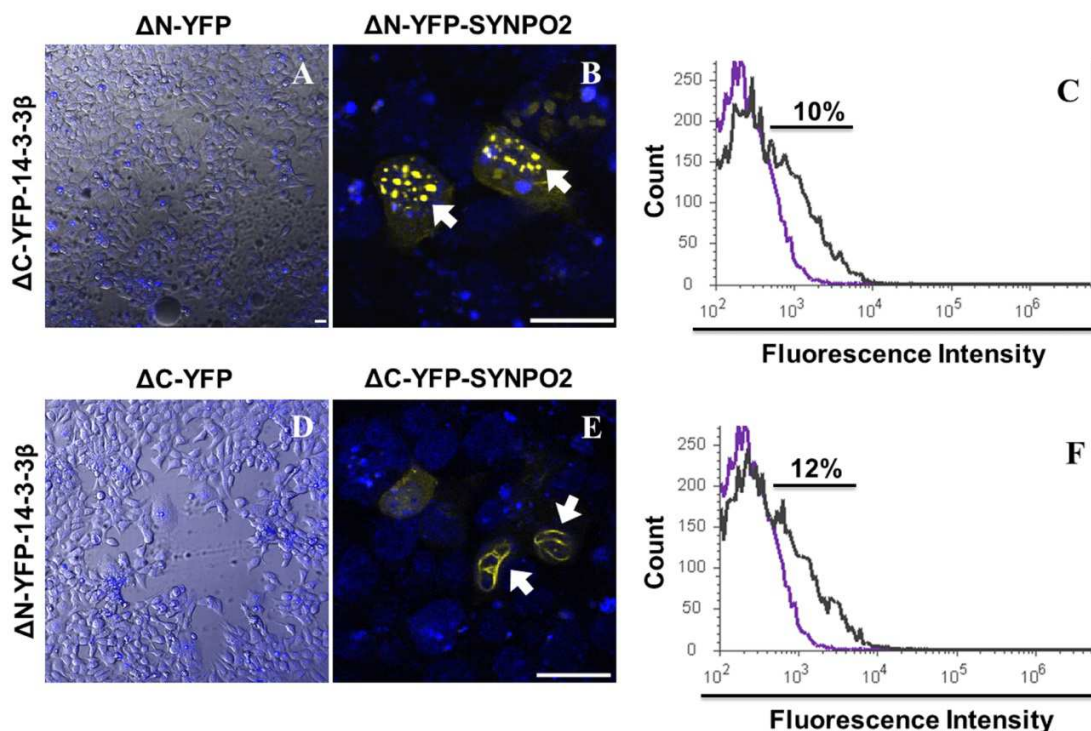


Fig. 26 SYNPO2 and 14-3-3 $\beta$  localized and formed a loop structure in the nucleus. HEK293 cells were transiently cotransfected with 300 ng of  $\Delta$ N-YFP &  $\Delta$ C-YFP-14-3-3 $\beta$  (A),  $\Delta$ N-YFP-SYNPO2 &  $\Delta$ C-YFP-14-3-3 $\beta$  (B),  $\Delta$ C-YFP &  $\Delta$ N-YFP-14-3-3 $\beta$  (D), and  $\Delta$ C-YFP-SYNPO2 &  $\Delta$ N-YFP-14-3-3 $\beta$  (E) using the calcium phosphate method. Quantitative FACS-BIFC analysis of 10,000 measured HEK293 cells cotransfected with  $\Delta$ N-YFP-SYNPO2 &  $\Delta$ C-YFP-14-3-3 $\beta$  (C), and  $\Delta$ C-YFP-SYNPO2 &  $\Delta$ N-YFP-14-3-3 $\beta$  (F).  $\Delta$ C-YFP/ $\Delta$ N-YFP cotransfected HEK293 cells was used as a control for FACS analysis (violet curve). At least three independent experiments were performed in triplicate. Scale bars present 20  $\mu$ m.

### 3.17.3 Preferred interaction of SYNPO2 and importin $\alpha$ in the nucleus

In order to investigate SYNPO2, importin $\alpha$  interaction in living cells, transiently cotransfected HEK293 cells seeded at 50% confluent on coverslips, were analyzed using an Olympus laser confocal microscope. HEK293 cells cotransfected with 300 ng of  $\Delta$ N-

YFP-SYNPO2/ $\Delta$ C-YFP-importin $\alpha$  (Fig. 27B) demonstrated a nuclear accumulation and/or interaction of SYNPO2 and importin $\alpha$ , while control experiment with HEK293 cells transfected with  $\Delta$ N-YFP/ $\Delta$ C-YFP-importin $\alpha$  did not show any fluorescence development (Fig. 27A). FACS analysis showed a population of around 12% of the cells in which fluorescence was detected (Fig. 27C). Confocal fluorescence imaging of the cells cotransfected with 300 ng of  $\Delta$ C-YFP-SYNPO2/ $\Delta$ N-YFP-importin $\alpha$  showed a nuclear distribution and/or interaction of SYNPO2/importin $\alpha$  (Fig. 27E). Analysis of the transiently transfected cells with  $\Delta$ C-YFP/ $\Delta$ N-YFP-Importin $\alpha$ , which was used as control experiment, revealed no fluorescent signal (Fig. 27D). Quantitative FACS-BIFC analysis of cells transfected with  $\Delta$ C-YFP-SYNPO2/ $\Delta$ N-YFP-Importin $\alpha$  demonstrated around 8% positive population of fluorescence positive cells (Fig. 27F). In both cases of the interaction study, an interaction/localization of SYNPO2-importin $\alpha$  complex in form of a loop were detected (Fig. 27B & E, white arrows).

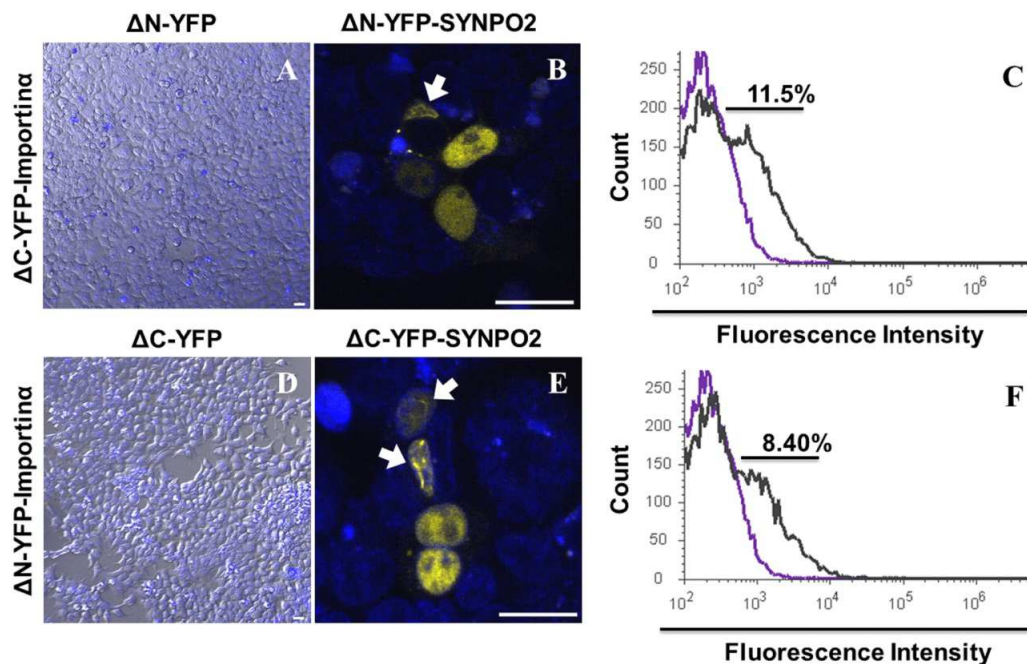


Fig. 27 Imaging of SYNPO2, importin $\alpha$  interaction using BIFC assay. SYNPO2, importin interaction analysis demonstrated a nuclear colocalization of SYNPO2-importin $\alpha$  complex. Confocal fluorescence images of transiently transfected HEK293 cells with 300 ng of  $\Delta$ N-YFP-SYNPO2/ $\Delta$ C-YFP (A),  $\Delta$ N-YFP-SYNPO2/ $\Delta$ C-YFP-Importin $\alpha$  (B),  $\Delta$ C-YFP-SYNPO2/ $\Delta$ N-YFP (D), and  $\Delta$ C-YFP-SYNPO2/ $\Delta$ N-YFP-Importin $\alpha$  (E). Quantitative FACS-BIFC analysis of 10000 measured HEK293 cells, cotransfected with  $\Delta$ N-YFP-SYNPO2/ $\Delta$ C-YFP-Importin $\alpha$  (C), and  $\Delta$ C-YFP-SYNPO2/ $\Delta$ N-YFP-Importin $\alpha$  (F) as a comparison with  $\Delta$ C-YFP/ $\Delta$ N-YFP (violet curve) cotransfected HEK293 cells are shown. Scale bars present 20  $\mu$ m.

### 3.18 Visualization of SYNPO2 homo-dimer using BIFC and FACS-BIFC based assay

In order to investigate and to visualize the SYNPO2 dimerization in living cells, HEK293 cells were transiently transfected with 300 ng  $\Delta$ N-YFP-SYNPO2/ $\Delta$ C-YFP (Fig. 28A),  $\Delta$ N-YFP/ $\Delta$ C-YFP-SYNPO2 (Fig. 28B) as controls or  $\Delta$ N-YFP-SYNPO2/ $\Delta$ C-YFP-SYNPO2 (Fig. 28C). Confocal fluorescence images of control HEK293 cells did not demonstrate any detectable fluorescence. However, cells transfected with  $\Delta$ N-YFP-SYNPO2/ $\Delta$ C-YFP-SYNPO2 showed a cytoplasmic accumulation of SYNPO2-dimers. Interestingly, SYNPO2-dimers were detected close to the cell membrane and also nucleus membrane (Fig. 28C, white arrow). FACS analysis of cells transfected with  $\Delta$ N-YFP-SYNPO2/ $\Delta$ C-YFP-SYNPO2 demonstrated an approximately 12% of cells which are fluorescence positive (Fig. 28D).

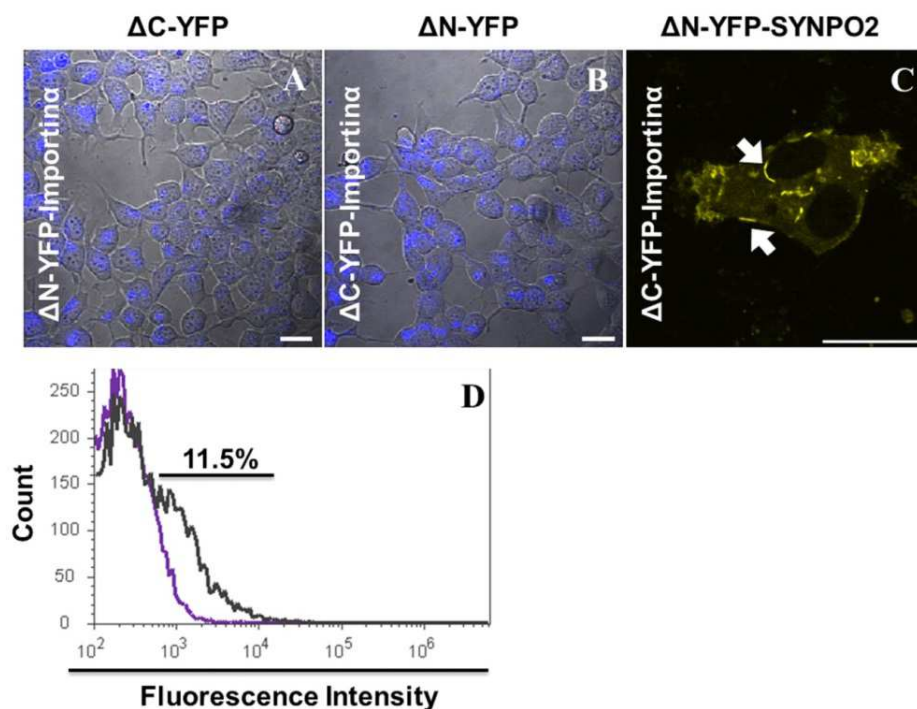


Fig. 28 Imaging of self-association of SYNPO2 to form homo-dimers in living cells. Confocal fluorescence analysis of transiently cotransfected HEK293 cells with 300 ng of  $\Delta$ C-YFP/ $\Delta$ N-SYNPO2 (A),  $\Delta$ C-SYNPO2/ $\Delta$ N-YFP (B), and  $\Delta$ C-SYNPO2/ $\Delta$ N-SYNPO2 (C) using the calcium phosphate method. FACS quantitative analysis of BIFC-SYNPO2 homo-dimerization is presented in the Dot-plot (D) and the histogram (E). Scale bars present 20  $\mu$ m

## 4 Discussion

### 4.1 Current state of knowledge as relevant to this work

VSMCs show a unique behavior that allows them to modulate their phenotype due to (de)differentiation<sup>10, 12</sup> and upon diseases like arteriosclerosis, high blood pressure and during vascular injuries<sup>11, 13, 40</sup>. Notably in response to vascular injury, VSMCs dramatically increase their rate of proliferation, migration, and synthetic activity and therefore play an essential role during vascular repair. Unfortunately this high degree of phenotype plasticity could also predispose the cells to abnormal environmental cues and signals that can lead to various adverse phenotype switches and in turn development of different vascular diseases. Additional examples of diseases associated with phenotype switch are cancer<sup>152</sup>, asthma<sup>153</sup>, obstructive bladder disease<sup>154</sup>, and numerous gastrointestinal pathologies<sup>155</sup>. Thus, the major challenge in understanding differentiation of the VSMCs is that these cells can exhibit a wide range of different phenotypes at different stage of tissue development and diseases. Accordingly, this is essential to advance our understanding of the mechanisms controlling VSMCs phenotype switch in health and disease. Several studies have provided evidence of the crucial role of the cytoskeleton and smooth muscle marker proteins during tissue development, cell (de)differentiation, phenotype switch, and various vascular diseases<sup>40, 156</sup>. The marker proteins for differentiated smooth muscle cells with the highest relevance are  $\alpha$ SMA<sup>157</sup>, smMHC<sup>158</sup>, smoothelin<sup>159</sup>, hCaD<sup>160</sup>, sm22<sup>161</sup>, and CaLP<sup>162</sup> proteins, which are mostly down-regulated during the phenotype switching from a contractile to a synthetic phenotype<sup>40, 41, 156</sup> (Table 20).

Protein	Contractile SMC	Synthetic SMC
Caldesmon	<i>h</i> -CaD ↑ <i>l</i> -CaD ↓	<i>h</i> -CaD ↓ <i>l</i> -CaD ↑
Smoothelin	↑	↓
Meta-vinculin	↑	↓
SM22	↑	↓
$\beta$ -actin	↓	↑
Vimentin	↓	↑

Table 20 Alteration of the marker proteins expression level in the smooth muscle cells during phenotype switch and/or diseases (Summarized according to Sobue et al. 1998 & 1999).

Furthermore, it has been reported that mechanotransduction affects phenotype modulation, whereby mechanical stimuli regulates target proteins or genes<sup>8, 163, 164</sup>. The sequence of events is initiated with the stimuli arising from the interaction of extracellular matrix proteins with the integrins protein family, which in turn passes the stimuli on to focal adhesion complexes<sup>165, 166</sup>. Afterwards the stimuli are transmitted to the cytoskeleton, leading to a remodeling of actin and quantitative changes of VSMC marker proteins<sup>163, 164</sup>. Actin is the most abundant protein in eukaryotic cells. Depending on its localization in the cell, it forms different cytoskeletal structures and plays different functions. Thus, actin plays crucial roles in processes such as the establishment of cellular shape, cell motility, cell adhesion, muscle contractility, differentiation, transcription, cytokinesis, and the formation and maintenance of neuronal synapses. Accordingly, actin dysfunction and mutations can be involved in to countless diseases, including muscle myopathies<sup>167</sup>, cancer<sup>168</sup>, Alzheimer's<sup>169, 170</sup>, Wiskott-Aldrich syndrome<sup>164</sup>, and neuronal retardation<sup>171</sup>. The structures of actin networks and their cellular functions are regulated by other hundreds of cytoskeletal proteins, generally known as actin binding proteins (ABPs). ABPs regulated elongation, shortening, capping or uncapping of the actin filaments as well as the formation of bundles and branches<sup>56</sup>. While the functions of some of these proteins are known, the physiological functions of newly discovered ABPs still remain unclear. One of these recently identified ABPs is synaptopodin 2 (SYNPO2), a member of the synaptopodin family<sup>75, 77, 88, 92</sup>.

SYNPO2 is an actin nucleator and actin filament binding protein<sup>75, 88, 172</sup>. Its close association with actin links SYNPO2 to the reorganization of the actin cytoskeleton and therefore to differentiation aspects involved in phenotype modulation. Previous studies showed that SYNPO2 (murine GFP-myopodin) shuttles between the cytoplasm and the nucleus during differentiation and heat shock in striated muscle and cardiomyocytes<sup>77, 100, 101</sup>. SYNPO2 is also a tumor suppressor protein and its shuttling has also been reported in carcinogenesis and metastasis of bladder and prostate cancer<sup>94, 95</sup>. The Mundel laboratory reported that the loss of nuclear expression of SYNPO2 in bladder cancer predicts the clinical outcome. In differentiated cells and during carcinogenesis SYNPO2 is accumulated in the cytoplasm while in the non-differentiated cells and after application of heat shock

SYNPO2 was mainly in the nucleus<sup>80, 94</sup>. Although many reports discussed a crucial role for SYNPO2 in striated muscle and cancer cells, the role of SYNPO2 in VSMCs is so far unknown.

With this notion that SYNPO2 is a part of the ABP-complex and therefore may be involved in the regulation of cell differentiation, phenotype switch of VSMCs and regulation of vascular tones, we have focused on the subcellular localization and expression level of endogenous SYNPO2 under conditions that promoted a differentiated versus dedifferentiated vascular smooth muscle phenotype. Therefore, the goal of this proposal was to address this lack of understanding, by using a multi-disciplinary approach, spanning cell through molecular biology. This research will considerably advance our understanding of the mechanisms controlling SYNPO2 dynamic and functions in cells in health and disease.

#### **4.2 Phenotype switch of VSMCs affects the subcellular distribution of SYNPO2**

In order to elucidate the relation between SYNPO2 and the phenotype switch of VSMCs, cells were freshly isolated from rat aorta<sup>131</sup> and characterized using anti-CD90 directed against fibroblast and specific smooth muscle marker antibodies like anti-smMHC, anti-desmin, and anti- $\alpha$ -SMA (Fig. 9). Isolated VSMCs demonstrated strong expression of all three smooth muscle marker proteins, while less than 3% positive signal was detected when cells treated with anti-CD90 antibody. A coimmunostaining of SYNPO2,  $\alpha$ -SMA, and smMHC showed a strong colocalization of SYNPO2 and  $\alpha$ -SMA (Fig. 10 B), while colocalization of SYNPO2 and smMHC was found to be diffuse (Fig. 10 A). This result may suggest that the binding of SYNPO2 to actin seems to be direct while its binding to myosin is an indirect interaction which is controlled by actin. In addition, VSMCs were characterized based on the expression of marker proteins, characteristic for a contractile or a non-contractile phenotype (Table 20). Consistent with the known literature<sup>41, 156</sup>, we found high expression levels of contractile markers on the first day of cell preparation. The phenotype was assessed by determination of markers of contractile and synthetic phenotype by qRT-PCR and Western Blotting. Our results revealed high expression levels

of contractile markers like *sm22*, *Smtn*, and *hCaD*, on the first day of cell preparation while the expression of these markers rapidly decreased accompanied by the up-regulation of markers favored by the synthetic phenotype like *lCaD* during cultivation (Fig. 11)<sup>173</sup>. In respect to *SYNPO2* we found a mild, but significant down-regulation (~1.4 fold,  $p < 0.01$ ) of transcript levels with increasing cultivation time (Fig. 11 A). However, confocal microscopy and subcellular fractioning combined with Western blotting revealed more striking results (Fig. 12). These demonstrated different distribution of *SYNPO2* isoforms in the nucleus compared to cytoplasm and total cell lysis (Fig. 12D). A possible reason for this could be specific subcellular differences in the distribution of *SYNPO2* isoforms in the cell nucleus versus in the cytoplasm. During cultivation of VSMCs, *SYNPO2* changed its subcellular localization from the cytoplasm, on day 1 (contractile), to the nucleus, on passage 2 (Fig. 12A & B). The quantitative analysis of the subcellular localization of *SYNPO2* based on indirect immunofluorescence data showed that on the day 1 of isolation, *SYNPO2* was detected in 16% of the isolated cells in the nucleus, but in the majority of the cells *SYNPO2* was localized into the cytoplasm. In contrast, at passage 2, *SYNPO2* was located in the nucleus of 89% of the cells (Fig. 12 C).

Furthermore, to obtain a better insight into the mechanisms that regulate shuttling of *SYNPO2*, the phenotype rescue from non-contractile to the contractile phenotype was analyzed. The extracellular matrix (ECM) protein laminin has been shown to activate pathways involved in the formation of a contractile phenotype<sup>8, 146</sup>, while collagen I favors signaling leading to a dedifferentiated phenotype<sup>8, 34, 174</sup>. Thus, we applied conditions that promoted the development of a differentiated versus a dedifferentiated phenotype in VSMCs using laminin and collagen I. In order to avoid the very rigid matrix of a cell culture dish, a polyacrylamide matrix with a stiffness of 55 kPa, as found during atherosclerosis, was chosen as the cell culture basement.

Analysis of the cells by Western blotting, qRT-PCR, light microscopy, and confocal microscopy showed, in agreement with others<sup>8, 34, 146</sup> that laminin induced a differentiated phenotype in VSMCs (Fig. 13). However, VSMCs cultivated on collagen I maintained the dedifferentiated phenotype (also known as synthetic phenotype)<sup>174</sup>. In term of subcellular localization of *SYNPO2*, cells cultivated on collagen I showed an increased

accumulation of SYNPO2 in the nucleus (Fig. 14 A), while cultivation on laminin led to cytoplasmic localization of SYNPO2 with a significance level of  $p < 0.001$  (Fig. 14 B). Notably, beside to the cytoplasmic localization of SYNPO2 on laminin coated matrices, an up-regulation of SYNPO2 by more than 3-fold could be observed (Fig. 13 A). Based on the expression rates of SYNPO2 during isolation and cultivation on untreated culture dishes an upregulation to this extent was unexpected.

Interestingly, apart from reduction of SYNPO2 expression in non-contractile VSMCs and an up-regulation in laminin-treated VSMCs, these findings resemble the results reported before for striated muscles<sup>77</sup>. For example, a cytoplasmic localization of SYNPO2 in C2C12 cells has been described during differentiation from myoblasts to myotubes<sup>77</sup>. In the latter ones upon differentiation SYNPO2 was found in Z-lines<sup>77, 101</sup>, a structure closely related to smooth muscle dense bodies<sup>175</sup>. *In vivo* avian SYNPO2 (fesselin) has been shown to localize to the dense bodies in the gizzard<sup>97</sup>. Shuttling of SYNPO2 upon cell differentiation seems to be not only conserved but also important. For instance, under pathological conditions of urinary bladder and prostate cancer, subcellular localization of SYNPO2 is crucial for the clinical outcome<sup>94</sup>. A benign prognosis is associated with a nuclear localization and unchanged expression rates of SYNPO2, while a malignant outcome goes along with reduced expression and depletion of nuclear SYNPO2<sup>78, 94, 95</sup>. We have now detected for the first time under non-pathological condition a change in subcellular localization of SYNPO2 that is correlated with a change in expression level (Fig. 13 A). We found an upregulated expression rate of SYNPO2 in VSMCs upon phenotype switching from a non-contractile (proliferative phenotype) to a contractile phenotype (Fig. 13 A). This finding could explain the suppressor effect of SYNPO2 on proliferative phenotype compared to previous works, describing invasive cells in bladder and prostate cancer<sup>80, 94</sup>. However, the function of the increased SYNPO2 expression associated with its cytoplasmic accumulation as observed in differentiated VSMCs, is so far unknown. Possible reasons for this controversial results in terms of subcellular localization of SYNPO2 in VSMCs, compared to bladder and prostate cancers, could either be cell type-specific differences in the impact of SYNPO2 on the regulation of differentiation state in invasive cells and in VSMCs or variable experimental settings.

Taken together, these findings raised the hypothesis of a potential link of SYNPO2 trafficking as ABP and differentiation states of cells. We may conclude that the phenotype switching of VSMCs correlates with the subcellular localization and expression level of the novel ABP SYNPO2 via mechanisms involving VSMCs differentiation due to extracellular matrix components like laminin, as contractile inducer and collagen I, as non-contractile regulator, which still remains to be elucidated.

### 4.3 Actin dynamics and subcellular distribution of SYNPO2 in VSMCs

There is increasing information that SYNPO2 increased nucleation and polymerization of actin<sup>75, 89, 90, 97-99, 176</sup> and therefore it is a part of the actin cytoskeleton complex. Accordingly, the so far best studied function of SYNPO2 is its effect on the actin cytoskeleton<sup>76, 90, 99, 176</sup>. In order to test whether this interaction is reciprocal and participates in phenotype switching, depending on an operating SYNPO2 shuttling, we manipulated the actin cytoskeleton. Cytochalasin D (CCD) and jasplakinolide (JASP) are small components that are supposed to destabilize or stabilize, respectively, the actin cytoskeleton<sup>177, 178</sup>. The main difference of SYNPO2 distribution was observed in cells seeded on ECM protein-coated polyacrylamide matrices. We detected a nuclear localization of SYNPO2 when collagen I was used (Fig. 15 A) and a cytoplasmic distribution when VSMCs were cultivated on laminin (Fig. 15 E). As long as stress fibers were still intact, we still observed SYNPO2 in the nucleus when seeded on a collagen I coated matrix and in the cytoplasm, when cells were seeded on a laminin-coated matrix compared to control cells. The biggest effect has been observed on collagen I matrices with CCD, where nuclear localization of SYNPO2 was not as intense as in cells that were treated with the vehicle control or JASP (Fig. 15 B and C). In the case of laminin coating, cells showed in the presence of CCD a stronger accumulation of SYNPO2 in the nucleus (Fig. 15 F). The effects of JASP were more subtle and resembled those that were observed with the vehicle control (Fig. 15 G). However, a manipulation of the actin cytoskeleton, as evident by the formation of phalloidin-blisters, could only be observed when CCD was applied (Fig. 15 B and F). As a refutation, one could argue that cells might have already adhered when treated with CCD or JASP, and SYNPO2 might have already occupied its

final destination. However, this argument does not comply with a dynamic actin cytoskeleton. So, when the drugs were applied, the cells had already settled and developed actin stress fibers, SYNPO2, as an actin-binding protein, underlies a dynamic process as actin itself. However, the effect of SYNPO2 on the actin cytoskeleton and *vice versa* may be mutual. We assumed that the effect SYNPO2 has on the actin cytoskeleton is stabilization of F-actin<sup>75</sup>. In this case the presence of SYNPO2 in the cytoplasm may shift the F-actin/G-actin-ratio and control the actin that enters the nucleus and participates in transcription. With the notion that in VSMCs, up to 25% of actin exists as G-actin<sup>175</sup>, the F/G-actin ratio was determined using a G-actin/F-actin kit (Cytoskeleton) to indicate whether the F/G-actin ratio underlies the changes during differentiation of the VSMCs. VSMCs grown on laminin or collagen I-coated polyacrylamide matrices demonstrated the same F/G-actin ratio in response to the CCD and JASP as compared to the vehicle controls (Fig. 15). In case of VSMCs (passage 3) cultivated on laminin and treated with JASP, SYNPO2 was accumulated in the cytoplasm as compared to vehicle control and CCD treated cells (Fig. 15 G). However, incubating the VSMCs cultivated on collagen I with JASP did not affect the subcellular localization of SYNPO2 (Fig. 15 C), while the F-actin ratio was increased (Fig. 15 D). Possible reasons for these controversial results could either be cell phenotype-specific differences in the impact of JASP on actin polymerization in VSMCs and consequently SYNPO2 shuttling, or differences in the impact of laminin versus collagen I by so far unknown mechanism.

Previous reports have shown that heat stress regulates gene expression, controls synthesis of heat shock proteins and induces changes in morphology of nucleoli, cytoplasmic organelles, and actin cytoskeleton<sup>179, 180</sup>. Notably, it is already reported, that heat shock inhibits actin polymerization and therefore affects actin cytoskeleton dynamics<sup>181</sup>. However, there always exists an exception to the rule. Recently, heat-induced stress (43°C) has been reported to affect the subcellular localization of murine SYNPO2<sup>77, 101</sup>. These observations were only reported in C2C12 cells transfected with a GFP-fused murine SYNPO2. Because the shuttling of GFP-SYNPO2 could be due to the diffusion of the GFP through the nuclear pores<sup>182, 183</sup> the subcellular localization of SYNPO2 in VSMCs was investigated by means of specific antibodies directed against the

endogenous protein. In contrast to results that were obtained in cardio myocytes and skeletal muscle cells, using fusion-proteins of GFP-SYNPO2<sup>77</sup>, stress applied in the form of heat shock did not trigger shuttling of SYNPO2 to the nucleus (Fig. 16). Possible reasons for this controversial results could either be cell type-specific differences in the impact of heat shock stress on distribution and function of SYNPO2 or variable experimental settings.

There is increasing evidence about the crucial roles of Rho-GTPase signaling pathways in the cell functions and especially its role in smooth muscle contraction, and actin organization<sup>16, 105, 184, 185</sup>. The roles of the GTPase Rho and its downstream effectors, the Rho-associated protein serine/threonine kinase (ROCK) family, have been intensively studied. Many studies point to the significant regulatory roles of the Rho-ROCK signaling pathway in various cellular functions like actin cytoskeleton organization<sup>105, 186</sup>, cytokinesis, cell motility<sup>187</sup>, contraction of the smooth muscle cells (Fig. 29), and vascular contraction<sup>16, 188-190</sup>.

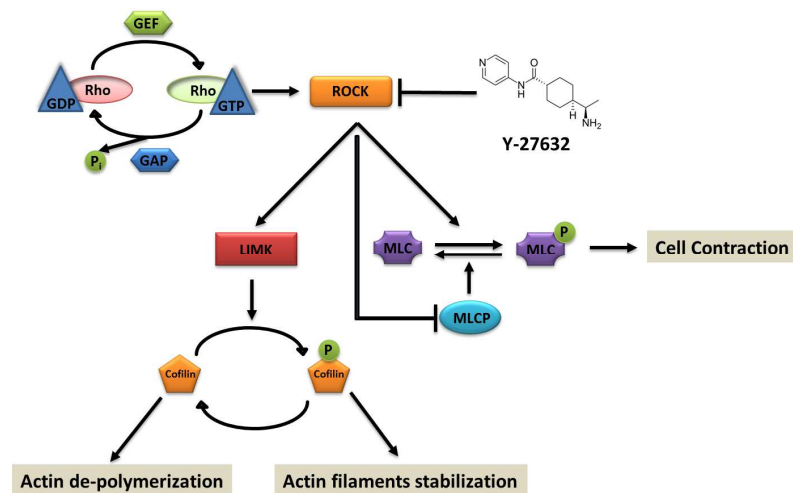


Fig. 29 Schematic illustration of actin cytoskeleton dynamics depending on Rho-Rock signaling pathway (modified from Alan Hall, science, 1998). The Rho-associated kinase as a main downstream effector protein of the small GTPase Rho, plays different crucial roles in the cells and is one of the major regulators of cytoskeleton. Rock inhibits de-polymerization of actin filaments indirectly by phosphorylation and activation of LIM kinase, which in turn phosphorylates cofilin, and therefore stabilizes actin filaments.

The Duncan Laboratory showed that SYNPO2 can promote cell migration via activation of Rho-ROCK signaling pathway<sup>191</sup>. SYNPO2 has been shown to affect cell migration in

response to different chemokinetic stimuli (NIH 3T3 CM or 10% FBS as chemo-attractants), which in turn was dependent on Rho-ROCK signaling that regulates the actin cytoskeleton and in turn the cell migration<sup>191</sup>. The NIH 3T3 conditioned medium (CM) activate Rho-Rock signaling pathway and therefore it promotes migration of PC3 cells (embryonal carcinoma cells) while FBS demonstrates a modest effect on this pathway. Therefore, in order to elucidate the role of Rho-ROCK signaling pathway for SYNPO2 trafficking in the VSMCs, cells were treated with a commercial inhibitor (Y27632) directed against Rho-associated protein serine/threonine kinase (ROCK) as a downstream effector of Rho-GTPase signaling pathway. Treatment the VSMCs from passage 3 (non-contractile phenotype) with Y27632 disrupted actin cytoskeleton as reported before, but this disruption of actin cytoskeleton was not accompanied by alteration of the subcellular distribution of SYNPO2 (Fig. 19). Previous studies showed that the inhibition of Rho-ROCK signaling pathway results in the inhibition of cell polarization, lamellipodia formation, and in turn cell migration<sup>192-194</sup>. Why inhibition of ROCK does not effect on distribution of SYNPO2 is unclear. As described before a major challenge in understanding differentiation of VSMC is that the cells exhibit different phenotypes at different stages of development and especially in cell culture condition. Accordingly, possible reasons for this result could either be cell phenotype differences in the impact of the cell culture or variable experimental settings.

#### **4.4 The cAMP mediated signaling is involved in the subcellular shuttling of SYNPO2 between the nucleus and the cytoplasm**

Recently, several studies showed that murine SYNPO2 altered its subcellular localization between the cytoplasm and the nucleus due to its phosphorylation status<sup>77, 96, 100, 101</sup>. *In vitro* studies demonstrated a crucial role of PKA and CaMK-II during this process, in which SYNPO2 was first phosphorylated on two 14-3-3 binding motifs<sup>100</sup>. *In vitro* phosphorylation studies of murine SYNPO2 showed that PKA phosphorylated the both binding sites, while CaMK-II phosphorylated only one of the binding sites<sup>100</sup>. These results suggest that cAMP-dependent signaling pathways like the PKA pathway (not shown for VSMCs) as the main controlling pathways for the functions of SYNPO2 in the cells (Fig.

30). Until now, most investigations on SYNPO2 were performed in striated muscle cells like skeletal and cardiac muscle<sup>77, 100, 101</sup> and in bladder or prostate cancers<sup>78, 80, 94, 95</sup>. Most information about the role of SYNPO2 is limited to these tissues, and therefore its role in vascular muscle systems and notably in the vascular smooth muscle cells are completely unclear. Thus, more information about this shuttling in VSMCs will considerably advance our understanding of the mechanisms controlling SYNPO2 functions and in turn actin dynamics in cells in health and disease.

The cAMP-dependent pathway is a G-protein-coupled receptor-triggered signaling cascade. As described before, an increase in the cAMP level leads to the activation of PKA, a cAMP dependent protein kinase, and EPAC, a cAMP-regulated guanine nucleotide exchange factor (GEF)<sup>16, 195</sup>. In this case, the activated  $\alpha$ -subunit of the G protein binds to and activates adenylyl cyclase (AC), which, in turn, catalyzes the production of cyclic adenosine monophosphate (cAMP) from ATP. The produced cAMP activates the cAMP-dependent pathways like PKA and EPAC. These pathways can either be activated directly by stimulation of adenylyl cyclase, PKA and EPAC<sup>196</sup>, or by blocking the phosphodiesterase using commercial small molecules.

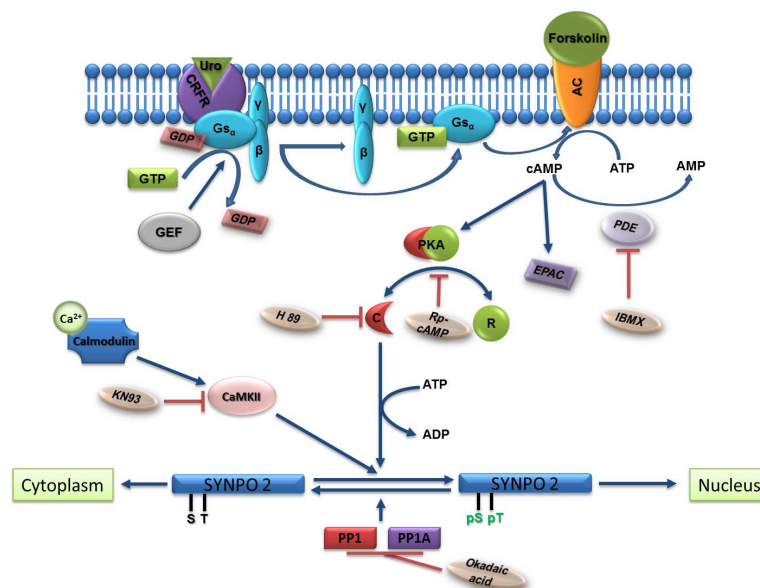


Fig. 30 Schematic illustration of PKA (R= regulatory domain, C= catalytic domain) and CaMKII-dependent phosphorylation of SYNPO2 used in this work (modified from Faul et al. 2007).

To provide more mechanistic insides, it was investigated, whether PKA and CaMKII could control the subcellular distribution of SYNPO2 in VSMCs. In order to investigate the effects of cAMP levels and also cAMP dependent signaling pathways, VSMCs were treated with different components. Interestingly, increased cAMP levels in VSMCs (day 1 of isolation) induced accumulation of SYNPO2 in the nucleus as described before<sup>100</sup>, when adenylyl-cyclase was directly activated by forskolin, Sp-5.6-DCI-cBIMPS and urocortin as activators (Fig. 17 B-D). Furthermore, the treated VSMCs with these activators demonstrated an increase in the numbers of nuclear SYNPO2-displaying cells in comparison with vehicle cells (Fig. 17 F). A combination of forskolin as activator for adenylyl cyclase and IBMX as an inhibitor for PDEs, resulted a reduction of nuclear SYNPO2-displaying cells (Fig. 17 E & F) and a diffuse localization of SYNPO2 around the nucleus. A possible mechanism for the decreased nuclear SYNPO2-displaying cells could be that increased cAMP levels activate an alternative cAMP-mediated pathway like EPAC which may affect export of SYNPO2 from the nucleus by a so far unknown mechanism.

Furthermore, to assess the functionality effect of the PKA and CaMKII on SYNPO2 trafficking, VSMCs from passage 3 (SYNPO2 in the nucleus) were treated by inhibitors directed against PKA and CaMKII. The inhibition of PKA with H89, Rp-8-PIP-cAMPS demonstrated a stronger reduction of nuclear SYNPO2 as compared to the VSMCs in which CaMKII was inhibited with KN93 (Fig. 18). This may be explained by the fact that the PKA phosphorylated both threonine, and serine, while CaMKII phosphorylated only threonine<sup>100</sup> on 14-3-3 binding motifs.

Phosphorylation/de-phosphorylation of proteins regulated by protein kinases and phosphatases, affects one third of all proteins in the cells, which in turn control numerous cellular processes<sup>197, 198</sup>. Our data suggest that the activation of CaMKII and PKA by an increased concentration of cAMP could affect subcellular localization of SYNPO2. Therefore, it was essential to investigate whether phosphatases affect subcellular localization of SYNPO2. Accordingly, VSMCs were treated with Okadaic acid (OA), which inhibits protein phosphatase 1 (PP1, IC50 = 3 - 15  $\mu$ M) and protein phosphatase 2A (PP2A, IC50 = 0.1-1 nM) specifically<sup>199, 200</sup>. Interestingly, we detected that the inhibition of phosphatases causes an accumulation of SYNPO2 in the cytoplasm and around the cell

nucleus (Fig. 20). On the one hand, this result may suggest that the phosphorylated forms of the SYNPO2 are essential for its shuttling in both directions (cytoplasm ↔ nucleus), which in turn could also be crucial for its regulation in the both cell nucleus and the cytoplasm. PP2A is a trimeric holoenzyme that acts as a tumor suppressor. A number of studies showed that the OA inhibits PP2A and therefore it promotes tumor growth and invasion<sup>201, 202</sup>. Therefore, it can be speculated that the inhibition of PP2A by OA, which causes a migrative phenotype, and in turn also phosphorylation of SYNPO2 in the nucleus may regulate the loss of nuclear SYNPO2. On the other hand, unfortunately the concentration that we used, 100 nM OA, inhibits only PP2A in VSMCs and not PP1. So far, it is not clear how the PP1 is communicated to the SYNPO2 shuttling, but one hypothesis is that it works independently of the PP2A, directly dephosphorylating SYNPO2, which in turn causes cytoplasmic accumulation of SYNPO2 in VSMCs via a so far unknown mechanism.

#### **4.5 Imaging of SYNPO2, 14-3-3 $\gamma/\beta$ , and Importin $\alpha$ interaction in living cells**

Phosphorylation as a post-translational modification (PTM) affects approximately one third of all proteins in the cell<sup>198, 203</sup>. 14-3-3 interactions with phosphorylated parts (RSXpS/TXP, phospho-serine or -threonine) of different proteins were a way to read this PTM in signaling cascades. 14-3-3 proteins form hetero- and homodimeric structures that bind to a large number of phosphorylated signaling proteins and control their nuclear and cytoplasmic distribution<sup>204-206</sup>. Moreover, It is widely accepted today that the binding of 14-3-3 proteins to disorder proteins is crucial for their stabilization, activity and especially protein-protein interactions<sup>206-208</sup>.

One novel class of such proteins is SYNPO2, which belongs to the natively unfolded proteins<sup>172</sup>. It has been recently reported that 14-3-3 polypeptides, acting as chaperone-like adaptor proteins, are able to bind a specific sequence of SYNPO2<sup>101</sup>, which in turn is crucial for the shuttling of SYNPO2 from the cytoplasm into the nucleus as shown for striated muscle cells<sup>96, 101</sup>. This could of course also imply a functional relevance of 14-3-3 isoforms at the differentiation state of VSMCs and in turn also for the trafficking of SYNPO2. However, no reports are currently available to test the functionality of the 14-3-

3 isoforms experimentally in this term. Accordingly, to test this, the expression levels of seven 14-3-3 isoforms were analyzed using quantitative real-time PCR. As shown in Fig. 21, the mRNA level of the 14-3-3 $\tau$ ,  $\eta$ , and  $\zeta$  were more abundant on the first day of isolation than at passage 3, while the mRNA level of isoform  $\sigma$  was higher at passage 3. The significance level of 14-3-3 $\eta$  expression was  $p < 0.02$  as determined by a two-tailed student's t-test. For 14-3-3 $\tau$ , and isoform  $\zeta$  the significance was  $p < 0.001$ . We found a higher expression of 14-3-3 $\sigma$  upon dedifferentiation of VSMCs with a significance level of  $p < 0.005$ . Interestingly, no significant changes in mRNA level of the isoforms  $\beta$ ,  $\gamma$ ,  $\epsilon$  was detected at passage 3 in VSMCs compared to cells from day 1.

Although no conclusive results could be shown for the 14-3-3 isoforms  $\beta$ ,  $\gamma$  during phenotype switch, three arguments suggest that probably both, 14-3-3 $\beta$ , and  $\gamma$ , act together in the trafficking of SYNPO2 in VSMCs during its phenotype modulation: first, several studies showed that interaction of SYNPO2 with 14-3-3 $\beta$  leads to its accumulation in the nucleus of C2C12 cells<sup>100, 101</sup>; second, it is already reported that of the seven isoforms comprising this family, 14-3-3 $\gamma$  and  $\beta$  are highly expressed in VSMCs<sup>147-150</sup>; and finally, it has been previously reported that the oxidation of 14-3-3 $\gamma$  by a PDGF mediated pathway induces VSMC migration<sup>209</sup>. So far, nothing is known about the function of different 14-3-3 isoforms in VSMCs in term of subcellular trafficking of SYNPO2, which could also be important for the phenotype switch, disease and beyond.

Furthremore, this import into the nucleus of cells is dependent on a signal, in the form of nuclear localization sequences (NLSs), cytosolic factors, binding to the nuclear pore, and subsequent translocation through the nuclear pore. The G protein Ran/TC4<sup>210, 211</sup> and an interacting partner, importin $\alpha$ <sup>212</sup> were found to be the active components of the cytosolic factors that are implicated in the nuclear-cytoplasmic shuttling of SYNPO2. This synergy strongly depends on the phosphorylation form of SYNPO2 as shown by *in vitro* experiments<sup>100</sup>. Nevertheless, this evidence required more physiological information about these proteins in the cellular context. Accordingly, we next investigated the subcellular localization of SYNPO2, 14-3-3 $\gamma/\beta$ , and importin $\alpha$  and their interaction together in living cells by designing and combining different fluorescent proteins (Fig. 22 A and B).

Modern fluorescence techniques like FRET, FACS and BIFC assay have emerged as the most promising techniques to study the subcellular localization and protein-protein interaction studies in living cells<sup>118, 125, 126</sup>. This included the incorporation of different fluorescent dyes at different positions in the proteins of interest, in case of FRET (Fig. 5) and/or different non-fluorescent fragments in the proteins of interest, in case of BIFC assay (Fig. 6). Although, FRET is a powerful method for colocalization and protein-protein interaction studies, its limitations include the crucial distance  $\sim 10$  nm, and the choice of the best sites for ligation of fluorescent proteins remains a significant challenge<sup>117, 122</sup>. Therefore optimizing and characterizing the best FRET constructs can be time-consuming. In this work, various fluorescent conjugated proteins, such as 14-3-3 $\gamma/\beta$ , Importin $\alpha$ , and SYNPO2 were used. These provided insights into the molecular mechanism of protein-protein interactions, between SYNPO2 and its partners, in living cells. Since it could be difficult to interpret and to predict whether the resulted fluorescence displays an interaction between two and more proteins or subcellular localization, two different fluorescence-based assays such as common fluorescence imaging and BIFC assays in combination with FACS analysis were used.

SYNPO2 alters its subcellular localization during differentiation, heat shock stress (not detected in VSMCs), and also during smooth muscle phenotype modulation (see 4.2). Even though the precise function in the cellular context remains to be elucidated, it likely involves the actin polymerization and complex formation of SYNPO2 with 14-3-3 $\gamma$  or  $\beta$  and the importin $\alpha$  during shuttling between the cell cytoplasm and the nucleus (Fig. 31). Accordingly, these findings raised the hypothesis of a possible ternary complex formation of SYNPO2/14-3-3 $\gamma$ /importin $\alpha$  or SYNPO2/14-3-3 $\beta$ /importin $\alpha$  with actin in the nucleus. Since the shuttling action of SYNPO2 should itself be tightly regulated, we established a BiFC-based assay that allows the visualization of SYNPO2-14-3-3 $\gamma$  and  $\beta$ , and importin $\alpha$  complexes and their quantification by confocal microscopy and FACS analysis. With these techniques, the subcellular localization of SYNPO2, 14-3-3 $\gamma/\beta$  and importin $\alpha$ , and the regulatory effects of 14-3-3 $\gamma/\beta$  and importin $\alpha$  on the SYNPO2 shuttling can be analyzed in a cellular context fashion.

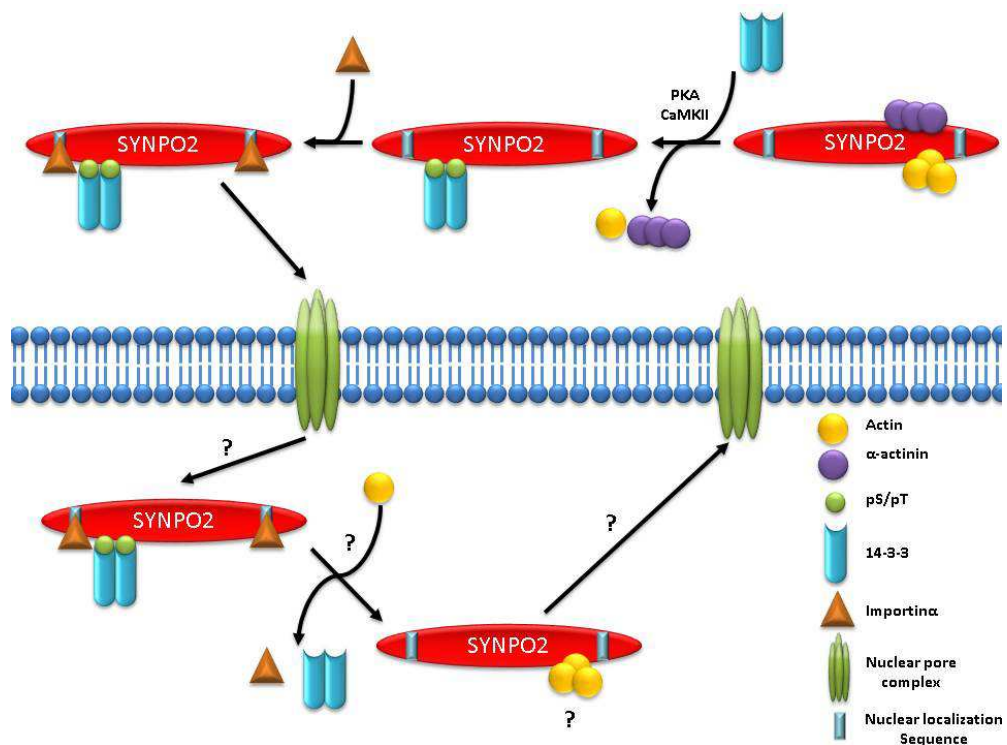


Fig. 31 Schematic illustration of nuclear-cytoplasmic trafficking of SYNPO2 (According to Faul et al. 2005). PKA and CaMKII phosphorylate SYNPO2 in both 14-3-3 binding motifs. These phosphorylations affect dissociation of  $\alpha$ -actinin and actin from SYNPO2, which in turn allow its interaction with 14-3-3. Finally, SYNPO2-14-3-3 complex forms a ternary complex with importin $\alpha$ , which govern SYNPO2 transport to the nucleus.

In order to provide flexibility for independent motion of the fluorescent protein fragments and the interaction partners, N-terminal CFP fused proteins, with a **SGLRS**-linker, between CFP and the protein of interest were used. The **GSAPVAT**-linker was used for C-terminal conjugated CFP and to design C-terminal and N-Terminal conjugated YFP proteins, **SGLRSRA** and **GSRPVAT** were used between YFP and the proteins, respectively (Fig. 22 A). In order to generate BIFC constructs with high fluorescence yield and minimal background several plasmid variants with **RSITLAAA**-linker were used (Fig. 22 B). Western blot analysis of fluorescent and non-fluorescent fragments-fused constructs demonstrated expected molecular weight for each protein (Fig. 23).

In terms of subcellular localization of SYNPO2, 14-3-3 $\beta/\gamma$ , and importin $\alpha$ , our conventional fluorescent fused constructs demonstrated a nuclear localization for SYNPO2, and importin $\alpha$ , while 14-3-3 $\gamma$  and 14-3-3 $\beta$  accumulated mainly in the cytoplasm (Fig. 24). Interestingly, we found the same nuclear distribution in distinct actin loop form

as it is reported for murine SYNPO2 fused to GFP (Fig. 24 A, white arrow)<sup>77</sup>. Transiently transfected cells with CFP-importin $\alpha$ , importin $\alpha$ -CFP, and YFP-SYNPO2 demonstrated also nuclear bodies-like structures for importin $\alpha$  (Fig. 24 G to H') and SYNPO2 (Fig. 24 A') by so far unknown functions.

In order to investigate the physical interaction between SYNPO2, 14-3-3 $\beta/\gamma$ , and importin $\alpha$  in the cellular context, it was verified whether both  $\Delta$ N-YFP-SYNPO2 and  $\Delta$ C-YFP-SYNPO2 interact with  $\Delta$ N-,  $\Delta$ C-YFP fused 14-3-3 $\beta/\gamma$  and importin $\alpha$  based on fluorescence development according to the BIFC assay. The BIFC method offers a simultaneous visualization of multiple proteins interacting in the living cells<sup>130</sup>. Confocal fluorescence images from the HEK293 cells transfected with  $\Delta$ C-YFP-14-3-3 $\gamma/\Delta$ N-YFP-SYNPO2 and  $\Delta$ C-YFP-SYNPO2/ $\Delta$ N-YFP-14-3-3 $\gamma$  demonstrated an interaction between SYNPO2 and 14-3-3 $\gamma$  in the cytoplasm (Fig. 25 B & D). We detected that the cells transfected with  $\Delta$ C-YFP-SYNPO2/ $\Delta$ N-YFP-14-3-3 $\gamma$  displayed highly punctuated pattern of structures in the cytoplasm (Fig. 25 D). In contrast to the 14-3-3 $\gamma$ , a nuclear localization of SYNPO2 was detected when a combination of  $\Delta$ C-YFP-SYNPO2/ $\Delta$ N-YFP-14-3-3 $\beta$  and  $\Delta$ C-YFP-14-3-3 $\beta/\Delta$ N-YFP-SYNPO2 was used (Fig. 26 B & E). A possible mechanism could be that the interaction of SYNPO2 with 14-3-3 $\gamma$  stabilizes its localization in the cytoplasm, while it's shuttling to the nucleus seems to be regulated by 14-3-3 $\beta$ . Moreover, we detected protein aggregation-like structure in the nucleus (Fig. 26 B), which may either occur due to overexpression of constructs or display a form of nuclear bodies with so far unknown function. Furthermore, we detected a nucleus colocalization of SYNPO2-14-3-3 $\beta$  complex in form of a loop structure in the nucleus (Fig. 26 C').

Murine SYNPO2 contains two putative NLSs that are crucial for the nuclear import of myopodin. According to the notion that the selective import of proteins into the cell nucleus is depending on (A) the presence of NLSs and (B) the interaction of importin $\alpha$  with NLSs, SYNPO2, importin $\alpha$  interaction was investigated using BIFC assay. Confocal fluorescence images of transiently transfected HEK293 cells with  $\Delta$ N-YFP-SYNPO2/ $\Delta$ C-YFP-Importin $\alpha$  and  $\Delta$ C-YFP-SYNPO2/ $\Delta$ C-YFP-Importin $\alpha$  demonstrated a nuclear accumulation of both proteins. Moreover, we found the same nuclear loops as described above for YFP-SYNPO2 (Fig. 24 A) and  $\Delta$ C-YFP-SYNPO2/ $\Delta$ N-YFP-14-3-3 $\beta$  (Fig. 26 E) when the cells were

transfected with  $\Delta$ N-YFP SYNPO2/ $\Delta$ C-YFP-Importin $\alpha$  and  $\Delta$ C-YFP-SYNPO2/ $\Delta$ C-YFP-Importin $\alpha$  (Fig. 27 B & E).

Interestingly, apart from nuclear localization and interaction between SYNPO2, 14-3-3 $\beta$ , and importin $\alpha$ , our findings may resemble the results reported before for actin polymerization in the nucleus<sup>213, 214</sup>. As described before, actin filaments and actin binding proteins (ABPs) are involved in different cytoplasmic processes like defining the cell shape, cell motility, cytokinesis, and intracellular transport. However, recently actin and ABPs have been also assigned numerous functional roles in the nucleus<sup>215</sup>.

For instance, works from Christian Baarlink et al.<sup>213</sup> and Kei Miyamoto et al.<sup>214</sup> suggests an essential role of nuclear actin polymerization in cell fate and cellular programming via SRF (serum response factor) and Oct4 (octamer-binding transcription factor 4) signaling. SRF is a transcription factor that plays essential role in numerous cellular functions like regulation of differentiation, cell adhesion, motility and contraction<sup>8, 12</sup>. Oct4 is a transcription factor that is critically involved in the cell division of embryonic stem cells. Oct4 is also strongly expressed in the numerous cancers<sup>216, 217</sup>. Taken together, our findings raised the hypothesis of a potential link of SYNPO2, polymerization of nuclear actin and signaling involved in health (e.g. cellular development) and diseases (e.g. atherosclerosis, and cancer).

#### **4.6 Visualization of SYNPO2 homo-dimerization using BIFC assay in living cells**

Principally, many proteins form homodimers or homo-oligomers<sup>218</sup>. Recent studies show that protein homo-dimerization or oligomerization is an essential factor in the regulation of proteins such as enzymes, ion channels, receptors and transcription factors<sup>219</sup>. For instance, protein dimerization can be a mechanism for activation<sup>220</sup> or inhibition<sup>221</sup>. Although, self-association and/or oligomerization seem to be very common to generate a biological response in the cells, it is often difficult to quantify, because the stoichiometry of self-association for proteins has not been characterized by robust biophysical methods. It is already known that many ABPs either contain two or more actin binding motifs, or they interact with actin as a homodimer or oligomer<sup>222-224</sup>.

SYNPO2 is a strong candidate to exhibit such a feature because previous studies showed that SYNPO2 regulates actin nucleation, polymerization and further controls cross-linking of actin filaments into thick bundles. Furthermore, since SYNPO2 as a novel ABP demonstrated a direct interaction with actin<sup>92</sup>, similar to  $\alpha$ -actinin, filamin (actin cross-linking proteins), it may also play its role as homodimer or/and oligomer.

Although, recently the Fürst laboratory reported homodimerization of murine SYNPO2 by using biochemical methods<sup>92</sup>, it has not been a subject in a cellular context study. Accordingly, these findings raised the hypothesis of a potential link of SYNPO2 dimerization and its function in the cells. To address this possible mechanism, HEK293 cells were transiently transfected with  $\Delta$ C-YFP-SYNPO2/ $\Delta$ N-YFP-SYNPO2.

Our transiently cotransfected HEK293 cells with  $\Delta$ C-YFP-SYNPO2/ $\Delta$ N-YFP-SYNPO2 corroborated the previous finding that the SYNPO2 self-associate in the form a homodimer. SYNPO2-homodimer demonstrated a cytoplasmic distribution and not nuclear (Fig. 28). Interestingly, SYNPO2-dimers were detected close to the cell membrane and also to the nuclear membrane (Fig. 28 C, white arrow). Further quantitative analysis of the relative efficiency of BIFC complex formation by using a FACS-BIFC based assay demonstrated a significant population of positive BIFC-cells as compared to the cells transfected with or without  $\Delta$ C-YFP/ $\Delta$ N-YFP (as control experiments). Collectively, it can be speculated that the dimerization of SYNPO2 and its localization at plasma membrane may play an autoregulatory effect on its role in cell motility or cell junctions.

## 5 Conclusion and Outlook

Immunofluorescence, biophysical and molecular approaches not only showed that SYNPO2 changed its subcellular localization but also its transcript levels in VSMCs upon phenotype switch from contractile to non-contractile. Rat vascular smooth muscle cells (rVSMCs) developed a non-contractile phenotype (Passage 3) from contractile cells (day 1 of isolation) in primary cell culture, which was associated with an accumulation of SYNPO2 in the nucleus and a down-regulation of its expression.

Cultivation of VSMCs (passage 3) on laminin or collagen I coated matrices, induced a contractile or a non-contractile phenotype, respectively. This further supported the shuttling hypothesis of SYNPO2 depending on a phenotype switch and indicated a potential impact of SYNPO2 on phenotype switch.

Furthermore, the results of this thesis suggest an essential role of the cAMP-regulated kinase PKA for the regulation of the SYNPO2 shuttling in VSMCs. Increased cAMP levels in VSMCs (contractile) induced accumulation of SYNPO2, when adenylyl-cyclase was directly activated by forskolin, Sp-5.6-DCl-cBIMPS and urocortin as activators. Supporting these results, inhibition of PKA using specific inhibitors, like H89, Rp-8-PIP-cAMPS demonstrated an accumulation of SYNPO2 in the cytoplasm of VSMCs from passage 3. However, we detected that the increased cAMP level induced by forskolin and 3-Isobutyl-1-methylxanthine (IBMX) together caused a diffuse accumulation of SYNPO2 within and around the nucleus. In addition, treating the cells from passage 3 with okadaic acid demonstrated a reduction in the number of nuclear SYNPO2-displaying VSMCs.

Possible reasons for these results could be cell type-specific. Differences in the impact of cAMP or increased cAMP levels might not only be as pronounced as a PKA-mediated trafficking of SYNPO2. As recently reported, cAMP regulates not only the PKA signalling pathway, but also EPAC, a cAMP-regulated guanine nucleotide exchange factor (GEF). Like PKA, EPAC contains a cAMP binding domain, which activates the small GTPase family Rap1 and Rap2. In addition, several studies have shown that the activation of EPAC/Rap regulates actin remodeling and adherent junctions. Therefore, it appears that EPAC may be involved in SYNPO2 trafficking, due to its role in actin remodeling. Accordingly, a

better understanding of the mechanism played by cAMP-mediated pathways during SYNPO2 trafficking in the cells is needed. Thus, future experiments using specific and selective activators, and/or inhibitors of EPAC should be aimed to elucidate this lack of information.

Furthermore, interaction of SYNPO2 with 14-3-3 and importin- $\alpha$  in the cytoplasm of striated muscles regulated its accumulation in the nucleus by so far incompletely understood mechanisms. Notably, a BIFC assay demonstrated an increasing fluorescence in the nucleus developed after interaction between SYNPO2, 14-3-3 $\beta$ , and importin $\alpha$  as well as an enhanced cytoplasmic fluorescence in terms of interaction with 14-3-3 $\gamma$ . In conclusion, this indicates that the nuclear accumulation of SYNPO2 could be the result of the interaction between SYNPO2 and 14-3-3 $\beta$  and importin $\alpha$ , and not with 14-3-3 $\gamma$ . Up to now it is not known which isoforms of 14-3-3 are involved and how is the shuttling of SYNPO2 regulated in VSMCs. In this regard, using a SYNPO2 containing mutant 14-3-3 binding domains and thereby inhibiting the interaction between SYNPO2 and the different 14-3-3 isoforms might serve as a better model to study the mechanism that regulate trafficking of SYNPO in cells. Further suggested methods would be interaction studies using pull-down assays, Immunoprecipitation, BIFC assays, and finally generating, 14-3-3 knock-out cells to study SYNPO2 trafficking depending on 14-3-3 isoforms.

Localization of SYNPO2 and its interaction with 14-3-3 $\beta$  in the nucleus of HEK293 cells led to the formation of either nuclear dot-like shapes that are similar to the recently reported nuclear bodies or loop-like structure. Possible reasons for these observations could either be a protein aggregation due to overexpression of SYNPO2 in the nucleus or SYNPO2 could be involved in the formation of nuclear bodies and F-actin loops by a so far unknown mechanism. Accordingly, some future approaches like co-immunostaining with known proteins like perimyelocytic leukemia (PML) which is found in nuclear bodies should therefore be performed to elucidate this lack of information.

The future goal of this project would be to address this lack of understanding by using systematic approaches on different levels spanning transcriptional regulation, protein level, during development, after injury and under pathological conditions like cancer. For instance, embryonic stem cells (ESCs) could be an excellent model to study SYNPO2's

unknown functions because developmental processes *in vivo* can be recapitulated *in vitro* to a certain extent in a time- and cost-effective manner.

## 6 Bibliography

1. Somlyo AP, Somlyo AV. Signal transduction and regulation in smooth muscle. *Nature* 1994; **372**(6503): 231-6.
2. Somlyo AP, Somlyo AV. Smooth muscle: excitation-contraction coupling, contractile regulation, and the cross-bridge cycle. *Alcoholism, clinical and experimental research* 1994; **18**(1): 138-43.
3. Murphy RA, Herlihy JT, Megerman J. Force-generating capacity and contractile protein content of arterial smooth muscle. *The Journal of general physiology* 1974; **64**(6): 691-705.
4. Somlyo AP, Somlyo AV. Ultrastructural aspects of activation and contraction of vascular smooth muscle. *Federation proceedings* 1976; **35**(6): 1288-93.
5. Horowitz A, Menice CB, Laporte R, Morgan KG. Mechanisms of smooth muscle contraction. *Physiol Rev* 1996; **76**(4): 967-1003.
6. Nguyen AT, Gomez D, Bell RD, Campbell JH, Clowes AW, Gabbiani G *et al.* Smooth muscle cell plasticity: fact or fiction? *Circ Res*; **112**(1): 17-22.
7. Owens GK. Regulation of differentiation of vascular smooth muscle cells. *Physiol Rev* 1995; **75**(3): 487-517.
8. Mack CP. Signaling mechanisms that regulate smooth muscle cell differentiation. *Arterioscler Thromb Vasc Biol* 2011; **31**(7): 1495-505.
9. Majesky MW. Developmental basis of vascular smooth muscle diversity. *Arterioscler Thromb Vasc Biol* 2007; **27**(6): 1248-58.
10. Alexander MR, Owens GK. Epigenetic control of smooth muscle cell differentiation and phenotypic switching in vascular development and disease. *Annual review of physiology* 2012; **74**: 13-40.
11. Gomez D, Owens GK. Smooth muscle cell phenotypic switching in atherosclerosis. *Cardiovasc Res* 2012; **95**(2): 156-64.
12. Owens GK, Kumar MS, Wamhoff BR. Molecular regulation of vascular smooth muscle cell differentiation in development and disease. *Physiol Rev* 2004; **84**(3): 767-801.

13. Regan CP, Adam PJ, Madsen CS, Owens GK. Molecular mechanisms of decreased smooth muscle differentiation marker expression after vascular injury. *J Clin Invest* 2000; **106**(9): 1139-47.
14. Volkmann N, Hanein D. Actomyosin: law and order in motility. *Current opinion in cell biology* 2000; **12**(1): 26-34.
15. Volkmann N, Hanein D, Ouyang G, Trybus KM, DeRosier DJ, Lowey S. Evidence for cleft closure in actomyosin upon ADP release. *Nature structural biology* 2000; **7**(12): 1147-55.
16. Puetz S, Lubomirov LT, Pfitzer G. Regulation of smooth muscle contraction by small GTPases. *Physiology* 2009; **24**: 342-56.
17. Berridge MJ. Smooth muscle cell calcium activation mechanisms. *The Journal of physiology* 2008; **586**(Pt 21): 5047-61.
18. Somlyo AP, Somlyo AV. Ca<sup>2+</sup> sensitivity of smooth muscle and nonmuscle myosin II: modulated by G proteins, kinases, and myosin phosphatase. *Physiol Rev* 2003; **83**(4): 1325-58.
19. Isotani E, Zhi G, Lau KS, Huang J, Mizuno Y, Persechini A *et al.* Real-time evaluation of myosin light chain kinase activation in smooth muscle tissues from a transgenic calmodulin-biosensor mouse. *Proceedings of the National Academy of Sciences of the United States of America* 2004; **101**(16): 6279-84.
20. Kamm KE, Stull JT. The function of myosin and myosin light chain kinase phosphorylation in smooth muscle. *Annual review of pharmacology and toxicology* 1985; **25**: 593-620.
21. Kitazawa T, Gaylinn BD, Denney GH, Somlyo AP. G-protein-mediated Ca<sup>2+</sup> sensitization of smooth muscle contraction through myosin light chain phosphorylation. *J Biol Chem* 1991; **266**(3): 1708-15.
22. Kitazawa T, Masuo M, Somlyo AP. G protein-mediated inhibition of myosin light-chain phosphatase in vascular smooth muscle. *Proceedings of the National Academy of Sciences of the United States of America* 1991; **88**(20): 9307-10.
23. Kitazawa T, Somlyo AP. Modulation of Ca<sup>2+</sup> sensitivity by agonists in smooth muscle. *Advances in experimental medicine and biology* 1991; **304**: 97-109.
24. Pfitzer G. Invited review: regulation of myosin phosphorylation in smooth muscle. *Journal of applied physiology* 2001; **91**(1): 497-503.

25. Pfitzer G, Sonntag-Bensch D, Brkic-Koric D. Thiophosphorylation-induced Ca(2+) sensitization of guinea-pig ileum contractility is not mediated by Rho-associated kinase. *The Journal of physiology* 2001; **533**(Pt 3): 651-64.
26. Noda M, Yasuda-Fukazawa C, Moriishi K, Kato T, Okuda T, Kurokawa K *et al.* Involvement of rho in GTP gamma S-induced enhancement of phosphorylation of 20 kDa myosin light chain in vascular smooth muscle cells: inhibition of phosphatase activity. *FEBS Lett* 1995; **367**(3): 246-50.
27. Gong MC, Iizuka K, Nixon G, Browne JP, Hall A, Eccleston JF *et al.* Role of guanine nucleotide-binding proteins--ras-family or trimeric proteins or both--in Ca2+ sensitization of smooth muscle. *Proceedings of the National Academy of Sciences of the United States of America* 1996; **93**(3): 1340-5.
28. Otto B, Steusloff A, Just I, Aktories K, Pfitzer G. Role of Rho proteins in carbachol-induced contractions in intact and permeabilized guinea-pig intestinal smooth muscle. *The Journal of physiology* 1996; **496 ( Pt 2)**: 317-29.
29. Feng J, Ito M, Ichikawa K, Isaka N, Nishikawa M, Hartshorne DJ *et al.* Inhibitory phosphorylation site for Rho-associated kinase on smooth muscle myosin phosphatase. *J Biol Chem* 1999; **274**(52): 37385-90.
30. Amano M, Ito M, Kimura K, Fukata Y, Chihara K, Nakano T *et al.* Phosphorylation and activation of myosin by Rho-associated kinase (Rho-kinase). *J Biol Chem* 1996; **271**(34): 20246-9.
31. Kimura K, Ito M, Amano M, Chihara K, Fukata Y, Nakafuku M *et al.* Regulation of myosin phosphatase by Rho and Rho-associated kinase (Rho-kinase). *Science* 1996; **273**(5272): 245-8.
32. Hungerford JE, Owens GK, Argraves WS, Little CD. Development of the aortic vessel wall as defined by vascular smooth muscle and extracellular matrix markers. *Dev Biol* 1996; **178**(2): 375-92.
33. Moehle CW, Bhamidipati CM, Alexander MR, Mehta GS, Irvine JN, Salmon M *et al.* Bone marrow-derived MCP1 required for experimental aortic aneurysm formation and smooth muscle phenotypic modulation. *The Journal of thoracic and cardiovascular surgery* 2011; **142**(6): 1567-74.
34. Barnes MJ, Farndale RW. Collagens and atherosclerosis. *Exp Gerontol* 1999; **34**(4): 513-25.

35. Gittenberger-de Groot AC, DeRuiter MC, Bergwerff M, Poelmann RE. Smooth muscle cell origin and its relation to heterogeneity in development and disease. *Arterioscler Thromb Vasc Biol* 1999; **19**(7): 1589-94.
36. Gorenne I, Jin L, Yoshida T, Sanders JM, Sarembock IJ, Owens GK *et al.* LPP expression during in vitro smooth muscle differentiation and stent-induced vascular injury. *Circ Res* 2006; **98**(3): 378-85.
37. Gorenne I, Kavurma M, Scott S, Bennett M. Vascular smooth muscle cell senescence in atherosclerosis. *Cardiovasc Res* 2006; **72**(1): 9-17.
38. Hao H, Gabbiani G, Bochaton-Piallat ML. Arterial smooth muscle cell heterogeneity: implications for atherosclerosis and restenosis development. *Arterioscler Thromb Vasc Biol* 2003; **23**(9): 1510-20.
39. Karnik SK, Brooke BS, Bayes-Genis A, Sorensen L, Wythe JD, Schwartz RS *et al.* A critical role for elastin signaling in vascular morphogenesis and disease. *Development* 2003; **130**(2): 411-23.
40. Wamhoff BR, Hoofnagle MH, Burns A, Sinha S, McDonald OG, Owens GK. A G/C element mediates repression of the SM22alpha promoter within phenotypically modulated smooth muscle cells in experimental atherosclerosis. *Circ Res* 2004; **95**(10): 981-8.
41. Sobue K, Hayashi K, Nishida W. Expressional regulation of smooth muscle cell-specific genes in association with phenotypic modulation. *Mol Cell Biochem* 1999; **190**(1-2): 105-18.
42. Niessen P, Clement S, Fontao L, Chaponnier C, Teunissen B, Rensen S *et al.* Biochemical evidence for interaction between smoothelin and filamentous actin. *Exp Cell Res* 2004; **292**(1): 170-8.
43. van Eys GJ, Niessen PM, Rensen SS. Smoothelin in vascular smooth muscle cells. *Trends Cardiovasc Med* 2007; **17**(1): 26-30.
44. Rensen SS, Niessen PM, van Deursen JM, Janssen BJ, Heijman E, Hermeling E *et al.* Smoothelin-B deficiency results in reduced arterial contractility, hypertension, and cardiac hypertrophy in mice. *Circulation* 2008; **118**(8): 828-36.
45. Ridley AJ. Life at the leading edge. *Cell* 2011; **145**(7): 1012-22.
46. Olson MF, Sahai E. The actin cytoskeleton in cancer cell motility. *Clinical & experimental metastasis* 2009; **26**(4): 273-87.

47. Li N ZJ, Liang Y, Shao J, Peng F, Sun M, Xu N, Li X, Wang R, Liu S, Lu Y. A controversial tumor marker: is SM22 a proper biomarker for gastric cancer cells? *J Proteome Res.* 2007 **6**(8): 3304-12.
48. Muto A, Fitzgerald TN, Pimiento JM, Maloney SP, Teso D, Paszkowiak JJ *et al.* Smooth muscle cell signal transduction: implications of vascular biology for vascular surgeons. *J Vasc Surg* 2007; **45 Suppl A**: A15-24.
49. Folkman J, D'Amore PA. Blood vessel formation: what is its molecular basis? *Cell* 1996; **87**(7): 1153-5.
50. dos Remedios CG, Chhabra D, Kekic M, Dedova IV, Tsubakihara M, Berry DA *et al.* Actin binding proteins: regulation of cytoskeletal microfilaments. *Physiol Rev* 2003; **83**(2): 433-73.
51. Kim HR, Gallant C, Leavis PC, Gunst SJ, Morgan KG. Cytoskeletal remodeling in differentiated vascular smooth muscle is actin isoform dependent and stimulus dependent. *American journal of physiology. Cell physiology* 2008; **295**(3): C768-78.
52. Vandekerckhove J, Weber K. At least six different actins are expressed in a higher mammal: an analysis based on the amino acid sequence of the amino-terminal tryptic peptide. *Journal of molecular biology* 1978; **126**(4): 783-802.
53. Fatigati V, Murphy RA. Actin and tropomyosin variants in smooth muscles. Dependence on tissue type. *J Biol Chem* 1984; **259**(23): 14383-8.
54. North AJ, Gimona M, Lando Z, Small JV. Actin isoform compartments in chicken gizzard smooth muscle cells. *Journal of cell science* 1994; **107 ( Pt 3)**: 445-55.
55. Small JV, Herzog M, Barth M, Draeger A. Supercontracted state of vertebrate smooth muscle cell fragments reveals myofilament lengths. *J Cell Biol* 1990; **111**(6 Pt 1): 2451-61.
56. Pollard TD, Cooper JA. Actin and actin-binding proteins. A critical evaluation of mechanisms and functions. *Annual review of biochemistry* 1986; **55**: 987-1035.
57. Chamley-Campbell J CG, Ross R. The smooth muscle cell in culture. *Physiol Rev.* 1979; **59**(1): 1-61.
58. Hegyi G, Szilagyi L, Belagyi J. Influence of the bound nucleotide on the molecular dynamics of actin. *European journal of biochemistry / FEBS* 1988; **175**(2): 271-4.
59. Wegner A. Head to tail polymerization of actin. *Journal of molecular biology* 1976; **108**(1): 139-50.

60. Kinosian HJ, Selden LA, Estes JE, Gershman LC. Nucleotide binding to actin. Cation dependence of nucleotide dissociation and exchange rates. *J Biol Chem* 1993; **268**(12): 8683-91.
61. Carlier MF, Pantaloni D. Control of actin dynamics in cell motility. *Journal of molecular biology* 1997; **269**(4): 459-67.
62. Korn ED, Carlier MF, Pantaloni D. Actin polymerization and ATP hydrolysis. *Science* 1987; **238**(4827): 638-44.
63. Oosawa F AS, Hotta K, Ooi T. G-F transformation of actin as a fibrous condensation. *J Polymer Sci* 1959; **37**: 323-326.
64. Pollard TD, Blanchoin L, Mullins RD. Molecular mechanisms controlling actin filament dynamics in nonmuscle cells. *Annual review of biophysics and biomolecular structure* 2000; **29**: 545-76.
65. Amann KJ, Pollard TD. Cellular regulation of actin network assembly. *Curr Biol* 2000; **10**(20): R728-30.
66. Machesky LM, May RC. Arps: actin-related proteins. *Results and problems in cell differentiation* 2001; **32**: 213-29.
67. Evangelista M, Pruyne D, Amberg DC, Boone C, Bretscher A. Formins direct Arp2/3-independent actin filament assembly to polarize cell growth in yeast. *Nature cell biology* 2002; **4**(1): 32-41.
68. Pruyne D, Evangelista M, Yang C, Bi E, Zigmond S, Bretscher A *et al.* Role of formins in actin assembly: nucleation and barbed-end association. *Science* 2002; **297**(5581): 612-5.
69. Bamberg JR, Harris HE, Weeds AG. Partial purification and characterization of an actin depolymerizing factor from brain. *FEBS Lett* 1980; **121**(1): 178-82.
70. Blanchoin L, Pollard TD. Mechanism of interaction of Acanthamoeba actophorin (ADF/Cofilin) with actin filaments. *J Biol Chem* 1999; **274**(22): 15538-46.
71. Blanchoin L, Amann KJ, Higgs HN, Marchand JB, Kaiser DA, Pollard TD. Direct observation of dendritic actin filament networks nucleated by Arp2/3 complex and WASP/Scar proteins. *Nature* 2000; **404**(6781): 1007-11.
72. Pollard TD. Reflections on a quarter century of research on contractile systems. *Trends in biochemical sciences* 2000; **25**(12): 607-11.

73. Joseph M, Chalovich MMS. Synaptopodin family of natively unfolded, actin binding proteins: physical properties and potential biological functions. *Biophys Rev* 2010; **2**: 181-189.
74. Deller T, Mundel P, Frotscher M. Potential role of synaptopodin in spine motility by coupling actin to the spine apparatus. *Hippocampus* 2000; **10**(5): 569-81.
75. Beall B, Chalovich JM. Fesselin, a synaptopodin-like protein, stimulates actin nucleation and polymerization. *Biochemistry* 2001; **40**(47): 14252-9.
76. Schroeter MM, Chalovich JM. Fesselin binds to actin and myosin and inhibits actin-activated ATPase activity. *J Muscle Res Cell Motil* 2005; **26**(4-5): 183-9.
77. Weins A, Schwarz K, Faul C, Barisoni L, Linke WA, Mundel P. Differentiation- and stress-dependent nuclear cytoplasmic redistribution of myopodin, a novel actin-bundling protein. *J Cell Biol* 2001; **155**(3): 393-404.
78. Alvarez-Mugica M, Cebrian V, Fernandez-Gomez JM, Fresno F, Escaf S, Sanchez-Carbayo M. Myopodin methylation is associated with clinical outcome in patients with T1G3 bladder cancer. *The Journal of urology* 2010; **184**(4): 1507-13.
79. De Ganck A, De Corte V, Staes A, Gevaert K, Vandekerckhove J, Gettemans J. Multiple isoforms of the tumor suppressor myopodin are simultaneously transcribed in cancer cells. *Biochem Biophys Res Commun* 2008; **370**(2): 269-73.
80. Jing L, Liu L, Yu YP, Dhir R, Acquafondada M, Landsittel D *et al*. Expression of myopodin induces suppression of tumor growth and metastasis. *Am J Pathol* 2004; **164**(5): 1799-806.
81. Beqqali A, Monshouwer-Kloots J, Monteiro R, Welling M, Bakkers J, Ehler E *et al*. CHAP is a newly identified Z-disc protein essential for heart and skeletal muscle function. *Journal of cell science* 2010; **123**(Pt 7): 1141-50.
82. van Eldik W, Beqqali A, Monshouwer-Kloots J, Mummery C, Passier R. Cytoskeletal heart-enriched actin-associated protein (CHAP) is expressed in striated and smooth muscle cells in chick and mouse during embryonic and adult stages. *The International journal of developmental biology* 2011; **55**(6): 649-55.
83. Mundel P, Heid HW, Mundel TM, Kruger M, Reiser J, Kriz W. Synaptopodin: an actin-associated protein in telencephalic dendrites and renal podocytes. *J Cell Biol* 1997; **139**(1): 193-204.

84. Kremerskothen J, Plaas C, Kindler S, Frotscher M, Barnekow A. Synaptopodin, a molecule involved in the formation of the dendritic spine apparatus, is a dual actin/alpha-actinin binding protein. *Journal of neurochemistry* 2005; **92**(3): 597-606.
85. Asanuma K, Kim K, Oh J, Giardino L, Chabanis S, Faul C *et al.* Synaptopodin regulates the actin-bundling activity of alpha-actinin in an isoform-specific manner. *J Clin Invest* 2005; **115**(5): 1188-98.
86. Deller T, Merten T, Roth SU, Mundel P, Frotscher M. Actin-associated protein synaptopodin in the rat hippocampal formation: localization in the spine neck and close association with the spine apparatus of principal neurons. *The Journal of comparative neurology* 2000; **418**(2): 164-81.
87. Deller T, Korte M, Chabanis S, Drakew A, Schwegler H, Stefani GG *et al.* Synaptopodin-deficient mice lack a spine apparatus and show deficits in synaptic plasticity. *Proceedings of the National Academy of Sciences of the United States of America* 2003; **100**(18): 10494-9.
88. Leinweber BD, Fredricksen RS, Hoffman DR, Chalovich JM. Fesselin: a novel synaptopodin-like actin binding protein from muscle tissue. *J Muscle Res Cell Motil* 1999; **20**(5-6): 539-45.
89. Schroeter M, Chalovich JM. Ca<sup>2+</sup>-calmodulin regulates fesselin-induced actin polymerization. *Biochemistry* 2004; **43**(43): 13875-82.
90. Schroeter MM, Orlova A, Egelman EH, Beall B, Chalovich JM. Organization of F-actin by Fesselin (avian smooth muscle synaptopodin 2). *Biochemistry* 2013.
91. Kolakowski J, Wrzosek A, Dabrowska R. Fesselin is a target protein for calmodulin in a calcium-dependent manner. *Biochem Biophys Res Commun* 2004; **323**(4): 1251-6.
92. Linnemann A, Vakeel P, Bezerra E, Orfanos Z, Djinovic-Carugo K, van der Ven PF *et al.* Myopodin is an F-actin bundling protein with multiple independent actin-binding regions. *J Muscle Res Cell Motil* 2013; **34**(1): 61-9.
93. Linnemann A, van der Ven PF, Vakeel P, Albinus B, Simonis D, Bendas G *et al.* The sarcomeric Z-disc component myopodin is a multiadapter protein that interacts with filamin and alpha-actinin. *Eur J Cell Biol* 2010; **89**(9): 681-92.
94. Sanchez-Carbayo M, Schwarz K, Charytonowicz E, Cordon-Cardo C, Mundel P. Tumor suppressor role for myopodin in bladder cancer: loss of nuclear expression

- of myopodin is cell-cycle dependent and predicts clinical outcome. *Oncogene* 2003; **22**(34): 5298-305.
95. Yu YP, Luo JH. Phosphorylation and interaction of myopodin by integrin-link kinase lead to suppression of cell growth and motility in prostate cancer cells. *Oncogene* 2011; **30**(49): 4855-63.
96. De Ganck A, Hubert T, Van Impe K, Geelen D, Vandekerckhove J, De Corte V *et al.* A monopartite nuclear localization sequence regulates nuclear targeting of the actin binding protein myopodin. *FEBS Lett* 2005; **579**(29): 6673-80.
97. Renegar RH, Chalovich JM, Leinweber BD, Zary JT, Schroeter MM. Localization of the actin-binding protein fesselin in chicken smooth muscle. *Histochem Cell Biol* 2009; **131**(2): 191-6.
98. Schroeter MM, Beall B, Heid HW, Chalovich JM. In vitro characterization of native mammalian smooth-muscle protein synaptopodin 2. *Biosci Rep* 2008; **28**(4): 195-203.
99. Pham M, Chalovich JM. Smooth muscle alpha-actinin binds tightly to fesselin and attenuates its activity toward actin polymerization. *J Muscle Res Cell Motil* 2006; **27**(1): 45-51.
100. Faul C, Dhume A, Schechter AD, Mundel P. Protein kinase A, Ca<sup>2+</sup>/calmodulin-dependent kinase II, and calcineurin regulate the intracellular trafficking of myopodin between the Z-disc and the nucleus of cardiac myocytes. *Mol Cell Biol* 2007; **27**(23): 8215-27.
101. Faul C, Huttelmaier S, Oh J, Hachet V, Singer RH, Mundel P. Promotion of importin alpha-mediated nuclear import by the phosphorylation-dependent binding of cargo protein to 14-3-3. *J Cell Biol* 2005; **169**(3): 415-24.
102. Liang J, Ke G, You W, Peng Z, Lan J, Kalesse M *et al.* Interaction between importin 13 and myopodin suggests a nuclear import pathway for myopodin. *Mol Cell Biochem* 2008; **307**(1-2): 93-100.
103. Claeys KG, van der Ven PF, Behin A, Stojkovic T, Eymard B, Dubourg O *et al.* Differential involvement of sarcomeric proteins in myofibrillar myopathies: a morphological and immunohistochemical study. *Acta neuropathologica* 2009; **117**(3): 293-307.
104. Caron E, Hall A. Identification of two distinct mechanisms of phagocytosis controlled by different Rho GTPases. *Science* 1998; **282**(5394): 1717-21.

105. Hall A. Rho GTPases and the actin cytoskeleton. *Science* 1998; **279**(5350): 509-14.
106. Fields S, Song O. A novel genetic system to detect protein-protein interactions. *Nature* 1989; **340**(6230): 245-6.
107. Barrett B, Wood PA, Volwiler W. Quantitation of gamma globulins in human serum by immunoprecipitation. *The Journal of laboratory and clinical medicine* 1960; **55**: 605-15.
108. Ahmadova Z, Yagublu V, Forg T, Hajiyeva Y, Jesenofsky R, Hafner M *et al.* Fluorescent resonance energy transfer imaging of VEGFR dimerization. *Anticancer research* 2014; **34**(5): 2123-33.
109. Bhat RA, Lahaye T, Panstruga R. The visible touch: in planta visualization of protein-protein interactions by fluorophore-based methods. *Plant methods* 2006; **2**: 12.
110. Ciruela F. Fluorescence-based methods in the study of protein-protein interactions in living cells. *Current opinion in biotechnology* 2008; **19**(4): 338-43.
111. Boens N, Qin W, Basaric N, Hofkens J, Ameloot M, Pouget J *et al.* Fluorescence lifetime standards for time and frequency domain fluorescence spectroscopy. *Analytical chemistry* 2007; **79**(5): 2137-49.
112. Boevink P, McLellan H, Bukharova T, Engelhardt S, Birch P. In vivo protein-protein interaction studies with BiFC: conditions, cautions, and caveats. *Methods in molecular biology* 2014; **1127**: 81-90.
113. Gradinaru CC, Marushchak DO, Samim M, Krull UJ. Fluorescence anisotropy: from single molecules to live cells. *The Analyst* 2010; **135**(3): 452-9.
114. Blouin S, Craggs TD, Lafontaine DA, Penedo JC. Functional studies of DNA-protein interactions using FRET techniques. *Methods in molecular biology* 2009; **543**: 475-502.
115. Heyduk T. Measuring protein conformational changes by FRET/LRET. *Current opinion in biotechnology* 2002; **13**(4): 292-6.
116. Takanishi CL, Bykova EA, Cheng W, Zheng J. GFP-based FRET analysis in live cells. *Brain research* 2006; **1091**(1): 132-9.
117. Zheng J. Spectroscopy-based quantitative fluorescence resonance energy transfer analysis. *Methods in molecular biology* 2006; **337**: 65-77.

118. Truong K, Ikura M. The use of FRET imaging microscopy to detect protein-protein interactions and protein conformational changes in vivo. *Current opinion in structural biology* 2001; **11**(5): 573-8.
119. Day RN, Schaufele F. Imaging molecular interactions in living cells. *Molecular endocrinology* 2005; **19**(7): 1675-86.
120. Ebbinghaus S, Dhar A, McDonald JD, Gruebele M. Protein folding stability and dynamics imaged in a living cell. *Nature methods* 2010; **7**(4): 319-23.
121. Moraczewska J, Strzelecka-Golaszewska H, Moens PD, dos Remedios CG. Structural changes in subdomain 2 of G-actin observed by fluorescence spectroscopy. *The Biochemical journal* 1996; **317 ( Pt 2)**: 605-11.
122. Jares-Erijman EA, Jovin TM. FRET imaging. *Nature biotechnology* 2003; **21**(11): 1387-95.
123. Kerppola TK. Design of fusion proteins for bimolecular fluorescence complementation (BiFC). *Cold Spring Harbor protocols* 2013; **2013**(8): 714-8.
124. Kerppola TK. Bimolecular fluorescence complementation: visualization of molecular interactions in living cells. *Methods in cell biology* 2008; **85**: 431-70.
125. Hu CD, Grinberg AV, Kerppola TK. Visualization of protein interactions in living cells using bimolecular fluorescence complementation (BiFC) analysis. *Current protocols in protein science / editorial board, John E. Coligan ... [et al.]* 2005; **Chapter 19**: Unit 19 10.
126. Kerppola TK. Bimolecular fluorescence complementation (BiFC) analysis of protein interactions in live cells. *Cold Spring Harbor protocols* 2013; **2013**(8): 727-31.
127. Hu CD, Grinberg AV, Kerppola TK. Visualization of protein interactions in living cells using bimolecular fluorescence complementation (BiFC) analysis. *Current protocols in cell biology / editorial board, Juan S. Bonifacino ... [et al.]* 2006; **Chapter 21**: Unit 21 3.
128. Shyu YJ, Suarez CD, Hu CD. Visualization of AP-1 NF-kappaB ternary complexes in living cells by using a BiFC-based FRET. *Proceedings of the National Academy of Sciences of the United States of America* 2008; **105**(1): 151-6.
129. Shyu YJ, Suarez CD, Hu CD. Visualization of ternary complexes in living cells by using a BiFC-based FRET assay. *Nature protocols* 2008; **3**(11): 1693-702.

130. Hu CD, Kerppola TK. Simultaneous visualization of multiple protein interactions in living cells using multicolor fluorescence complementation analysis. *Nature biotechnology* 2003; **21**(5): 539-45.
131. Golovina VA, Blaustein MP. Preparation of primary cultured mesenteric artery smooth muscle cells for fluorescent imaging and physiological studies. *Nat Protoc* 2006; **1**(6): 2681-7.
132. Leik CE, Willey A, Graham MF, Walsh SW. Isolation and culture of arterial smooth muscle cells from human placenta. *Hypertension* 2004; **43**(4): 837-40.
133. Kisselbach L, Merges M, Bossie A, Boyd A. CD90 Expression on human primary cells and elimination of contaminating fibroblasts from cell cultures. *Cytotechnology* 2009; **59**(1): 31-44.
134. Weber SC, Gratopp A, Akanbi S, Rheinlaender C, Sallmon H, Barikbin P *et al.* Isolation and culture of fibroblasts, vascular smooth muscle, and endothelial cells from the fetal rat ductus arteriosus. *Pediatric research* 2011; **70**(3): 236-41.
135. Neumann S, Schneider M, Daugherty RL, Gottardi CJ, Eming SA, Beijer A *et al.* Nesprin-2 interacts with  $\alpha$ -catenin and regulates Wnt signaling at the nuclear envelope. *J Biol Chem* 2010; **285**(45): 34932-8.
136. Thakar K, Karaca S, Port SA, Urlaub H, Kehlenbach RH. Identification of CRM1-dependent Nuclear Export Cargos Using Quantitative Mass Spectrometry. *Mol Cell Proteomics* 2013; **12**(3): 664-78.
137. Towbin H, Staehelin T, Gordon J. Electrophoretic transfer of proteins from polyacrylamide gels to nitrocellulose sheets: procedure and some applications. *Proceedings of the National Academy of Sciences of the United States of America* 1979; **76**(9): 4350-4.
138. Schlunck G HH, Wecker T, Kampik D, Meyer-ter-Vehn T, Grehn F. Substrate rigidity modulates cell matrix interactions and protein expression in human trabecular meshwork cells. *Invest Ophthalmol Vis Sci.* 2008 **49**(1): 262-269.
139. Heras-Bautista CO, Katsen-Globa A, Schloerer NE, Dieluweit S, Abd El Aziz OM, Peinkofer G *et al.* The influence of physiological matrix conditions on permanent culture of induced pluripotent stem cell-derived cardiomyocytes. *Biomaterials* 2014.
140. Sneddon IN. The relation between load and penetration in the axisymmetric boussinesq problem for a punch of arbitrary profile. *International Journal of Engineering Science* 1965; (3): 47-57.

141. Hertz H. Uber die Berührung fester elastischer Körper. *J. Reine Angew. Mathematik*. 1882; (92): 156–171.
142. Weisenhorn AL, M. Khorsandi, S. Kasas, V. Gotzos, and H. J. Butt. Deformation and height anomaly of soft surfaces studied with an AFM. *Nanotechnology* 1993; (106).
143. Radmacher M, Fritz M, Hansma PK. Imaging soft samples with the atomic force microscope: gelatin in water and propanol. *Biophys J* 1995; **69**(1): 264-70.
144. Hutter JLB, J. Calibration of atomic-force microscope tips. *Review of Scientific Instruments* 1993; (64:): 1868-1873.
145. Worth NF, Rolfe BE, Song J, Campbell GR. Vascular smooth muscle cell phenotypic modulation in culture is associated with reorganisation of contractile and cytoskeletal proteins. *Cell Motil Cytoskeleton* 2001; **49**(3): 130-45.
146. Tran T TC, Tam JK, Qiao Y, Chin CY, Chong OK, Stewart AG, Harris T, Wong WS, Guan SP, Leung BP, Gerthoffer WT, Unruh H, Halayko AJ. Laminin drives survival signals to promote a contractile smooth muscle phenotype and airway hyperreactivity. *FASEB J* 2013; **27**: 1-13.
147. Autieri MV. Inducible expression of the signal transduction protein 14-3-3gamma in injured arteries and stimulated human vascular smooth muscle cells. *Experimental and molecular pathology* 2004; **76**(2): 99-107.
148. Autieri MV, Carbone CJ. 14-3-3Gamma interacts with and is phosphorylated by multiple protein kinase C isoforms in PDGF-stimulated human vascular smooth muscle cells. *DNA and cell biology* 1999; **18**(7): 555-64.
149. Autieri MV, Haines DS, Romanic AM, Ohlstein EH. Expression of 14-3-3 gamma in injured arteries and growth factor- and cytokine-stimulated human vascular smooth muscle cells. *Cell growth & differentiation : the molecular biology journal of the American Association for Cancer Research* 1996; **7**(11): 1453-60.
150. Ellis JJ, Valencia TG, Zeng H, Roberts LD, Deaton RA, Grant SR. CaM kinase IIdeltaC phosphorylation of 14-3-3beta in vascular smooth muscle cells: activation of class II HDAC repression. *Mol Cell Biochem* 2003; **242**(1-2): 153-61.
151. Matera AG. Nuclear bodies: multifaceted subdomains of the interchromatin space. *Trends Cell Biol* 1999; **9**(8): 302-9.

152. Morikawa S, Baluk P, Kaidoh T, Haskell A, Jain RK, McDonald DM. Abnormalities in pericytes on blood vessels and endothelial sprouts in tumors. *The American journal of pathology* 2002; **160**(3): 985-1000.
153. Panettieri RA, Jr. Airway smooth muscle: an immunomodulatory cell. *The Journal of allergy and clinical immunology* 2002; **110**(6 Suppl): S269-74.
154. Levin RM, Haugaard N, O'Connor L, Buttyan R, Das A, Dixon JS *et al.* Obstructive response of human bladder to BPH vs. rabbit bladder response to partial outlet obstruction: a direct comparison. *Neurourology and urodynamics* 2000; **19**(5): 609-29.
155. Golder M, Burleigh DE, Belai A, Ghali L, Ashby D, Lunniss PJ *et al.* Smooth muscle cholinergic denervation hypersensitivity in diverticular disease. *Lancet* 2003; **361**(9373): 1945-51.
156. Sobue K, Hayashi K, Nishida W. Molecular mechanism of phenotypic modulation of smooth muscle cells. *Hormone research* 1998; **50** Suppl 2: 15-24.
157. Gabbiani G, Schmid E, Winter S, Chaponnier C, de Ckhashtonay C, Vandekerckhove J *et al.* Vascular smooth muscle cells differ from other smooth muscle cells: predominance of vimentin filaments and a specific alpha-type actin. *Proceedings of the National Academy of Sciences of the United States of America* 1981; **78**(1): 298-302.
158. Babij P, Kelly C, Periasamy M. Characterization of a mammalian smooth muscle myosin heavy-chain gene: complete nucleotide and protein coding sequence and analysis of the 5' end of the gene. *Proceedings of the National Academy of Sciences of the United States of America* 1991; **88**(23): 10676-80.
159. van der Loop FT, Schaart G, Timmer ED, Ramaekers FC, van Eys GJ. Smoothelin, a novel cytoskeletal protein specific for smooth muscle cells. *J Cell Biol* 1996; **134**(2): 401-11.
160. Frid MG, Shekhonin BV, Koteliansky VE, Glukhova MA. Phenotypic changes of human smooth muscle cells during development: late expression of heavy caldesmon and calponin. *Dev Biol* 1992; **153**(2): 185-93.
161. Duband JL, Gimona M, Scatena M, Sartore S, Small JV. Calponin and SM 22 as differentiation markers of smooth muscle: spatiotemporal distribution during avian embryonic development. *Differentiation* 1993; **55**(1): 1-11.

162. Miano JM, Carlson MJ, Spencer JA, Misra RP. Serum response factor-dependent regulation of the smooth muscle calponin gene. *J Biol Chem* 2000; **275**(13): 9814-22.
163. Qu MJ, Liu B, Wang HQ, Yan ZQ, Shen BR, Jiang ZL. Frequency-dependent phenotype modulation of vascular smooth muscle cells under cyclic mechanical strain. *Journal of vascular research* 2007; **44**(5): 345-53.
164. Liu B, Qu MJ, Qin KR, Li H, Li ZK, Shen BR *et al.* Role of cyclic strain frequency in regulating the alignment of vascular smooth muscle cells in vitro. *Biophysical journal* 2008; **94**(4): 1497-507.
165. Qu M, Liu B, Jiang Z. [Effect of frequency of cyclic tensile strain on extracellular matrix of rat vascular smooth muscle cells in vitro]. *Sheng wu yi xue gong cheng xue za zhi = Journal of biomedical engineering = Shengwu yixue gongchengxue zazhi* 2008; **25**(4): 826-30.
166. Schiller HB FR. Mechanosensitivity and compositional dynamics of cell-matrix adhesions. *EMBO Rep.* 2013 **14**(6): 509-519.
167. Laing NG, Dye DE, Wallgren-Pettersson C, Richard G, Monnier N, Lillis S *et al.* Mutations and polymorphisms of the skeletal muscle alpha-actin gene (ACTA1). *Human mutation* 2009; **30**(9): 1267-77.
168. Steeg PS. Tumor metastasis: mechanistic insights and clinical challenges. *Nature medicine* 2006; **12**(8): 895-904.
169. Penzes P, Vanleeuwen JE. Impaired regulation of synaptic actin cytoskeleton in Alzheimer's disease. *Brain research reviews* 2011; **67**(1-2): 184-92.
170. Ochs HD, Thrasher AJ. The Wiskott-Aldrich syndrome. *The Journal of allergy and clinical immunology* 2006; **117**(4): 725-38; quiz 739.
171. Pavone L, Corsello G, Pavone P, Iannetti P. Lissencephalic syndromes: brain and beyond. *Frontiers in bioscience* 2010; **2**: 85-95.
172. Khaymina SS, Kenney JM, Schroeter MM, Chalovich JM. Fesselin is a natively unfolded protein. *J Proteome Res* 2007; **6**(9): 3648-54.
173. Ueki N, Sobue K, Kanda K, Hada T, Higashino K. Expression of high and low molecular weight caldesmons during phenotypic modulation of smooth muscle cells. *Proceedings of the National Academy of Sciences of the United States of America* 1987; **84**(24): 9049-53.

174. Yamamoto M, Yamamoto K, Noumura T. Type I collagen promotes modulation of cultured rabbit arterial smooth muscle cells from a contractile to a synthetic phenotype. *Exp Cell Res* 1993; **204**(1): 121-9.
175. Gabella G. Structural apparatus for force transmission in smooth muscles. *Physiol Rev* 1984; **64**(2): 455-77.
176. Schroeter MM, Beall B, Heid HW, Chalovich JM. The actin binding protein, fesselin, is a member of the synaptopodin family. *Biochem Biophys Res Commun* 2008; **371**(3): 582-6.
177. Cooper JA. Effects of cytochalasin and phalloidin on actin. *J Cell Biol* 1987; **105**(4): 1473-8.
178. Selden LA, Gershman LC, Estes JE. A proposed mechanism of action of cytochalasin D on muscle actin. *Biochem Biophys Res Commun* 1980; **95**(4): 1854-60.
179. Welch WJ, Suhan JP. Morphological study of the mammalian stress response: characterization of changes in cytoplasmic organelles, cytoskeleton, and nucleoli, and appearance of intranuclear actin filaments in rat fibroblasts after heat-shock treatment. *J Cell Biol* 1985; **101**(4): 1198-211.
180. Laszlo A. The effects of hyperthermia on mammalian cell structure and function. *Cell proliferation* 1992; **25**(2): 59-87.
181. Mounier N, Arrigo AP. Actin cytoskeleton and small heat shock proteins: how do they interact? *Cell stress & chaperones* 2002; **7**(2): 167-76.
182. Seibel NM, Eljouni J, Nalaskowski MM, Hampe W. Nuclear localization of enhanced green fluorescent protein homomultimers. *Analytical biochemistry* 2007; **368**(1): 95-9.
183. von Arnim AG, Deng XW, Stacey MG. Cloning vectors for the expression of green fluorescent protein fusion proteins in transgenic plants. *Gene* 1998; **221**(1): 35-43.
184. Allen RJ, Bogle ID, Ridley AJ. A model of localised Rac1 activation in endothelial cells due to fluid flow. *Journal of theoretical biology* 2011; **280**(1): 34-42.
185. Burns S, Thrasher AJ, Blundell MP, Machesky L, Jones GE. Configuration of human dendritic cell cytoskeleton by Rho GTPases, the WAS protein, and differentiation. *Blood* 2001; **98**(4): 1142-9.
186. Hall A. G proteins and small GTPases: distant relatives keep in touch. *Science* 1998; **280**(5372): 2074-5.

187. Horwitz AR, Parsons JT. Cell migration--movin' on. *Science* 1999; **286**(5442): 1102-3.
188. Puetz S, Schroeter MM, Piechura H, Reimann L, Hunger MS, Lubomirov LT *et al.* New insights into myosin phosphorylation during cyclic nucleotide-mediated smooth muscle relaxation. *J Muscle Res Cell Motil* 2012; **33**(6): 471-83.
189. Uehata M, Ishizaki T, Satoh H, Ono T, Kawahara T, Morishita T *et al.* Calcium sensitization of smooth muscle mediated by a Rho-associated protein kinase in hypertension. *Nature* 1997; **389**(6654): 990-4.
190. Takahara A, Sugiyama A, Satoh Y, Yoneyama M, Hashimoto K. Cardiovascular effects of Y-27632, a selective Rho-associated kinase inhibitor, assessed in the halothane-anesthetized canine model. *European journal of pharmacology* 2003; **460**(1): 51-7.
191. Kai F, Tanner K, King C, Duncan R. Myopodin isoforms alter the chemokinetic response of PC3 cells in response to different migration stimuli via differential effects on Rho-ROCK signaling pathways. *Carcinogenesis* 2012; **33**(11): 2100-7.
192. Ai S, Kuzuya M, Koike T, Asai T, Kanda S, Maeda K *et al.* Rho-Rho kinase is involved in smooth muscle cell migration through myosin light chain phosphorylation-dependent and independent pathways. *Atherosclerosis* 2001; **155**(2): 321-7.
193. Nishiguchi F, Fukui R, Hoshiga M, Negoro N, Ii M, Nakakohji T *et al.* Different migratory and proliferative properties of smooth muscle cells of coronary and femoral artery. *Atherosclerosis* 2003; **171**(1): 39-47.
194. Worthylake RA, Lemoine S, Watson JM, Burridge K. RhoA is required for monocyte tail retraction during transendothelial migration. *J Cell Biol* 2001; **154**(1): 147-60.
195. Grandoch M, Roscioni SS, Schmidt M. The role of Epac proteins, novel cAMP mediators, in the regulation of immune, lung and neuronal function. *British journal of pharmacology* 2010; **159**(2): 265-84.
196. Cheng X, Ji Z, Tsalkova T, Mei F. Epac and PKA: a tale of two intracellular cAMP receptors. *Acta biochimica et biophysica Sinica* 2008; **40**(7): 651-62.
197. Krebs EG, Beavo JA. Phosphorylation-dephosphorylation of enzymes. *Annual review of biochemistry* 1979; **48**: 923-59.
198. Gough NR, Foley JF. Focus issue: systems analysis of protein phosphorylation. *Science signaling* 2010; **3**(137): eg6.

199. Fernandez JJ, Candenas ML, Souto ML, Trujillo MM, Norte M. Okadaic acid, useful tool for studying cellular processes. *Current medicinal chemistry* 2002; **9**(2): 229-62.
200. Cohen P, Holmes CF, Tsukitani Y. Okadaic acid: a new probe for the study of cellular regulation. *Trends in biochemical sciences* 1990; **15**(3): 98-102.
201. Eichhorn PJ, Creighton MP, Bernards R. Protein phosphatase 2A regulatory subunits and cancer. *Biochimica et biophysica acta* 2009; **1795**(1): 1-15.
202. Lu J, Kovach JS, Johnson F, Chiang J, Hodes R, Lonser R *et al.* Inhibition of serine/threonine phosphatase PP2A enhances cancer chemotherapy by blocking DNA damage induced defense mechanisms. *Proceedings of the National Academy of Sciences of the United States of America* 2009; **106**(28): 11697-702.
203. Levene PA AC. THE CLEAVAGE PRODUCTS OF VITELLIN. . *J. Biol. Chem.* 1906; **2**(1 ): 127-133.
204. Muslin AJ, Xing H. 14-3-3 proteins: regulation of subcellular localization by molecular interference. *Cellular signalling* 2000; **12**(11-12): 703-9.
205. Brunet A, Kanai F, Stehn J, Xu J, Sarbassova D, Frangioni JV *et al.* 14-3-3 transits to the nucleus and participates in dynamic nucleocytoplasmic transport. *J Cell Biol* 2002; **156**(5): 817-28.
206. Morrison DK. The 14-3-3 proteins: integrators of diverse signaling cues that impact cell fate and cancer development. *Trends Cell Biol* 2009; **19**(1): 16-23.
207. Oldfield CJ, Meng J, Yang JY, Yang MQ, Uversky VN, Dunker AK. Flexible nets: disorder and induced fit in the associations of p53 and 14-3-3 with their partners. *BMC genomics* 2008; **9 Suppl 1**: S1.
208. Yaffe MB. How do 14-3-3 proteins work?-- Gatekeeper phosphorylation and the molecular anvil hypothesis. *FEBS Lett* 2002; **513**(1): 53-7.
209. Maheswaranathan M, Gole HK, Fernandez I, Lassegue B, Griendling KK, San Martin A. Platelet-derived growth factor (PDGF) regulates Slingshot phosphatase activity via Nox1-dependent auto-dephosphorylation of serine 834 in vascular smooth muscle cells. *J Biol Chem* 2011; **286**(41): 35430-7.
210. Moore MS, Blobel G. The GTP-binding protein Ran/TC4 is required for protein import into the nucleus. *Nature* 1993; **365**(6447): 661-3.

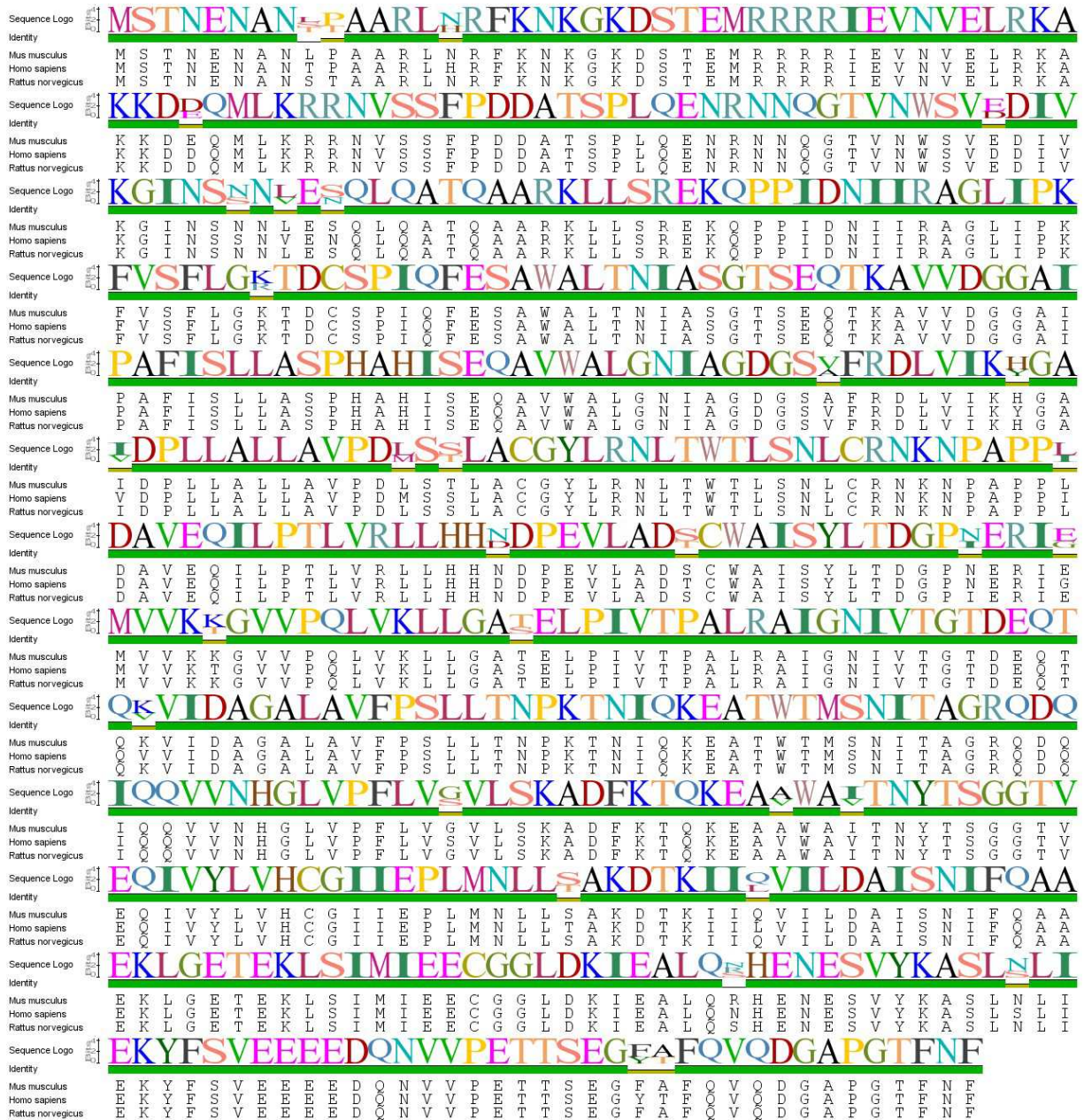
211. Melchior F, Paschal B, Evans J, Gerace L. Inhibition of nuclear protein import by nonhydrolyzable analogues of GTP and identification of the small GTPase Ran/TC4 as an essential transport factor. *J Cell Biol* 1993; **123**(6 Pt 2): 1649-59.
212. Moore MS, Blobel G. Purification of a Ran-interacting protein that is required for protein import into the nucleus. *Proceedings of the National Academy of Sciences of the United States of America* 1994; **91**(21): 10212-6.
213. Baarlink C, Wang H, Grosse R. Nuclear actin network assembly by formins regulates the SRF coactivator MAL. *Science* 2013; **340**(6134): 864-7.
214. Miyamoto K, Pasque V, Jullien J, Gurdon JB. Nuclear actin polymerization is required for transcriptional reprogramming of Oct4 by oocytes. *Genes & development* 2011; **25**(9): 946-58.
215. Nishimoto N, Watanabe M, Watanabe S, Sugimoto N, Yugawa T, Ikura T *et al.* Heterocomplex formation by Arp4 and beta-actin is involved in the integrity of the Brg1 chromatin remodeling complex. *Journal of cell science* 2012; **125**(Pt 16): 3870-82.
216. Wu G, Scholer HR. Role of Oct4 in the early embryo development. *Cell regeneration* 2014; **3**(1): 7.
217. Niwa H, Miyazaki J, Smith AG. Quantitative expression of Oct-3/4 defines differentiation, dedifferentiation or self-renewal of ES cells. *Nature genetics* 2000; **24**(4): 372-6.
218. Goodsell DS, Olson AJ. Structural symmetry and protein function. *Annual review of biophysics and biomolecular structure* 2000; **29**: 105-53.
219. Marianayagam NJ, Sunde M, Matthews JM. The power of two: protein dimerization in biology. *Trends in biochemical sciences* 2004; **29**(11): 618-25.
220. Renatus M, Stennicke HR, Scott FL, Liddington RC, Salvesen GS. Dimer formation drives the activation of the cell death protease caspase 9. *Proceedings of the National Academy of Sciences of the United States of America* 2001; **98**(25): 14250-5.
221. Chen Z, Chang K, Capraro BR, Zhu C, Hsu CJ, Baumgart T. Intradimer/Intermolecular interactions suggest autoinhibition mechanism in endophilin A1. *Journal of the American Chemical Society* 2014; **136**(12): 4557-64.
222. Oku T, Itoh S, Ishii R, Suzuki K, Nauseef WM, Toyoshima S *et al.* Homotypic dimerization of the actin-binding protein p57/coronin-1 mediated by a leucine

- zipper motif in the C-terminal region. *The Biochemical journal* 2005; **387**(Pt 2): 325-31.
223. Pudas R, Kiema TR, Butler PJ, Stewart M, Ylanne J. Structural basis for vertebrate filamin dimerization. *Structure* 2005; **13**(1): 111-9.
224. Xu Y, Moseley JB, Sagot I, Poy F, Pellman D, Goode BL *et al.* Crystal structures of a Formin Homology-2 domain reveal a tethered dimer architecture. *Cell* 2004; **116**(5): 711-23.



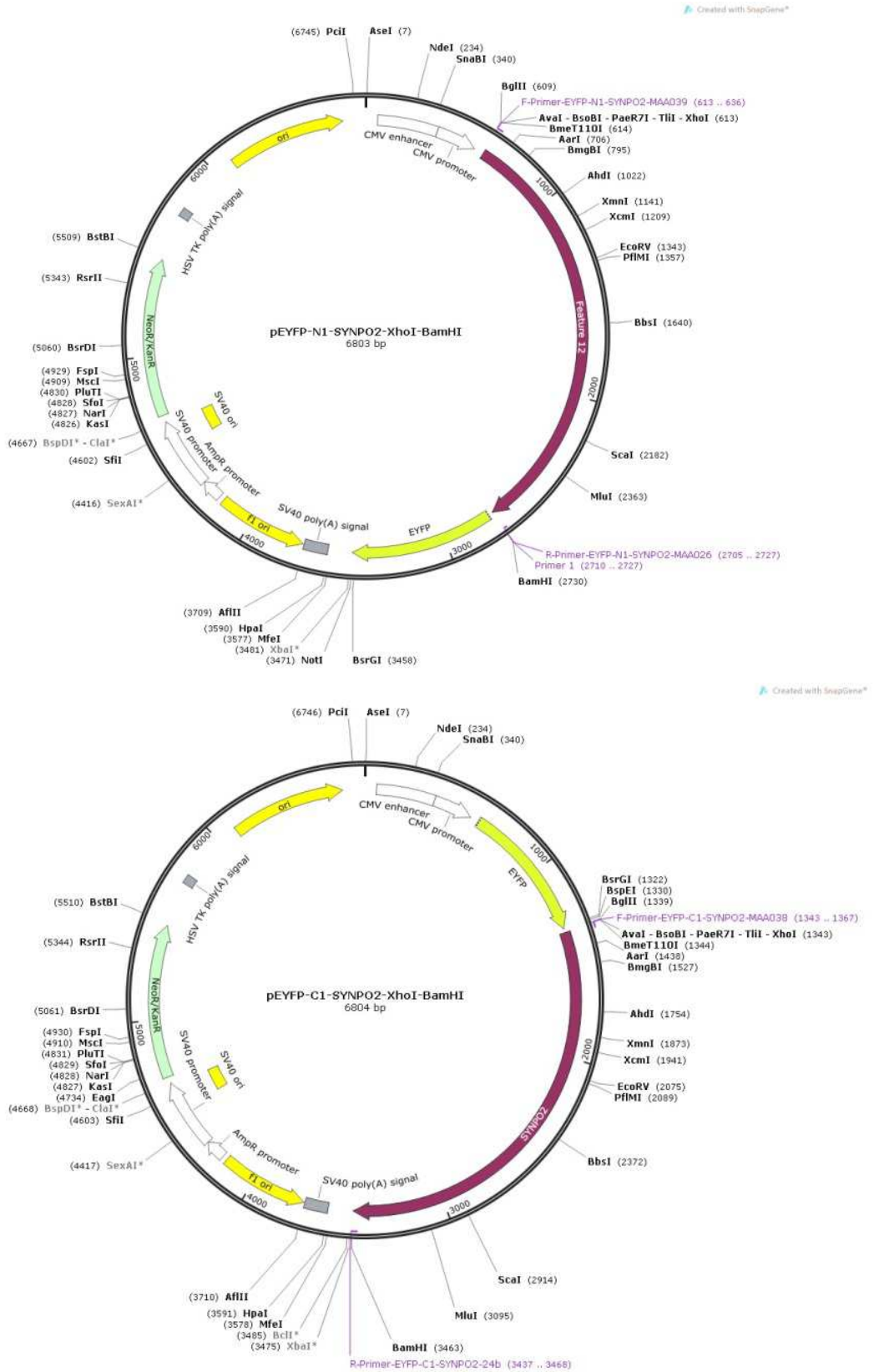


### 7.4 Importina

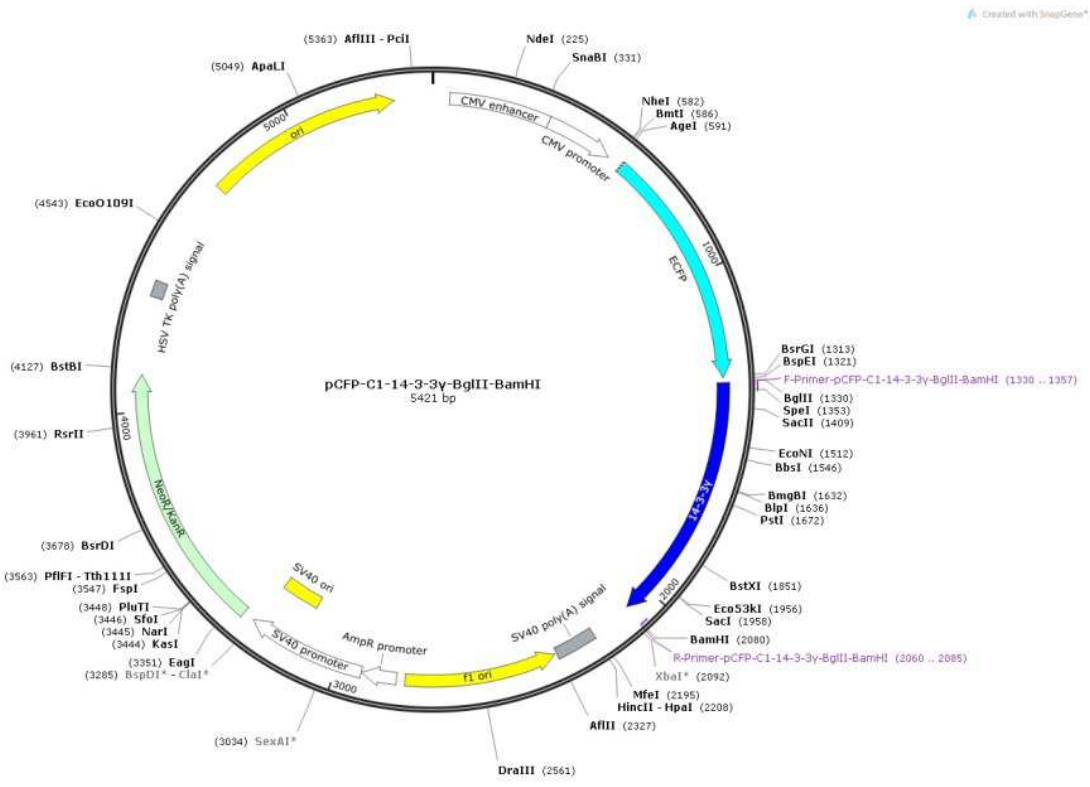
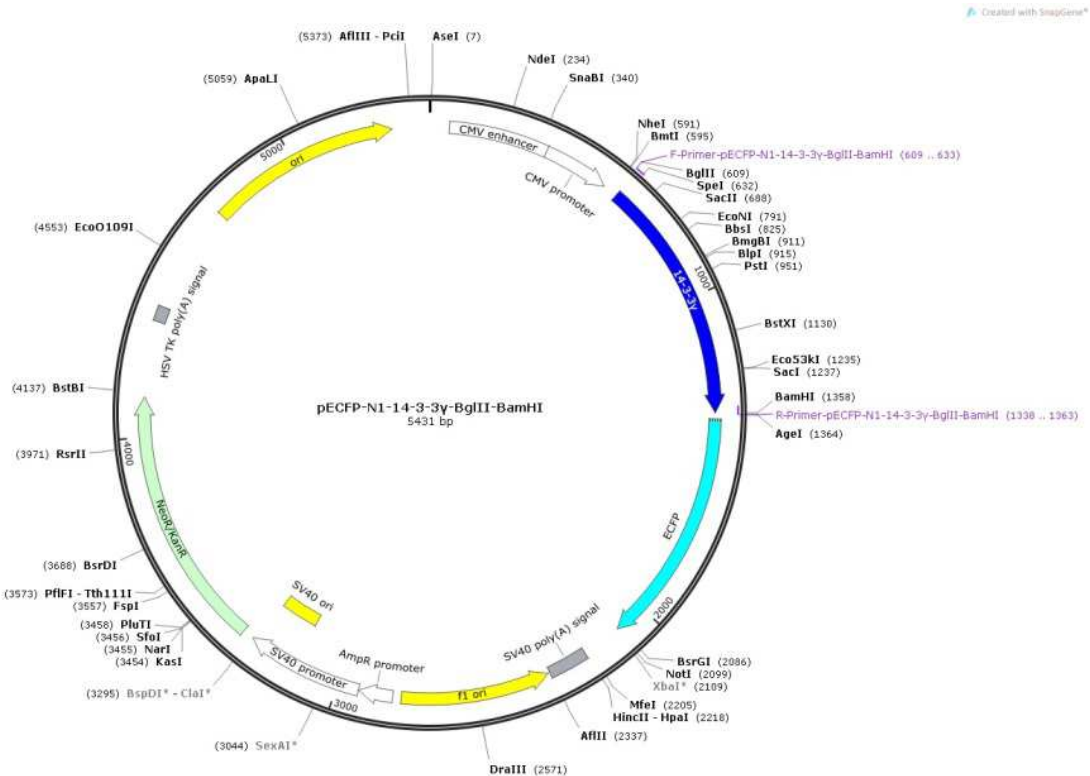


## 7.5 Plasmids

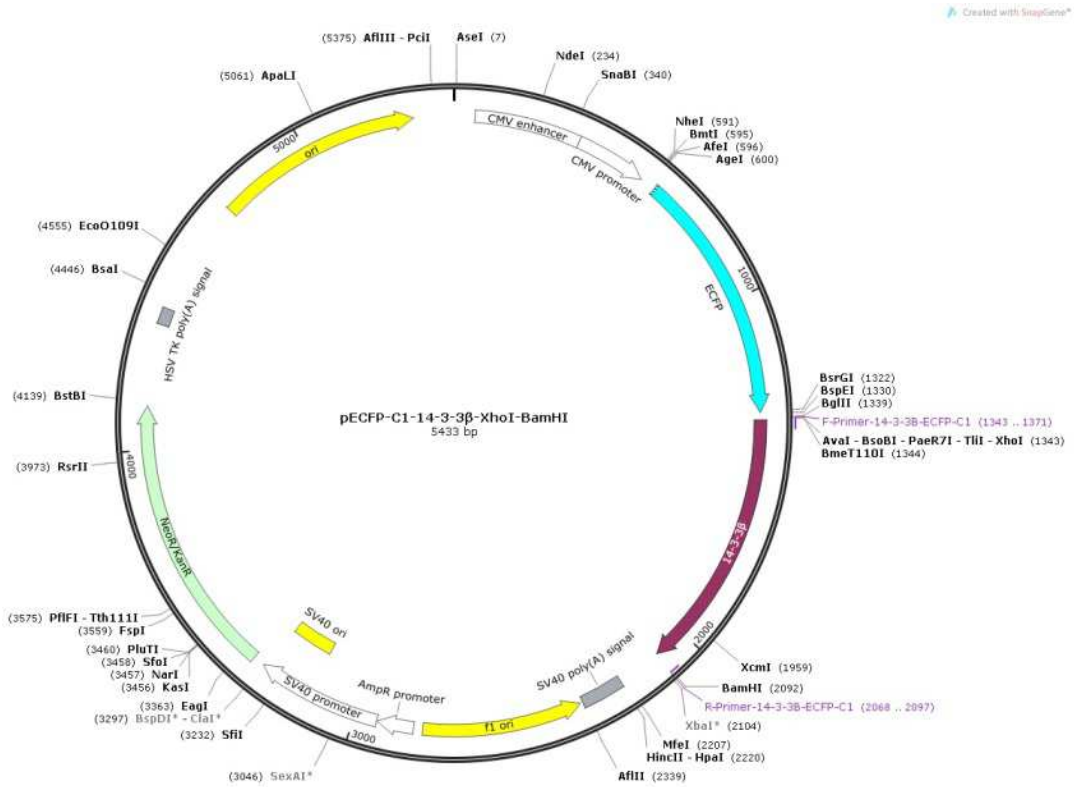
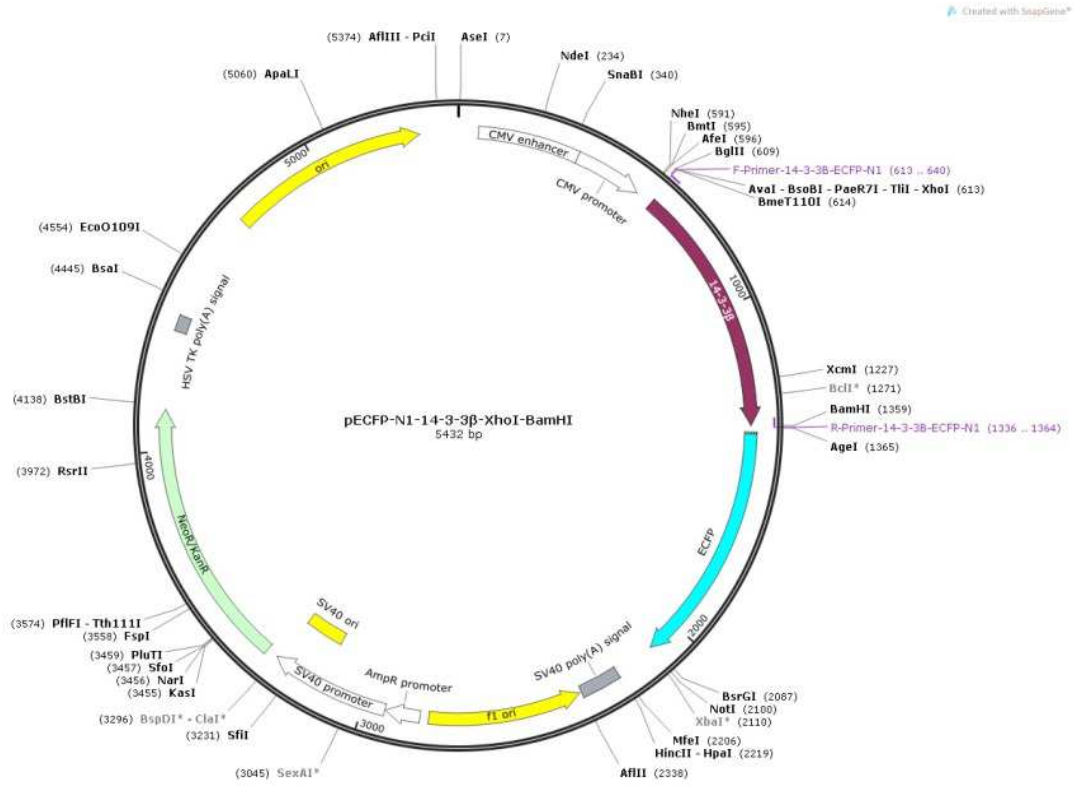
### 7.5.1 pEYFP-N1-SYNPO2 and pEYFP-C1-SYNPO2



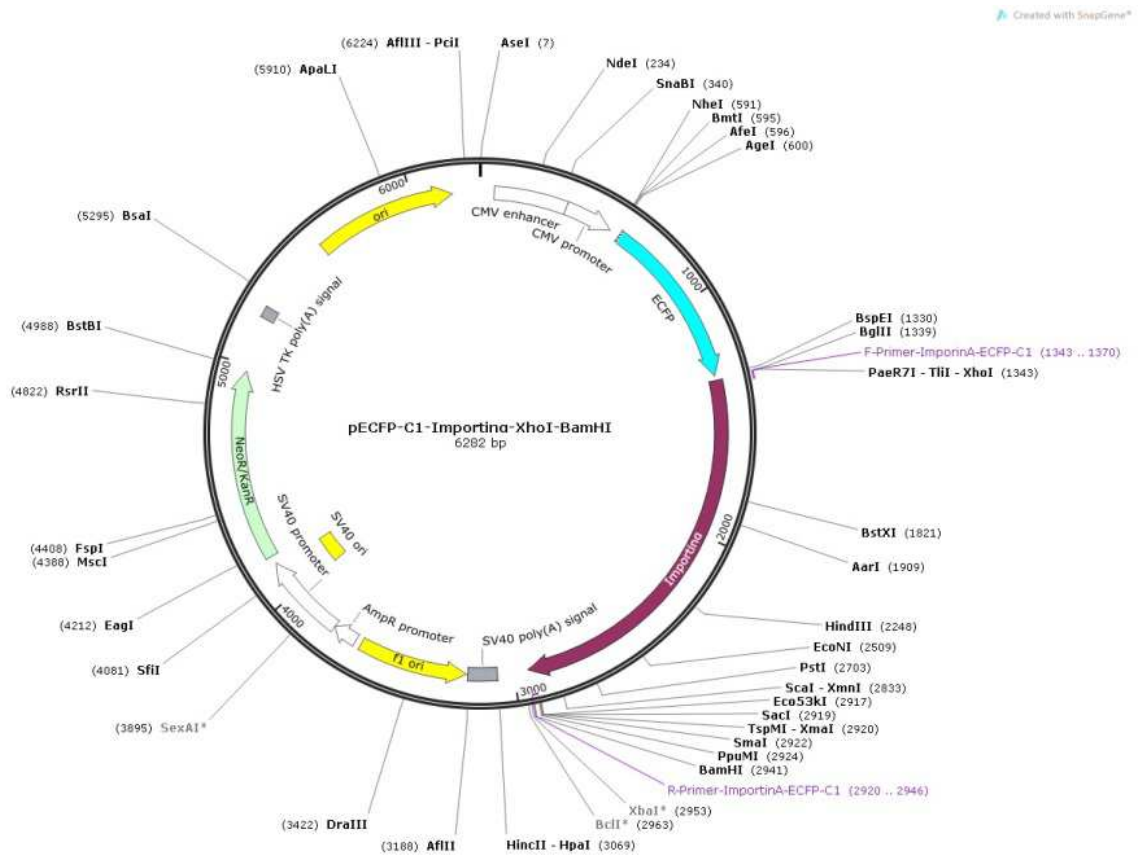
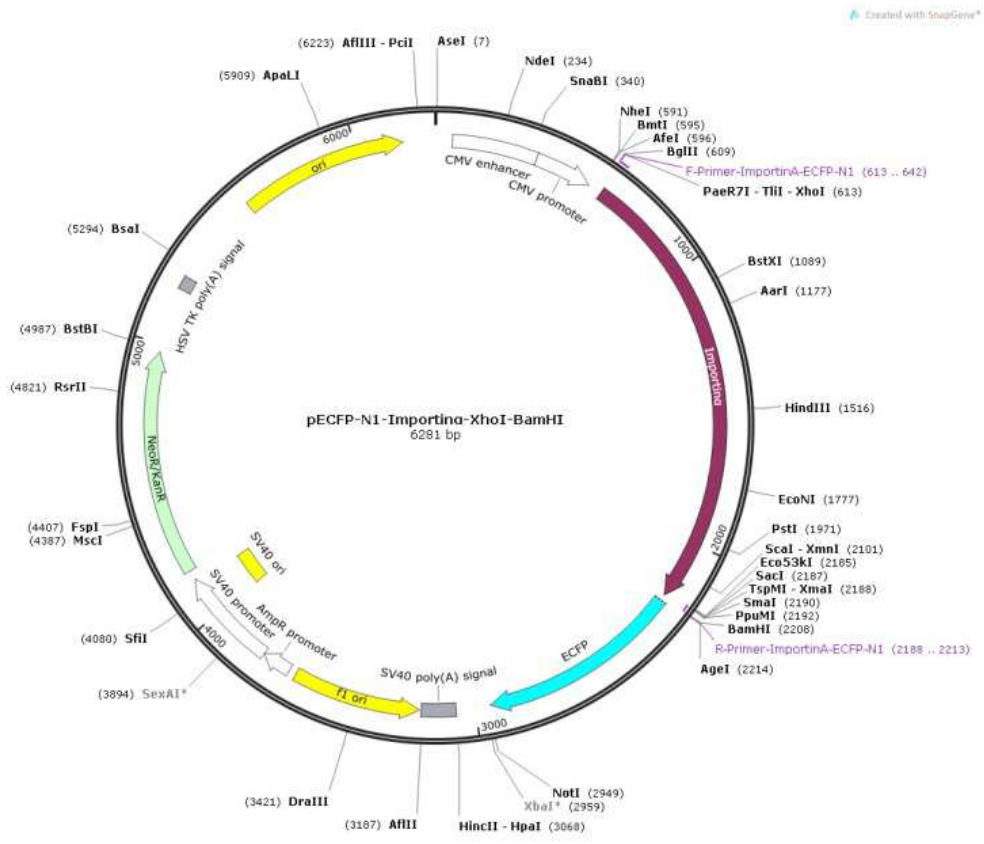
7.5.2 pECFP-N1-14-3-3y and pECFP-C1-14-3-3y



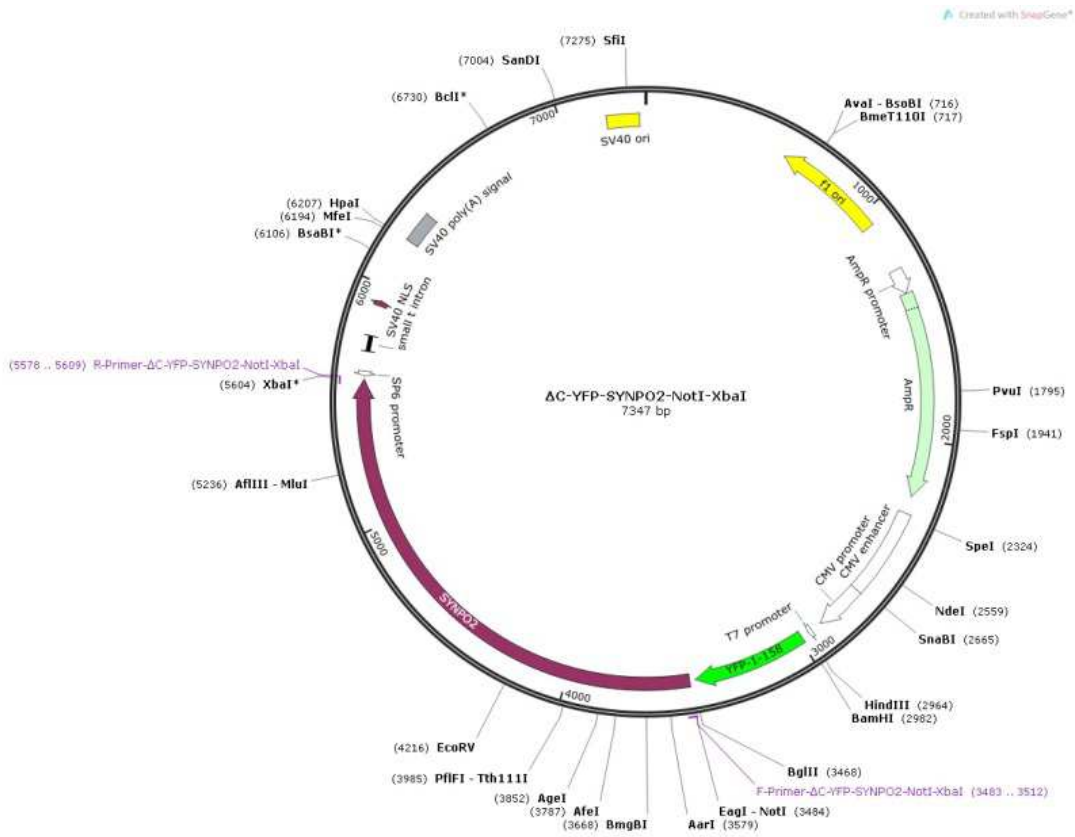
7.5.3 pECFP-N1-14-3-3β and pECFP-C1-14-3-3β



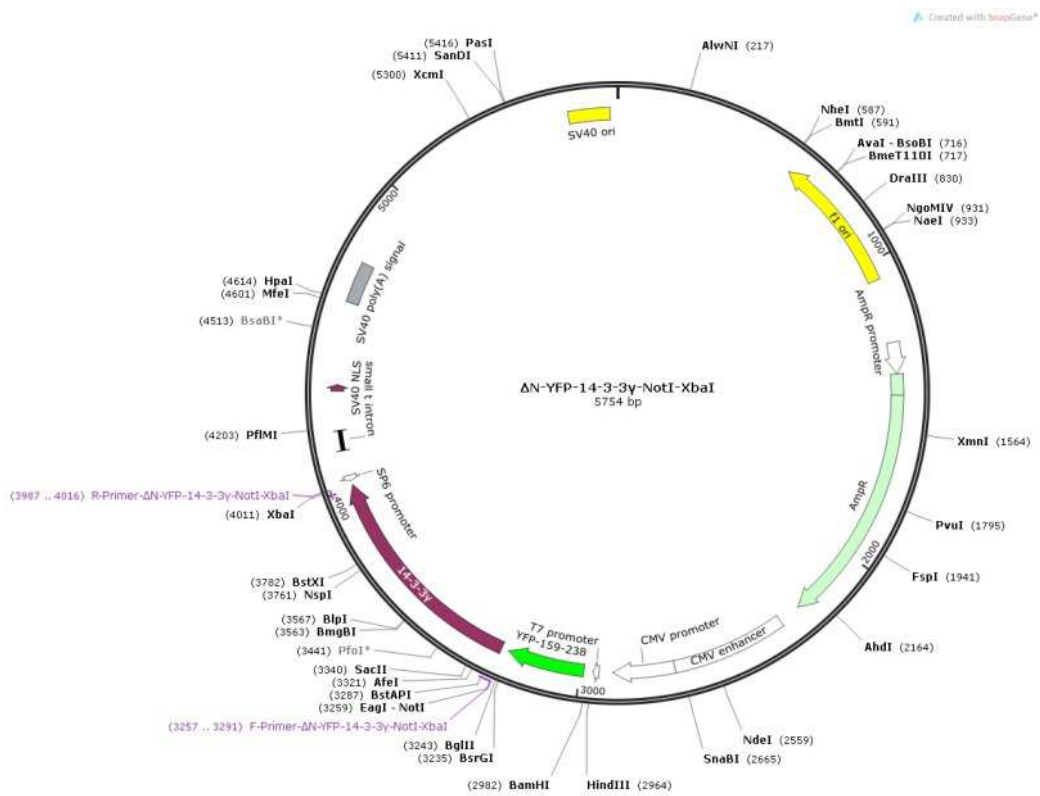
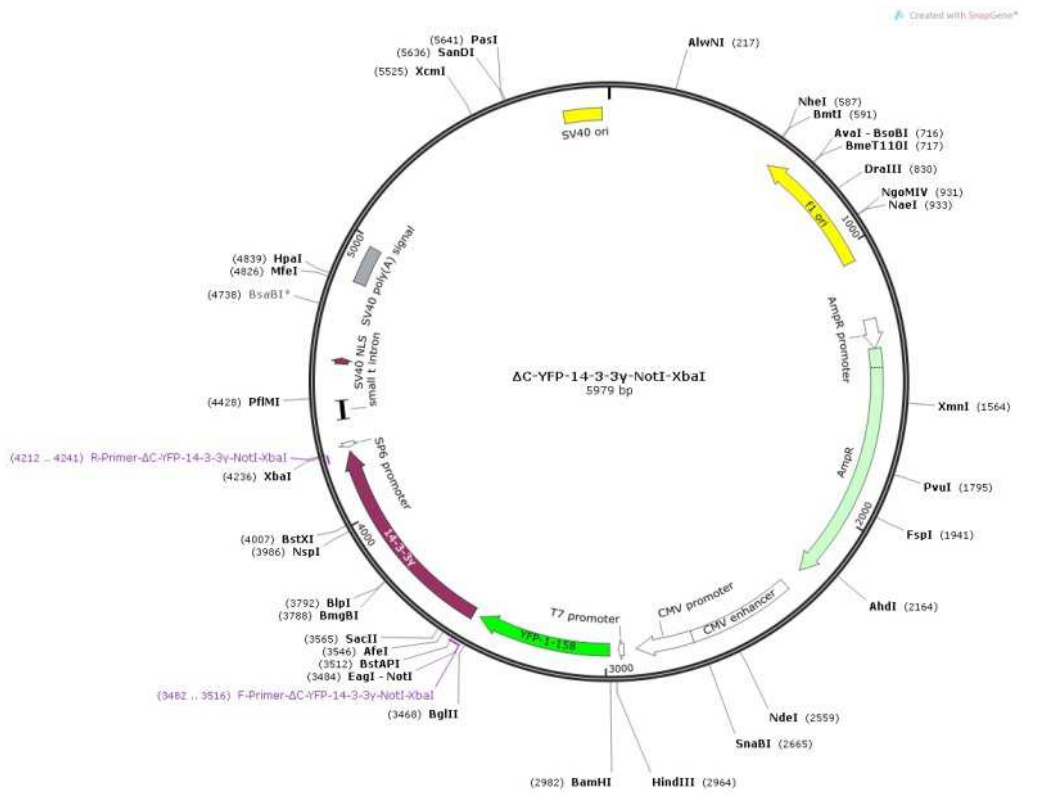
7.5.4 pECFP-N1-importin $\alpha$  and pECFP-C1-importin $\alpha$



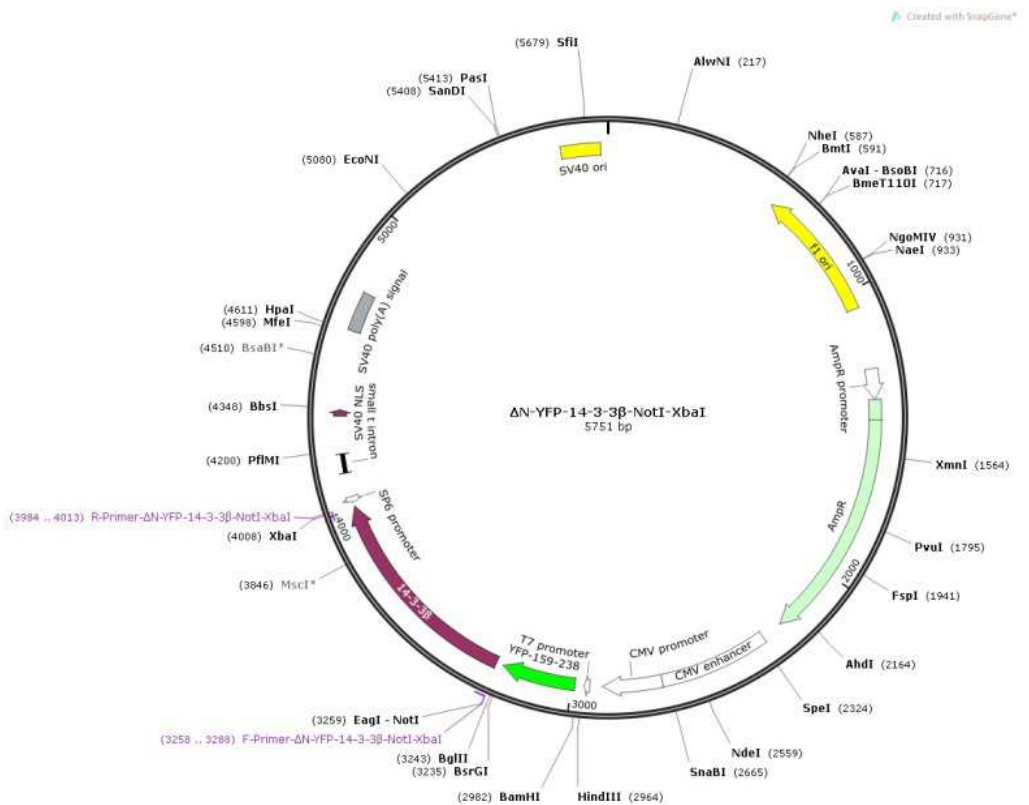
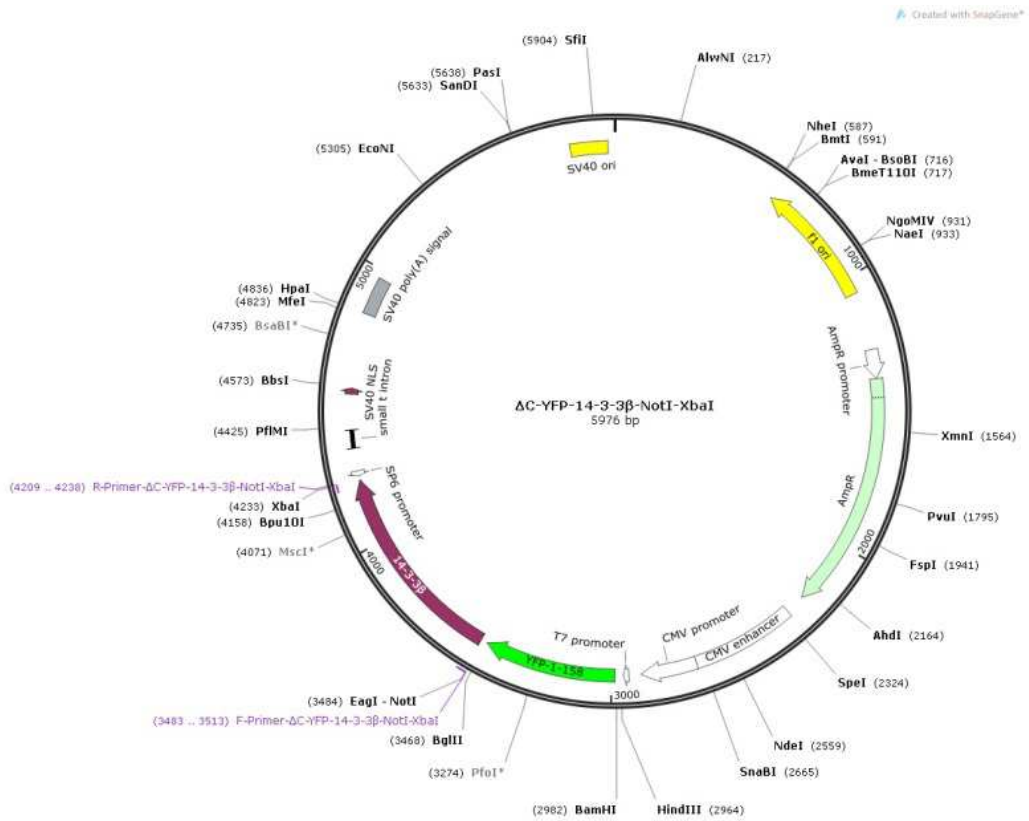
7.5.5 ΔC- and ΔN-YFP-SYNPO2



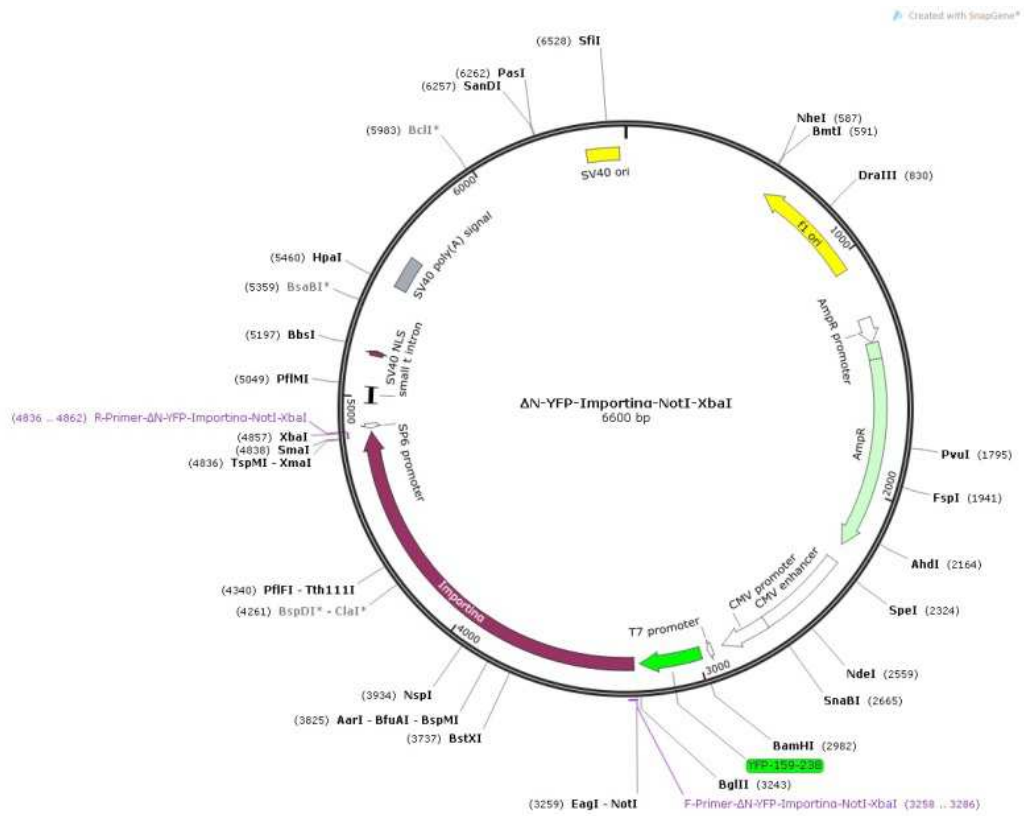
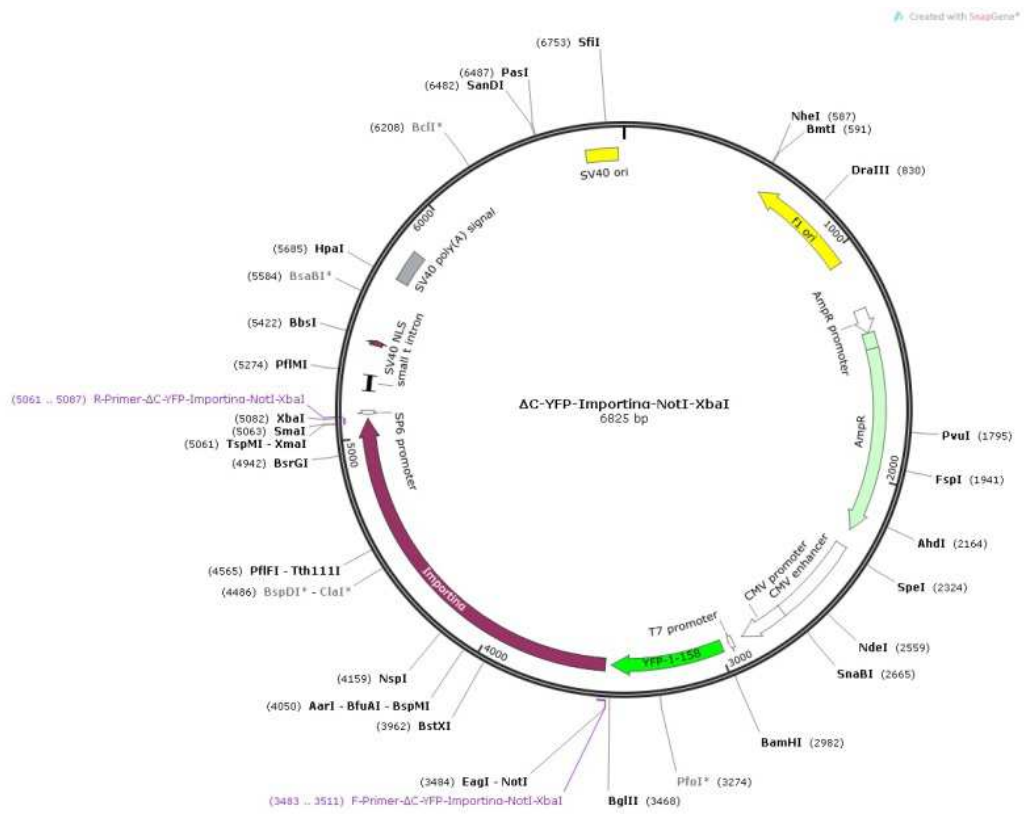
7.5.6 ΔC- and ΔN-YFP-14-3-3y



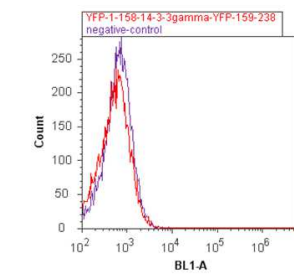
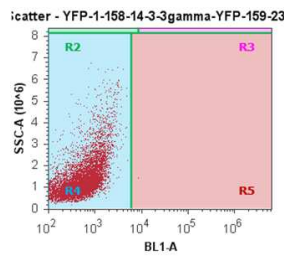
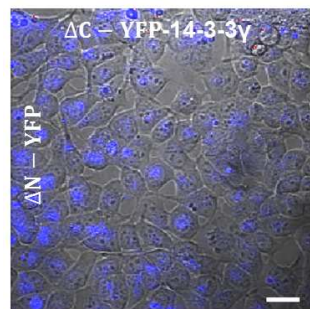
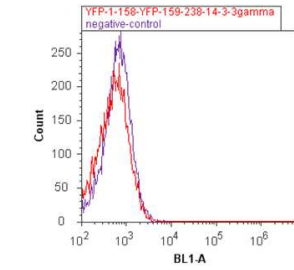
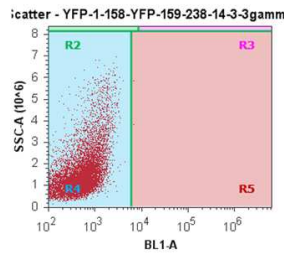
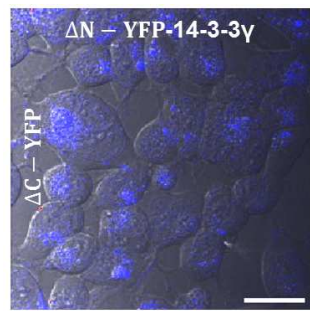
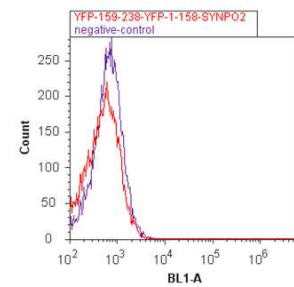
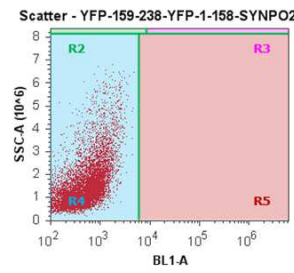
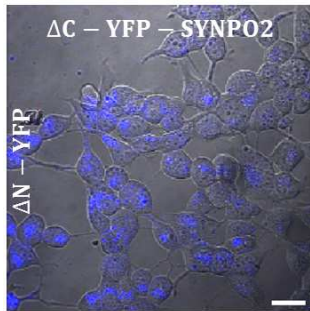
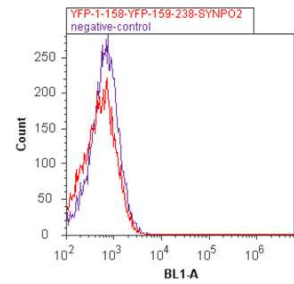
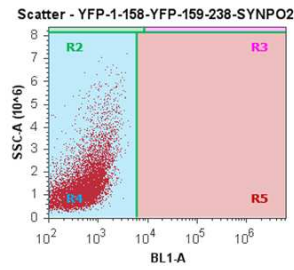
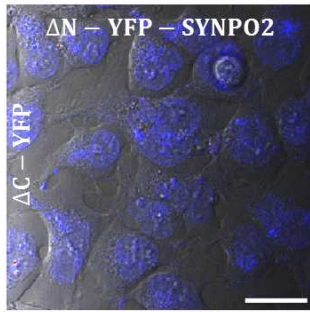
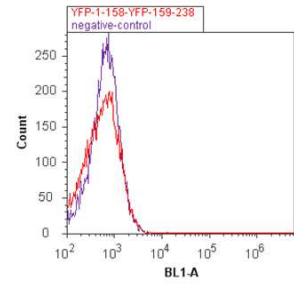
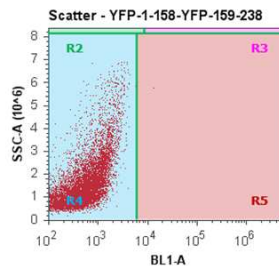
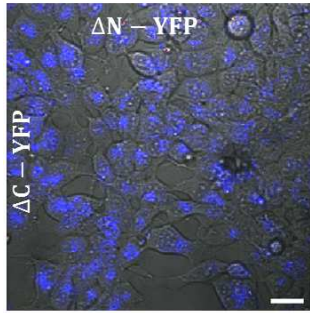
7.5.7 ΔC- and ΔN-YFP-14-3-3β

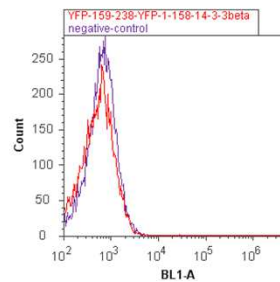
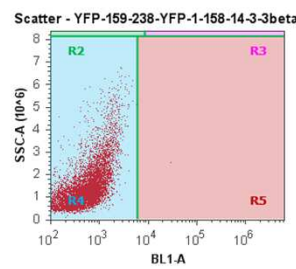
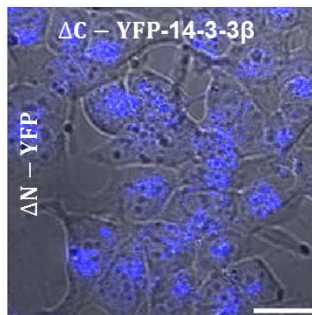
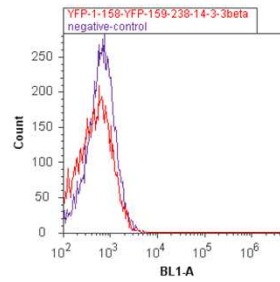
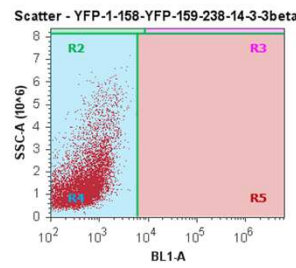
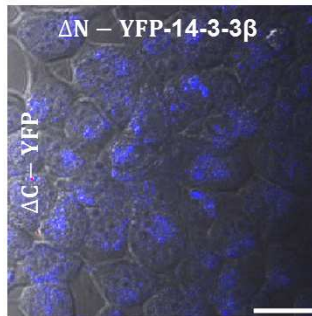
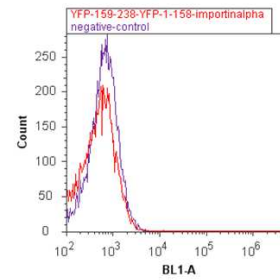
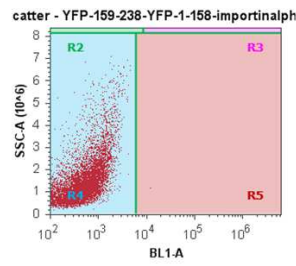
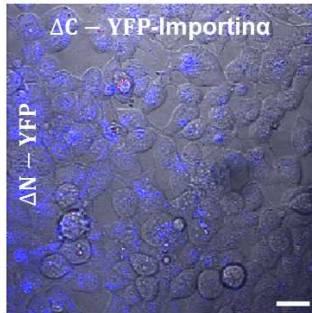
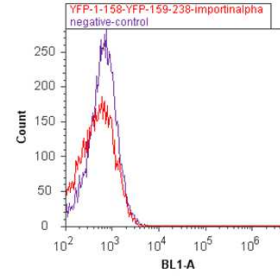
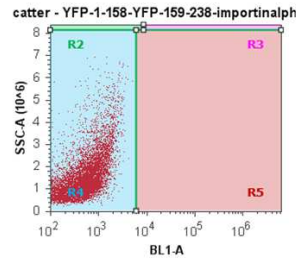
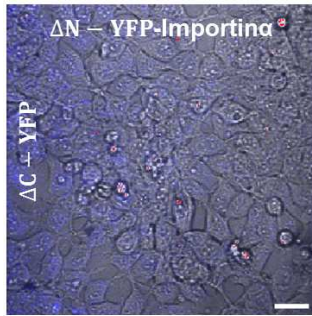


7.5.8 ΔC- and ΔN-YFP- Importina



7.6 BIFC control experiments





## 8 Acknowledgment

**Praise to the Almighty God who guided me to the path of knowledge.**

This thesis is the ultimate product of my arduous and long journey to obtain my goal. This thesis has been kept on fast track and its completion has been possible with the support and encouragement of numerous people which includes my well-wishers, friends and various institutions. And the end of my thesis, it is a pleasant task to express my thanks to all those who contributed in many ways to the success of this study and made it an unforgettable experience for me.

I express a deep sense of gratitude and thankfulness to my supervisor **Prof. Gabriele Pfitzer**, Chair, Department of Medicine, Institute of Vegetative Physiology, University of Cologne, Germany. She has helped me at each and every point of my research work with the patience and enthusiasm. She has taught me, both consciously and unconsciously, how to become a good researcher. I am also thankful for the excellent example, she provided as a successful Scientist and Professor.

I am indebted to **Dr. Mechthild Schroeter**, Institute of Vegetative Physiology, for all her cooperation, guidance and support during the course of my research.

I would like to thank my first thesis supervisor and reviewer of my thesis, **Prof. Dr. Günter Schwarz** for his supervision during my PhD work.

I owe my sincere thanks to my second supervisor and reviewer of my thesis, **Prof. Dr. Angelika A. Noegel**, Chair, Department of Medicine, Institute of Biochemistry I, who has always been a constant source of inspiration and support.

I would also like to thank **Prof. Dr. Thorsten Hoppe**, the chair of my thesis committee.

I would like to appreciate,

**PD. Dr. Kurt Pfannkuche** and **Dr. Carlos Omar Heras Bautista**, Institute of Neurophysiology, for preparing acrylamide matrices I consumed throughout my studies.

**Prof. Dr. Symen Papadopoulos**, who helped with the confocal microscopy.

**Prof. Dr. Kurt Beam**, Department of Physiology and Biophysics, University of Colorado, Denver, USA, for the gift of BIFC vectors.

**Prof. Dr. Tim Hucho**, Department of Anesthesiology and Intensive Care, University of Cologne, for supplying rat organs.

**Dr. Hue-Tran Hornig-Do** for her kind guidance to me during my PhD work.

**Dr. Stefan Lanz** for his kind help during my PhD thesis.

**Dr. Lubomir Lubomirov** for his suggestions and comments on my thesis, especially in case of the cAMP signaling pathway.

**Nina Flizitas Linde**, who helped to design and to perform SYNPO2 mutations and with confocal microscopy.

**Maike Schlemminger, and Alina Bouwer** for technical assistance in the lab.

I cannot skip thanking my family and my best friends, **Abolfazl, Zahra, Leila, Feli, Anna, Dilyana, Desi, Jan, Stefan, Katrin, Jonni, David, Jenni, and Dr. Fatiha Elhamine**, for their everlasting love and prayers that really gave me the strength to complete this thesis and faithful support during the final stages of the preparation of this thesis is so appreciable. I thank them for everything, for being so understanding and for putting up with me through the toughest moment of my life.

I would like to thank the Graduate School for Biological Sciences (**GSfBS**) for setting the opportunity of becoming a member. My sincere gratitude goes to **Dr. Isabell Witt** for her kind support and help in official matters.

**Mostafa Abootorabi Ardestani**

## 9 Erklärung

Ich versichere, dass ich die von mir vorgelegte Dissertation selbständig angefertigt, die benutzten Quellen und Hilfsmittel vollständig angegeben und die Stellen der Arbeit – einschließlich Tabellen, Karten und Abbildungen –, die anderen Werken im Wortlaut oder dem Sinn nach entnommen sind, in jedem Einzelfall als Entlehnung kenntlich gemacht habe; dass diese Dissertation noch keiner anderen Fakultät oder Universität zur Prüfung vorgelegen hat; dass sie – abgesehen von unten angegebenen Teilpublikationen – noch nicht veröffentlicht worden ist, sowie, dass ich eine solche Veröffentlichung vor Abschluss des Promotionsverfahrens nicht vornehmen werde. Die Bestimmungen der Promotionsordnung sind mir bekannt. Die von mir vorgelegte Dissertation ist von Prof. Dr. Angelika A. Noegel und Prof. Dr. Guenter Schwarz betreut worden.

Teilpublikationen liegen nicht vor.

Mostafa Abootorabi Ardestani,

Köln den 29.01.2015

## 10 Curriculum Vitae

Name: Mostafa Abootorabi Ardestani  
PhD-Student  
Institute of Vegetative Physiology  
Medical Faculty, University of Cologne  
Robert-Koch-Str. 39  
D-50931 Cologne, Germany  
Phone: +49 221 478 7853  
Email: mabootor@uni-koeln.de



**Date of Birth:** 22.11.1977, Iran

**Citizenship:** Iran/Germany

### EDUCATION

**PhD-Student**, Nov. 2011-Present

University of Cologne

Title of PhD-Thesis: "Mechanism of Synaptopodin 2 translocation to the cell nucleus and its role in Mechanotransduction in vascular smooth muscle cell"

Main Focus: Biochemistry and cell biology

**Master of Science (Chemical Biology)**, 2011

Technical University of Dortmund and Max Planck Institute, 2009-2011

Master Thesis: "Semi-Synthesis of Prenylated Rab Proteins"

Department: Physical Biochemistry at Max Planck Institute

**Bachelor of Science (Chemical Biology)**, 2009

Technical University of Dortmund and Max Planck Institut, 2007-2009

Bachelor Thesis: "Alternative Substrate for Arginin Kinase"

Department: Physical Biochemistry at Max Planck Institute

**Bachelor of Science**, 2002

Azad University of Qom, Iran, 1998 - 2002

Department: Microbiology and Cell Biology

### TEACHING ACTIVITIES

Teaching Assistant, Medical Student Physiology: Laboratory, University of Cologne, Cologne, Germany, since May 2012.

### TRAINED STAFF MEMBER

Maike Schlemminger, Technician, Department of Physiology, since July 2013

Janine Klask, Technician, Department of Physiology, since January 2014

Alina Bouwer, Technician, Department of Physiology, since August 2014

**TECHNICAL EXPERIENCES**

Primary Cell culture and Cell Characterization Methods (Cell Isolation from Tissues, Transfection, Immunofluorescence Staining, etc.)

Molecular Biology Techniques (DNA/RNA Isolation, Real-Time PCR, Cloning and Sub-Cloning etc.)

Protein Biochemistry Techniques (Protein Isolation and SDS-PAGE Analysis, Western Blot Analysis, and Recombinant Protein Purification)

Microscopy Methods (Fluorescence and Confocal Microscopy)

FACS Analysis, MS-MS and MALDI-ToF Analysis, ELISA

**Honors & Awards**

The Albertus Magnus Graduate Center the Medical Faculty, University of Cologne, Travel Grant for Conferences Abroad, 2014

**PUBLICATIONS**

"Semi-synthesis of Prenylated Rab GTPases by Click Ligation" Long Yi, **Mostafa Abootorabi**, Yao-Wen Wu, **2011**, *ChemBioChem*, 12, 2413–2417.

"Fam40b Is Required for Lineage Commitment of Murine Embryonic Stem Cells" Vilas Wagh, Michael Xavier Doss, Davood Sabour, Rabea Niemann, Kesavan Meganathan, Smita Jagtap, John Antonydas Gaspar, **Mostafa Abootorabi Ardestani**, Symeon Papadopoulos, Martin Gajewski, Johannes Winkler, Jürgen Hescheler and Agapios Sachinidis, **2014**, *Cell Death & Dis*, 5, e1320.

**WORK IN PROGRESS**

"Correlation of Phenotype Switch in Vascular Smooth Muscle Cells and Subcellular Localization of Synaptopodin 2" **M. A. Ardestani**, C. O. Heras Bautista, K. Pfannkuche, S. Papadopoulos, G. Pfitzer, M. M. Schroeter

**PRESENTATIONS, AND POSTERS**

"Elusive Role of Synaptopodin 2 in Smooth Muscle Cell Phenotype Switch" **M. A. Ardestani**, C. O. Heras Bautista, K. Pfannkuche, J. M. Chalovich, S. Papadopoulos, G. Pfitzer, M. M. Schroeter, European Muscle Conference 2013, Amsterdam, Netherland, (Poster presentation)

"Correlation of Phenotype Switch in Vascular Smooth Muscle Cells and Subcellular Localization of Synaptopodin 2" **M. A. Ardestani**, C. O. Heras Bautista, K. Pfannkuche, S. Papadopoulos, G. Pfitzer, M. M. Schroeter, 5<sup>th</sup> International Symposium Crossroads in Biology 2014, Cologne, Germany, (Poster presentation)

"Synaptopodin 2 in Synthetic versus Contractile Vascular Smooth Muscle Cells" **M. A. Ardestani**, C. O. Heras Bautista, K. Pfannkuche, S. Papadopoulos, G. Pfitzer, M. M.

Schroeter, 37<sup>th</sup> International Meeting of the German Society for Cell Biology (DGZ) 2014, Regensburg, Germany, (Poster presentation)

"Targeted deletion of total caldesmon in mice is perinatally lethal" Sandra Pütz, Manuel Koch, Marina Frohn, Vivek Peche, Doris Metzler, **Mostafa A. Ardestani**, Wolfram F. Neiss, Angelika A. Noegel, Mechthild M. Schroeter, Gabriele Pfitzer, 58<sup>th</sup> Annual Meeting of the Biophysical Society 2014, San Francisco, USA, (Poster presentation)

"Different regulation of basal tone and electric field stimulation (EFS) induced relaxation by e- and nNOS in aged compared to juvenile murine basilar arteries" G. Pfitzer, S. Pütz, J. Welter, **M.A. Ardestani**, D. Filipova, M., Schroeter, S. Papadopoulos, and L. T. Lubomirov, 11<sup>th</sup> International Symposium on Resistance Arteries 2014, Banff, AB, Canada, (Poster Presentation)

"14-3-3 $\beta$ , not 14-3-3 $\gamma$  supports nuclear localization of SYNPO2 in the nucleus" **M.A. Ardestani**, F.N. Linde, S. Papadopoulos, G. Pfitzer, M.M. Schroeter, American Society of Cell Biology Meeting, 6-10 Dec. 2014, Philadelphia, USA, (Poster Presentation)

#### PROFESSIONAL ASSOCIATIONS

German Society for Cell Biology, Student Member

#### PROFESSIONAL EXPERIENCE

- Military services in the Army Research Center of Iran, Tehran, Iran, 2002-2003  
**Department:** Immunology, Biochemistry, Microbiology and Parasitology
- Sales Manager, medical company (Fater Electronic Co.), Teheran, Iran, 2001-2002
- Lab Assistant, Medical Laboratory, (Tajik), Teheran, Iran, 2002-2004
- Research Assistant, Max Planck Institute, Dortmund, Germany, 2009